Development and Performance Investigation of Diamond Based Radiation Detectors

By

Amit Kumar

(Enrolment No. – PHYS01201304032)

Bhabha Atomic Research Centre, Mumbai, India

A thesis submitted to the

Board of Studied in Physical Sciences

In partial fulfillment of requirements

for the Degree of

DOCTOR OF PHILOSPHY

of

HOMI BHABHA NATIONAL INSTITUTE

November, 2019

STATEMENT BY AUTHOR

This dissertation has been submitted in partial fulfilment of requirements for an advanced degree at Homi Bhabha National Institute (HBNI) and is deposited in the Library to be made available to borrowers under rules of the HBNI.

Brief quotations from this dissertation are allowable without special permission, provided that accurate acknowledgement of source is made. Requests for permission for extended quotation from or reproduction of this manuscript in whole or in part may be granted by the Competent Authority of HBNI when in his or her judgment the proposed use of the material is in the interests of scholarship. In all other instances, however, permission must be obtained from the author.

(Amit Kumar)

DECLARATION

I, hereby declare that the investigation presented in the thesis has been carried out by me. The work is original and has not been submitted earlier as a whole or in part for a degree / diploma at this or any other Institution / University.

(Amit Kumar)

Dedicated

To

My Parents

ACKNOWLEDGEMENTS

I would first like to express my sincere gratitude to my guide Dr. Anita Topkar, Electronics Division, BARC for her guidance. Her Patience, motivation and immense knowledge helped me in all the time of research and completing my thesis work. Besides my guide, I am also thankful to Shri Debasis Das, Group Director, E & IG, BARC and Smt. Anita Behre, Head, Electronics Division, BARC for their constant support and encouragement to carry out the doctoral work.

I am also thankful to my doctoral committee members: Dr. D. S. Patil, Dr. S. C. Gadkari, Dr. V. Sudarshan and Prof. R. O. Dusane for their insightful comments and encouragement to widen my research from various perspectives.

My Sincere thank also goes to Dr. Amar Sinha and Dr. S. C. Gadkari to allow me to experiment at fast neutron facility. I would like to thanks Dr. Rekha Rao to help me in carrying out Raman spectroscopy of diamond substrates. I am also thankful to Smt. K. G. Girija to give me time to time support for processing diamond substrates in her Chemistry lab. I thank to my seniors Shri Arvind Singh and Ms. Bharti Aggrawal and other fellow lab mates:- Arvind, Soumyajit and Sebin for the stimulating discussions which help me to improve my work.

Last but not the least, I would like to thank my family members: my parents, my wife, my sisters and others for supporting me throughout my PhD tenure. Without their support and encouragement, this would not have been easy.

(Amit Kumar)

List of Publications:

List of publications in refereed journals:

1. Amit Kumar and Anita Topkar; "A study of the fast neutron response of a single-crystal diamond detector at high temperature", IEEE Trans. on Nucl. Scin. 6, 5630-635(January 2018).
2. Amit Kumar, Arvind Kumar, Anita Topkar and D. Das; "Prototyping and performance study of a single crystal diamond detector for operation at high temperature", Nucl. Instr. and Meth. in Phys. Res. A 858, 12-17 (March 2017).
3. Amit Kumar, Arvind Singh, Arvind Kumar and Anita Topkar; "Fabrication and characterization of polycrystalline diamond detectors for fast neutron monitoring" Nucl. Instr. and Meth. in Phys. Res.A 785, 55-60 (February 2015).

List of publications in conferences:

4. Amit Kumar, Pradeep Sarin and Anita Topkar; Proc. of the DAE Symp. on Nucl. Phys. 62, 996-997(2017).
5. Amit Kumar and Anita Topkar; "Alpha particle response study of polycrystalline diamond radiation detector", AIP Conf. Proc. 060001, 10.1063/1.4947807, 1731-1-3 (May 2016).
6. Arvind Singh, Amit Kumar and Anita Topkar; "Performance study of polycrystalline CVD diamond detectors for fast neutron monitoring", AIP Conf. Proc., 10.1063/1.4872692, 611-613 (February 2014).
7. Arvind Singh, Amit Kumar and Anita Topkar; 2nd Intern. Symp. on Neut. Scatt., held at BARC, Mumbai, 2013.

TABLE OF CONTENT

SYNOPSIS

In the recent years, diamond has become very popular in radiation detector application due to its outstanding properties such as large bandgap, high resistivity, high electron and hole mobility. It has several advantages such as low leakage current, low electronic noise, fast response and radiation hardness. It has great potential to work in applications which involve high radiation flux, high temperature and harsh environments. It is being widely used in medical dosimetry due to its tissue equivalence. Motivation to involve in the diamond related work came due to its radiation hardness and ability to withstand high temperature. BARC is involved in the development of detectors for neutron measurements in Indian test blanket module (TBM) where temperature and neutron flux are expected to be very high. Diamond is expected to be most suitable for this application due to its radiation hardness and crystal structure.

The present thesis is composed of seven chapters. First chapter is introduction to the thesis and outlines the objectives and scope of the thesis. chapter 2 presents literature review of diamond from the point of view of material as well as detector. chapter provides introduction to diamond from atomic scale to crystal structure and its several properties. Diamond as a radiation detector is further introduced in the chapter with its advantages over other semiconductor detectors. chapter 3 gives details of the characterization methods used for the characterization of diamond substrates and detectors. Experimental methodology to test the detectors with alpha particles and fast neutrons are also discussed in this chapter. Fabrication and characterization of poly crystalline diamond (pCVD) detectors and single crystal diamond (SCD) detectors are discussed in chapter 4 and chapter 5 respectively. Results of the measurements of several types of radiations such as alpha particles, fast neutrons and slow neutrons are also presented in the chapters. In chapter 6, performance of the detectors at high temperature is presented. Results and findings of the doctoral work are summarized in chapter 7. The details of each chapter are described below.

Chapter 1: Introduction

This chapter introduces the thesis considering objective and scope of the work. Main objectives of the work were development of detector fabrication methodology, realizations of low leakage currents, validation of response of diamond based detectors with different radiations at room temperatures and higher temperatures.

Chapter 2: Diamond - A Unique Material

This chapter introduces material aspect of diamond. Diamond is basically a tetrahedral arrangement of carbon atoms which forms a crystal class known as diamond cubic crystal. All carbon atoms are bonded to each other by σ-bonding which give very high strength to the material. The properties of diamond and its implications are discussed in this chapter which mainly focuses on large bandgap, high resistivity, high electron and hole mobility, hardness, etc. Further, techniques for diamond fabrication are discussed which are HPHT method and chemical vapor deposition (CVD) technique. In HPHT method, detectors are fabricated by recreating similar environment that exist beneath Earth which causes formation of natural diamond. CVD technique is the most reliable method to grow diamond substrates in a controlled way. Depending upon the number of grains in diamond crystal, it is classified into single crystal diamond (SCD) which have single orientations of atoms and Polycrystalline diamond (pCVD) having many grains having different orientations of atoms. Depending upon content of nitrogen impurity, diamond substrates are classified into type I having nitrogen impurity > 5 ppm and type II having nitrogen impurity < 5 ppm.

Further details of diamond from detector point of view are discussed. Excellent properties of diamond make it favourable for detector applications which are discussed in this chapter. Diamond detectors exhibit several advantages such as low leakage current, low electronic noise, fast timing response, high breakdown voltage and radiation hardness. Diamond detectors can work not only at room temperature but also at higher temperatures which make them promising for high temperature applications. Diamond has low Z which allows it to discriminate radiation particles from gamma background. As atomic number of carbon atom is close to that of tissue, diamond can be used for dosimetry. Diamond has great potential to monitor fast neutrons produced in D-T fusion. The detector fabrication methodology is presented considering the requirement of metal contact behaviour, adhesion of metal to diamond surface and area of applications. Subsequently principle of diamond detector is discussed to measure charged particles, neutrons and gamma rays. Charged particles can directly ionize diamond and create electron hole pairs which can be collected by applying electric field in diamond which gives rise to electronic signal. On the other hand neutrons cannot directly ionize diamond but these can be detected through conversion process in which neutrons produces charged particles either in diamond (fast neutron case) or in other converter layer (low energy neutrons). A brief review of the work done on diamond detector by various international group is also presented in this chapter starting from diamond as photo-conductive device to diamond detectors as radiation counters, dosimeters and neutron detectors. At the end of the chapter, application of diamond detectors in several fields are summarized such as beam conditioning and monitoring at LHC, fast neutron detector in ITER, medical dosimetry, etc.

Chapter 3: Experimental Methods

First part of the chapter discusses about the fabrication steps of diamond detector starting from the cleaning to metallization and then bonding and packaging. Several batches of SCD and pCVD detectors were fabricated with different dimensions of detectors and different combinations of metallization. Diamond substrates were cleaned to remove surface impurities. Some of the diamond substrates (mainly SCD) were treated with oxygen plasma to get highly insulating surface. Some of the detectors were annealed before metallization in nitrogen environment at different temperatures. Both sides of diamond substrates were metallized by sequential deposition of three different combination of metal - Ti/Au, Cr/Au and Ti/Pt/Au. Some of the samples were annealed after metallization in the same nitrogen environment. Finally, detectors were packaged on a TO header and wire bonding was done to make electrical contact.

In the second part of chapter, characterization and testing methods are discussed with complete description of experimental setups and principle of the methods. Raman spectrum of pCVD and SCD substrates were obtained after cleaning the substrates to get information about the phase of material. Lau pattern of the diamond substrates was obtained to study crystal nature of substrate and identify single crystalline and pCVD nature. XPS was done on oxygen plasma treated substrates to study the surface termination. After the fabrication of the detector, leakage current measurement was done at different bias voltages to study metal diamond interface. Further study was done using alpha particles emitted from ^{238}Pu+^{239}Pu dual energy alpha source and fast neutrons from D-T reaction. The experimental setup comprised of a high voltage source, pre-amplifier, amplifier, multichannel analyser (MCA) and CRO. For alpha response measurements, the detector was mounted in a vacuum chamber. Fast neutron measurement was done in air where detector was enclosed inside an aluminium box. Dynamics of charge carriers generated inside diamond was studied using transient current technique. Fast current amplifier having bandwidth of 2 GHz and gain of 53 dB was used to collect charge carriers while detector was biased through a T-Bias.

Chapter 4: pCVD Based Detectors

Two thicknesses of pCVD substrates (100 µm and 300 µm) were used for the fabrication of detectors with three different types of metallization Ti/Au, Ti/Pt/Au and Cr/Au. Just after the fabrication, I-V measurement was done to study metal-diamond contact behaviour. The detectors having Ti/Au and Cr/Au metallisation have shown near ohmic behaviour with leakage current of ~ 1 nA. On the other hand, pCVD detectors with Ti/Pt/Au metallization have shown leakage current of 3 nA at +100 V and current at -100 V was twice of that at positive bias. Subsequently response of detectors to charged particles was studied by obtaining pulse height spectrum (PHS) of alpha particles using the electronics setup discussed in chapter 4. PHS was observed to be a continuum in energy domain. The stability test of the detectors was done by continuously monitoring the PHS for a long time. It was observed that count rate reduces with time which was attributed to polycrystalline nature of substrate where probability of occurrence trap centres is more at grain boundaries. Priming of the pCVD detectors was done to saturate the trap centres using β-particles. For a net dose of 30 Gy, the response of the detector was observed to be stable with time. The PHS after the priming has shown a shift towards higher channel (compared to PHS before priming) which indicated the improvement in charge collection. The effect of thickness of the substrate on charge collection has been studied by taking two pCVD detectors having thicknesses of 100 µm and 300 µm. The PHS of alpha particles obtained using the two detectors have shown that the thin detector has better charge collection compared to the thicker one. This was due to the trap centres in pCVD detectors which offer high probability of trapping as electrons and holes transport through longer path in a thicker detector. These findings were published in NIMA 785, 55-60 (2015) The pCVD detectors were subsequently tested with fast neutrons generated by D-T reaction. The PHS with fast neutrons was obtained up to a neutron flux of 8.76 x 10^6 n $cm^{-2}s^{-1}$ using 100 μm and 300 μm thick detectors. No peaks were observed in the spectrum to get energy information about neutrons. Similar effect of thickness as for alpha particle response was observed for neutron related charge collection. The detectors have shown quite linear response to neutrons with respect to change in the neutron flux. Therefore, pCVD detectors have shown the potential for counting application of alpha particles and fast neutrons. However, the detectors were unable to give energy information. De-trapping of the saturated trap sites was observed after heating the detector at above 50^oC. Further measurements were done to study the effect of different parameters of electronics components such as bias voltage and shaping time on count rate and charge collection. The detectors have shown improved count rate and better charge collection at higher shaping times.

Chapter 5: SCD Based Detectors

As pCVD detectors did not show any indication of energy information of neutron radiation, further work was done using SCD substrates whose details and results are presented in this chapter. The Raman spectrum of the SCD substrate has shown peak at 1332 cm^{-1} indicating the presence of only sp^3 carbon and absence of graphite phase. The Laue diffraction pattern has shown dots corresponding to the set of planes which satisfy Bragg condition. The observed pattern has shown single crystalline nature of the substrate. XPS spectrum of SCD substrate has shown presence of oxygen termination of the surface after oxygen plasma treatment. SCD detectors were fabricated using 5 mm x 5 mm x 400 μm single crystal substrates with Cr/Au metallisation on both sides of the substrates. The detectors have shown leakage current of few hundred pA at 400 V. The oxygen plasma treatment of the detectors has shown decrease in leakage current by at least one order of magnitude. The PHS was obtained using dual energy alpha source. The spectrum has shown two peaks corresponding to the two energies of alpha particles. The detectors have shown energy resolution of 1.9 % for 5.5 MeV alpha particles. GEANT4 based Monte Carlo simulation was done to study the interaction between carbon and fast neutrons. The PHS was obtained through simulations by calculating energy deposition in the detector. Several peaks in the spectrum were observed corresponding to different channel of nuclear reaction between neutron and carbon. Similar PHS has been experimentally measured for 14.2 MeV fast neutrons from compact D-T neutron source. The (n, α) peak at 8.5 MeV was observed to be well separated from the other peaks which can be used to deduce energy information of neutrons. The detector has demonstrated an energy resolution of 4 % for 8.5 MeV peak in the spectrum.

Chapter 6: Study of SCD Detectors for High Temperature Applications

Performance investigation of SCD detector at high temperatures is discussed in this chapter. A high temperature setup was designed and fabricated for experiments at high temperatures. The setup included a heating disk placed in a vacuum chamber where temperature can be sensed and adjusted using an integrated temperature controller and a temperature sensor. There was a provision to mount alpha source in the chamber and obtain electrical signal from the detector to subsequent chain of electronics. The adhesion of metal deposited on diamond at high temperatures was studied by annealing three types of metallization on diamond films - Ti/Au, Ti/Pt/Au and Cr/Au (thickness of Ti, Pt & Cr was 20 nm and Au was 200 nm). It has been observed that Ti/Pt/Au and Cr/Au can withstand temperature higher than 300^{o}C. The SCD detectors fabricated using Cr/Au metallization were studied at high temperatures as it had relatively low leakage currents and better ohmic behaviours as compared to pCVD detector. The PHS with alpha particles was obtained at high temperature up to 300^{o}C and no measurable change in the spectrum was observed. The resolution of the detectors was observed to be unchanged up to 300^{o}C. Subsequently, the detectors were tested with fast neutrons at high temperatures. For this purpose, a detector enclosure was designed and fabricated to conduct various experiments. The package was made of a long aluminium tube where the detector was mounted at one end of the enclosure and connected to a BNC connector at the other end by an 1 mm SS wire. The PHS with neutrons was obtained at room temperatures (RT), 100^{o}C, 200^{o}C, 250^{o}C and 300^{o}C and all peaks were observed to be the same without any change. Total integrated count rate, count rate under (n, α) peak and energy resolution were analysed at different temperatures. No significant change in the count rate with temperature was observed. The energy resolution was observed to be between 3.3 % to 3.8 % with a standard deviation of ±0.2 %. This was the first international experimental demonstration of SCD detector to measure energy of alpha and fast neutrons at 300^{o}C and the results were published (IEEE Trans. on Nucl. Scin. 6, 5630-635 (2018)).

Chapter 7: Summary

Important results and findings of the work have been summarized in this chapter. The thesis presents investigation of performance of diamond based detector for radiation measurements. The work was initiated with pCVD substrates of different dimensions and different combination of metallization. Cr/Au metallisation was observed to be the best for diamond as it showed ohmic behaviour with low leakage current. One of the major findings of the work on pCVD detector was the effect of thickness of diamond substrates on the charge collection properties. It has been observed that pulse height (in the PHS of alpha particles and neutrons) in thin detector is more than that in thicker detector which was attributed to more trapping phenomena in thicker detector than thinner one. Therefore, thin detector offers better charge collection compared to thicker detectors. The pCVD detectors were shown to have instable response as count rate was observed to decrease with time. Priming of the pCVD substrate using β-irradiation for a total dose of 30 Gy resulted in the stable response of detector and count rate was observed to be constant with time. The pCVD detectors were shown to have potential for counting application but were unable to provide energy information.

The doctoral work was further carried out using SCD substrates. The SCD detectors have shown leakage current few hundred pico-amperes for Cr/Au and Al metalized detectors. The charge collection study of the detector in terms of charge collection distance CCD shows full charge collection at an applied bias voltage corresponding to 0.13 V/μm. The SCD detectors have shown alpha response with peaks corresponding to the different energies of alpha emitting from ^{238}Pu+^{239}Pu source. Energy resolution shown by the fabricated detectors was about 2 % for 5.5 MeV alphas.The PHS of fast neutrons has shown several peaks corresponding to different channel of nuclear reaction between carbon and neutrons. The experimentally observed PHS was in good agreement with the Monte Carlo simulation results. The SCD detector response is quite linear with respect to variation in neutron flux. The SCD detector along with a ^{10}B neutron converter film can be used for the measurement of thermal neutrons.

The thesis work was further carried out to explore the potential of diamond detector for the measurements of fast neutrons at high temperatures. A complete experimental setup and detector package for fast neutron experiments at high temperatures was designed and fabricated. The SCD detector when tested at high temperatures did not show degradation in the detector response up to the studied temperature of 300^{o}C. The energy resolution of the detector was observed to be approximately same with different temperatures up to 300^{o}C and was about 2 % for 5.5 MeV alpha particles and about 4 % for fast neutrons.

List of Figures

List of Tables

CHAPTER 1: INTRODUCTION

Semiconductor detectors are most widely used detectors in the area of radiation detection where precise energy measurement is a prime concern. Semiconductor detectors are compact, fast and give better energy resolution compared to other widely used detectors such as scintillators and gas detectors. In these detectors, the basic information carriers are electron hole pairs instead of electron ion pairs as in the case of gas detectors. Silicon and germanium are most widely used materials for semiconductor detectors. Germanium detectors require cooling to reduce the leakage currents to obtain better energy resolution. These detectors also suffer degradation due to radiation damage which limits their applications in high radiation areas. Diamond as a detector material exhibits several outstanding properties such as a wide bandgap of 5.5 eV, a high break down field, high carrier mobilities and high radiation hardness. Due to its high radiation hardness and wide bandgap, diamond detectors have potential to sustain the harsh environment involving high radiation flux and/or high temperature. In the upcoming fusion tokamak facilities such as the International Thermonuclear Experimental Reactor (ITER), detectors are required to operate in a high gamma and neutron radiation environment, and at temperatures well above the room temperature. The measurement of various radiations is considered important but one of the most challenging task due to the harsh environment of ITER. Considering the outstanding properties of diamond and its compact size, diamond detectors have potential for building a compact neutron spectrometer for the neutron diagnostics at ITER.

1.1. Motivation of doctoral work

BARC is involved in several types of research activities in which radiation detectors are required to monitor radiations for several applications such as nuclear physics experiments, nuclear waste processing, thermal neutron flux monitoring, etc. India is one of the participating countries in the ITER experiment and a Test Blanket Module (TBM) developed by India will be installed at ITER to study the breeding of tritium. For the neutron diagnostics in the Indian TBM, compact neutron detectors withstanding the high neutron flux as well as the temperatures much higher than the room temperatures are required. The neutron flux and temperatures inside the TBM at various locations are expected to be 10^{10} - 10^{13} n / cm^2 s and 300 - 500 °C respectively. The neutron flux and temperatures outside the TBM at various locations such as shield block, pipe forest, etc, are expected to be 10^{4-} 10^{10} n / cm^2 s and ~ 50 - 100 °C respectively. Considering the requirements of small size and operation in a high temperature and high flux environment, diamond detectors are the best choice for fast neutron counting and spectrometry. Hence, in recent years, there has been a significant interest internationally in the development of diamond based detectors for measuring the fast neutron spectrum from the fusion plasmas.

1.2. Objective of doctoral work

Main objectives of the doctoral work are as follows:

a. Development of fabrication methodology for diamond based detectors involving surface treatments, contact metal selection, post metallization annealing, packaging, etc.

b. Realizing low leakage currents for improving the noise performance of the diamond detectors.

c. Development of characterization setups for operations from room temperature (RT) to high temperature (300°C).

d. To validate the performance of the detectors at RT to charged particles, fast neutrons, thermal neutrons, etc.

e. Performance investigation of diamond based detectors with alphas and fast neutrons at higher temperatures.

1.3. Layout of the thesis

The present thesis investigates suitable fabrication techniques for diamond detectors and their performance to several types of radiations. The response of the fabricated detectors is also studied at high temperatures. The thesis consists of seven chapters.

In chapter 2, details of diamond from material point of view to detector point of view are presented. This includes discussions on allotropes of carbon, crystal structure and band structure of diamond. Further several properties of diamond, methods to grow diamond substrate, types of diamond substrates, etc., are presented in this chapter. The advantages of diamond as a detector over other semiconductor detectors are further explained. Subsequently, fabrication methods of diamond detectors, principle of radiation detection, and response of the detectors to several types of radiation particles are described. A brief review of the work reported in the literature in the area of diamond detectors is also presented this chapter.

chapter 3 provides details of diamond detector fabrication methods which have been developed during the doctoral work. This is followed by a description of characterization techniques which have been used to evaluate the characteristics and quality of diamond detectors. Subsequently, the experimental setup and measurement methods have been presented to study the performance of detector to several types of radiations.

In chapter 4, the study of polycrystalline diamond (pCVD) detectors is presented. This comprises of fabrication and characterization of several batches of detectors. The stability tests and priming of pCVD detector are further presented in this chapter with results showing how the detector response can be stabilised by the method of priming.

In chapter 5, the study of single crystal diamond (SCD) detector is presented with characterization results to study structure of crystal and chemical state of surface. The response of SCD detectors to alpha particles and neutrons are presented.

In chapter 6, the performance study of diamond detectors at high temperature is presented. This chapter discusses details of the experimental setup developed to evaluate the detector performance at high temperatures. The results of the detector performance at high temperature have been discussed in this chapter to demonstrate the potential of detectors for high temperature applications.

At the end of the thesis, in chapter 7, all the results have been summarized with highlights of major findings of the doctoral work.

CHAPTER 2: LITERATURE REVIEW

Diamond has been known since centuries mostly for its appearance and has been used in jewellery such as rings and necklaces due to durability and lustre. Apart from the appearances, people quickly recognized other potentials in diamond mostly its hardness and hence widely used it as an abrasive for cutting, drilling and polishing. Diamond has a very high thermal conductivity due to light carbon atoms and rigid chemical bonds. Thermal conductivity of diamond (2200 W/(m.K)) is around five times more than copper (385 W/(m.K)) which makes it a suitable heat sink to extract heat from the electronic chips. The word diamond comes from the Greek word meaning unbreakable.

This chapter begins with the introduction to carbon and its allotropes and how the mixing of s and p orbitals in sp^3 hybridization leads to a very strong and stable tetrahedral structure of diamond. Overview of crystal structure of diamond, band gap model of the diamond, various properties of diamond, fabrication techniques of diamond substrate and types of diamond substrate, etc., are presented. Subsequently a brief discussion on the detector fabrication methods as reported by various researchers is presented. At the end of the chapter, few applications of diamond detector are also discussed.

2.1. Allotropes of Carbon

Carbon exists in several allotropic forms such as diamond, graphite, carbon nano tubes, fullerene, etc. Carbon atom has six electrons and in ground state they are arranged in orbitals as shown in the Diagram 2.1.

Diagram 2.1: C: $\underset{1s}{\underline{\uparrow\downarrow}}\,\underset{2s}{\underline{\uparrow\downarrow}}\,\underset{2p_x}{\underline{\;\uparrow\;}}\,\underset{2p_y}{\underline{\;\uparrow\;}}\,\underset{2p_z}{\underline{\quad}}$

The ground state orbitals cannot be used for bonding in C, while exciting a 2s electron into a 2p orbital (shown in Diagram 2.2) would allow for four bonds according to the valence band theory. The resultant hybrid orbits are used in the bonding in carbon. In crystalline phase, valence electrons are arranged in 2s, 2px, 2py and 2pz orbitals. As energy difference between 2s and 2p levels is smaller than the binding energy of C-C, the electronic wave function prefers to mix with each other to enhance binding energy [1].

Diagram 2.2: $C^*: \frac{\uparrow\downarrow}{1s}\,\frac{\downarrow}{2s}\,\frac{\uparrow}{2p_x}\,\frac{\uparrow}{2p_y}\,\frac{\uparrow}{2p_z}$

Depending upon the circumstances, the 2s orbital electron will mix with different number of p orbital electrons which leads to different hybridization of carbon atoms. There are three possible ways in which 2s orbital may mix with the three p orbitals and form three different types of hybridizations as shown in Diagram 2.3 and Figure. 2.1 (a) – (c).

$\frac{\uparrow\downarrow}{1s}\,\frac{\uparrow}{sp^3}\,\frac{\uparrow}{sp^3}\,\frac{\uparrow}{sp^3}\,\frac{\uparrow}{sp^3}$ $\qquad$ $\frac{\uparrow\downarrow}{1s}\,\frac{\uparrow}{sp^2}\,\frac{\uparrow}{sp^2}\,\frac{\uparrow}{sp^2}\,\frac{\uparrow}{p}$ $\qquad$ $\frac{\uparrow\downarrow}{1s}\,\frac{\uparrow}{sp}\,\frac{\uparrow}{sp}\,\frac{\uparrow}{p}\,\frac{\uparrow}{p}$

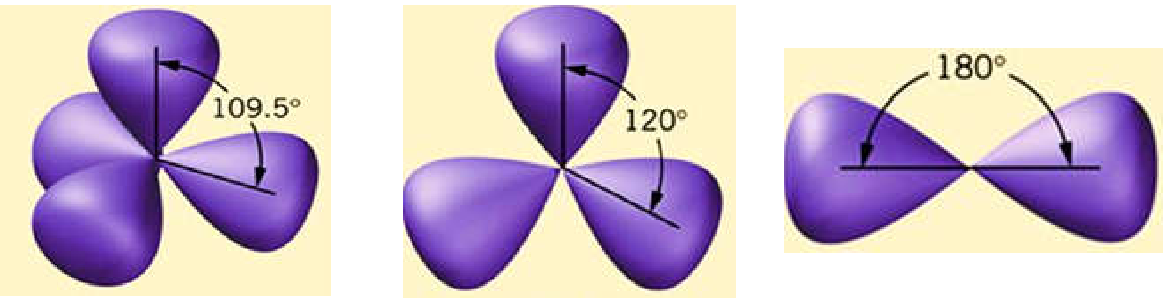

(a) sp^3 hybridization (b) sp^2 hybridization (c) sp hybridization

Fig. 2.1. (a) Tetrahedral arrangement of carbon atom due to sp^3 hybridization, (b) Planar arrangement of carbon atoms due to sp^2 hybridization, (c) Linear arrangement of carbon atoms due to sp hybridization.

Carbon atoms in diamond have sp^3 hybridization and they are arranged in tetrahedral form with all bonds making an angle of 109.5^o with each other. The covalent bonds between carbon atoms are made by pairing valence electrons of each carbon atom along the axis of joining the atoms which results in strong σ-bonding. Three different types of hybridization lead to different vibrational modes of atoms/molecules. In Raman spectroscopy, these modes can be excited by laser photons which lead to shift in the energy of the photons which can be used for the study of hybridization and phase of the material. The quality of diamond substrates is normally discussed in terms of the ratio of sp^3 to sp^2 bonded carbon atoms i.e. fraction of graphite content in diamond.

2.2. Crystal structure of diamond

The lattice structure of diamond is called diamond cubic crystal where each carbon atom is at the centre of a tetrahedron with its four nearest neighbours at the four corners of the tetrahedron. A unit cell of diamond cubic crystal is shown in Figure 2.2 (a), (b) which may be visualized as two interpenetrating face cenetred cubic (FCC) C lattice along the diagonals which are displaced with respect to one another by (1/4, 1/4, 1/4) a, where ‘a’ is the dimension of the cubic unit cell.

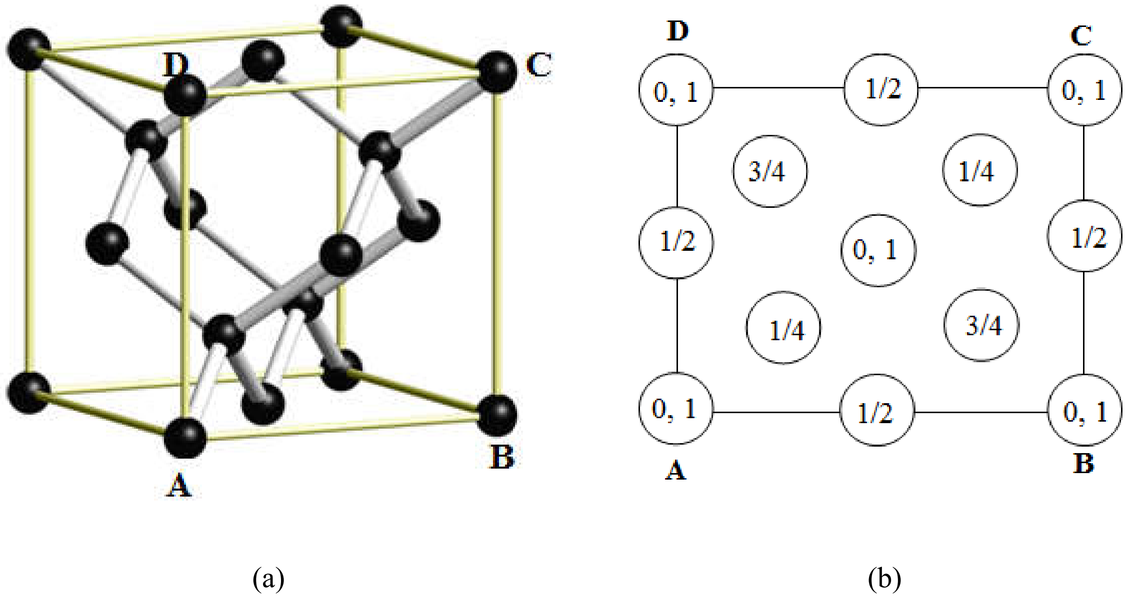

Fig. 2.2. Lattice structure of diamond; (a) Unit cell with carbon atoms arranged in tetrahedral from, (b) Plane view of the unit cell looking from the face ABCD. The circled numbers denote location of atoms in scale of lattice parameter a.

For better understanding of the relative locations of carbon atoms in the crystal, a plane view of the unit cell looking along the face ABCD is as shown in Figure 2.2 (b). There are two indices at corner and central circle which indicate two atoms, one at face ABCD and second on the opposite of face ABCD. The circles at the centre of edges indicate face centred atoms and circles represented by 1/4 and 3/4 are atoms completely inside the unit cell along diagonals. Therefore, the unit cell can be viewed as two FCC sub-lattices interpenetrating each other so that if the central atom of tetrahedron is on one FCC sub-lattice then the four corner atoms are all on the other sub-lattice. Silicon and germanium also have the same crystal structure as that of diamond.

2.2.1. Atoms per unit cell

The number of atoms per unit cell is contributed by corner atoms, face centred atoms and atoms inside the unit cell. The corner atoms represented by (0, 1) are shared by 8 unit cells, face centred atoms represented by 1/2 and central (0, 1) are shared by two unit cells and atoms inside the unit cell represented by 1/4 and 3/4 are not shared by any other unit cell. Therefore,

The total number atoms per unit cell of diamond cubic crystal are;

$$= \frac{1}{8} \times \text{number of atoms at corner} + \frac{1}{2} \times \text{number of face centred atoms}$$

$$+ \text{number of atoms completely inside the unit cell}$$

$$= \frac{1}{8} \times 8 + \frac{1}{2} \times 6 + 4$$

$$\text{No. of atoms per unit cell of diamond cubic crystal} \quad = 8 \qquad (2.1)$$

If we consider atoms at the location A, then the nearest atom to this atom is atom at the location R in the same unit cell which is as shown in Figure 2.3 (a), (b). As atom at the location A is shared by eight unit cells, there will be three more atoms at the same distance in other four cells which are represented as 3/4 location in Figure 2.2 (b). Total number of atoms at the nearest neighbour distance is called co-ordination number. Therefore, co-ordination number in diamond cubic crystal is 4.

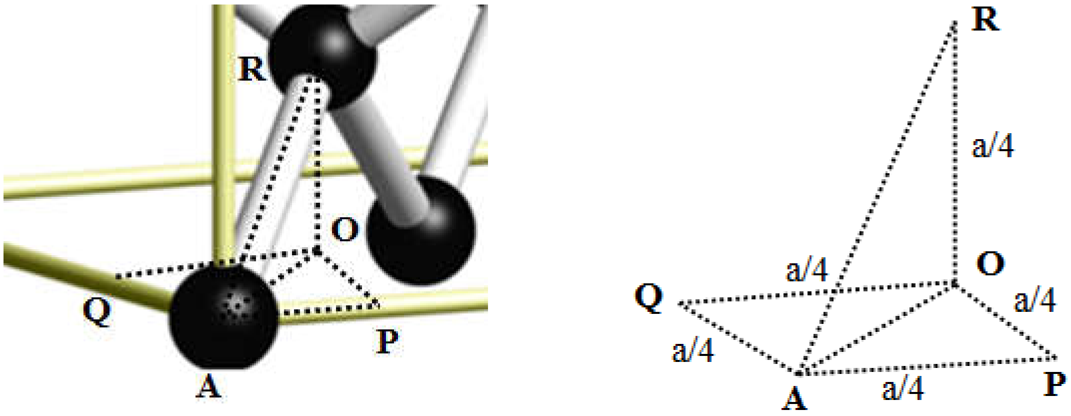

(a)

(b)

Fig. 2.3. (a) Carbon atom at corner A and its nearest neighbour atom at R in the same unit cell, (b) AR is nearest neighbour distance.

2.2.2. Nearest neighbour distance

The distance between two nearest carbon atoms in a diamond cubic crystal is called nearest neighbour distance of the crystal. The nearest neighbour distance is represented by AR (in Figure 2.3) which is the distance between two closest carbon atoms at A and R as in Figure 2.3 (b).

In ΔAOP

$$\mathrm{AO} \; = \sqrt{\mathrm{AP}^2 + \mathrm{AO}^2}$$

$$= \sqrt{\left(\frac{a}{4}\right)^2 + \left(\frac{a}{4}\right)^2}$$

$$AO = \frac{a}{2\sqrt{2}} \tag{2.2}$$

in ΔAOR

$$AR = \sqrt{AO^2 + OR^2}$$

$$= \sqrt{\left(\frac{a}{2\sqrt{2}}\right)^2 + \left(\frac{a}{4}\right)^2}$$

$$\text{Nearest neighbour distance} = AR = \frac{\sqrt{3}}{4}a \tag{2.3}$$

2.2.3. Atomic radius and dimensions of a unit cell

Let radius of each carbon atoms be r and the lattice constant be a. The atoms having centre at A and R in Figure 2.3 (a) actually touch each other. Therefore,

$$AR = r + r$$

$$\Rightarrow \frac{\sqrt{3}}{4}a = 2r$$

$$\text{Relation between atomic radius and unit cel parameter } r = \frac{\sqrt{3}}{8}a \tag{2.4}$$

Atomic packing fraction

$$APF = \frac{\text{Volume of atoms in one unit cell}}{\text{volume of unit cell}}$$

$$= \frac{8 \times \frac{4}{3}\pi r^3}{a^3}$$

$$= \frac{8 \times \frac{4}{3}\pi r^3}{\left(\frac{8r}{\sqrt{3}}\right)^3}$$

$$\text{Atomic packing fraction} \quad = 0.34 \tag{2.5}$$

This means only 34 % of the diamond unit cell volume can be occupied by hard carbon atom spheres.

2.3. Reciprocal lattice and Brillouin zone of diamond cubic crystal

Reciprocal lattice vector ($G = n_1b_1+n_2b_2+n_3b_3$) of diamond crystal can be constructed using $b_j.a_i = 2\pi\delta_{ij}$ where $a_1(011)$, $a_2(101)$ and $a_3(110)$ are basis vectors of direct lattice of diamond crystal. The first Brillouin zone can be made by drawing bisector planes to each possible nearest neighbour distances in the reciprocal lattice of diamond. First Brillouin zone of FCC lattice is shown in Figure 2.4 which is a truncated octahedron with eight regular hexagonal faces and six square faces [2].

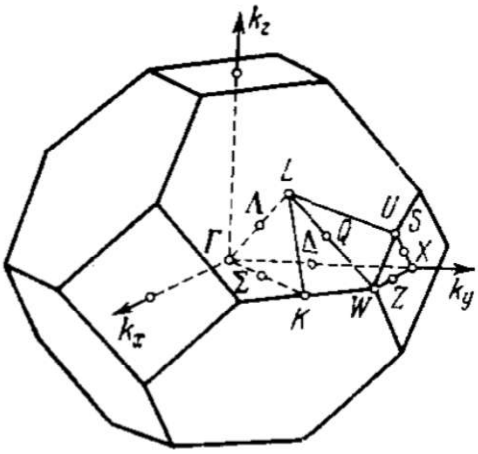

Fig. 2.4. Brillouin zone of diamond with symmetry directions.

The Brillouin zone of diamond crystal has been made by considering Γ as a centre of the Brillouin zone. X represents boundary of the first Brillouin zone and L represent boundary along the [1 1 1] axis. Δ, Σ, Λ, Z are lines of high symmetry. In the region of Brillouin zone, electrons have travelling wave like solution, on the other hand the zone boundaries meet the

Bragg condition so that electrons get diffracted. The Bragg diffraction at the boundary of first Brillouin zone leads to the origin of bandgap which will be discussed in next section.

2.4. Band structure of diamond

Diamond is an insulator but it can be considered as a semiconductor with a high bandgap. The first calculation of energy band structure of diamond was done by Herman *et. al.* [3] using orthogonalized plane wave method. The valence band was obtained to be doubly degenerate which touches each other at Γ_{25} where the valence band reaches its maxima as shown in Figure 2.5 (a). The conduction band was calculated to be quadruply degenerate. The simplified band gap model is shown in Figure 2.5 (b) which consists of valence band and conduction band separated by a band gap of 5.45 eV.

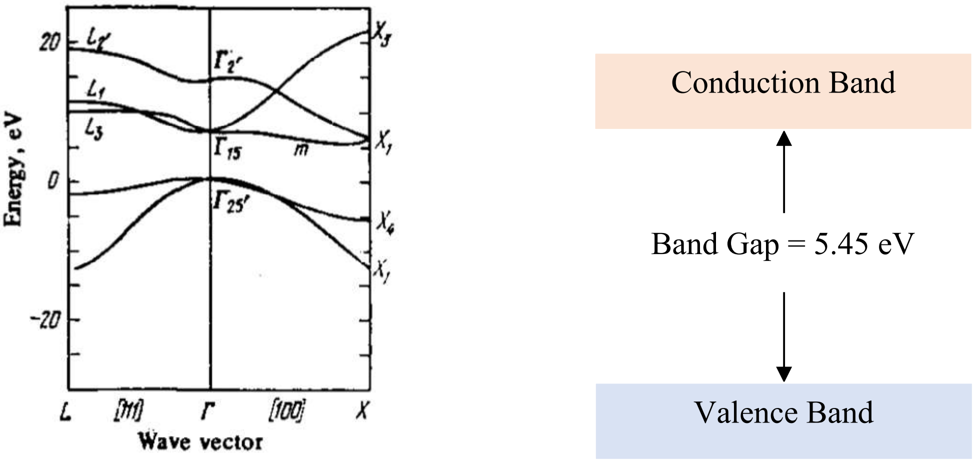

(a) (b)

Fig. 2.5. (a) Band gap model of diamond calculated by Herman [3], (b) Simplified band gap model of diamond.

The valence band represents the outer shell electrons of carbon atoms which are bound to lattice points in crystal. On the other hand, conduction band represents electrons which are free to move within the crystal lattice. The band gap represents the region which forbids the electrons.

2.5. Properties of diamond and its superiority over other semiconductors

Diamond possess outstanding properties such as large bandgap, high mobility, low dielectric constant, low atomic number, high thermal conductivity, etc. The properties of diamond are compared to other semiconductor materials in Table 2.1.

Table 2.1. The properties of diamond compared to other semiconductors [4-7].

Properties (at room temperature)	**Diamond**	**Silicon**	**Germanium**
Bandgap (eV)	5.45	1.12	0.67
Resistivity (Ω.m)	$>10^{12}$	$\sim 10^{5}$	50
Electron mobility (cm^2 V^{-1} s^{-1})	4800	1350	3900
Hole mobility (cm^2 V^{-1} s^{-1})	3500	480	1900
Break down voltage ($V.\mu m^{-1}$)	1-2	0.2	0.1
C displacement energy (eV)	43	15	20
Z	6	14	32
Energy to create e-h (eV)	13	3.6	3
Dielectric constant	5.7	11.9	16.3
Intrinsic carrier density (cm^{-3})	$<10^{3}$	10^{10}	10^{13}

2.5.1. Semiconducting properties of diamond

Diamond has high bandgap (5.45 eV) which is approximately five times more than bandgap of silicon and ten times more than that of germanium. Due to high band gap, the concentration of thermally generated electrons is very small in diamond. Other semiconductors such as silicon and germanium have high concentration of thermally generated electrons at room temperature which results in relatively more electronic noise when they are used for detector applications. The energy required to create electron hole pairs is approximately three times the bandgap of the semiconductor. The average energy required to create one electron-hole pair in diamond is 13 eV which is approximately three times more than that required in silicon. Therefore, the number of electron hole pairs generated in diamond is approximately one third of that in silicon. The intrinsic carrier density in diamond is less than 10^3 carriers per cm^3 which is seven orders of magnitude less than that in silicon and ten orders of magnitude less than that in germanium.

2.5.2. Electrical properties of diamond

The high band gap of diamond results in very low concentration of intrinsic charge carriers. As the resistivity of material is inversely proportional to the free charge carrier density, the resistivity of diamond ($>10^{12}$ Ω.m) is approximately seven orders of magnitude more than that of silicon (~ 10^5 Ω.m) and ten orders of magnitude more than that of germanium (~50 Ω.m).

Rigid covalent bonds between carbon atoms are very less affected by the externally applied electric field. Therefore, the shift of positive and negative charge centres is quite less compared to silicon and germanium which results in a very small dielectric polarization. The strong bonding in diamond results in relatively small dielectric constant (5.7) which is just half of the dielectric constant of silicon. Low dielectric constant of diamond leads to low capacitance of the material which has a very significant impact on the electronic performance when it is used for detector application.

2.5.3. Transport properties of diamond

The carrier transport in diamond is caused by either externally applied electric field or due to the variation in the carrier density which are called carrier drift and diffusion respectively.

The motion of charge carriers in the bulk of material causes current in the external circuit. When an electric field is applied, the electrons move in the direction opposite to the electric field and hole in the direction of electric field.

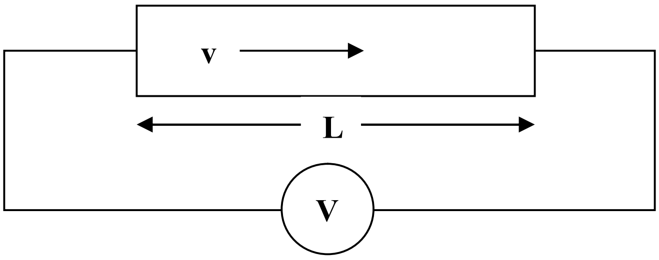

Fig. 2.6. Carrier drift in a conductor of length L due to applied electric field E.

If all carriers having charge Q drift with same speed through a conductor of length L and area A having resistivity of ρ, then current and current density is;

$$I = \frac{Q}{t} = \frac{Q}{\frac{L}{v}} \tag{2.6}$$

$$J = \frac{I}{A} = \frac{Q}{AL}v = \rho v \tag{2.7}$$

Current density given by equation 2.7 is constituted by both electrons and holes. If n_n and n_p are density of electrons and hole then net current is given by:

$$J = qn_pv_p + qn_nv_n \tag{2.8}$$

The force experienced by the charge carriers is composed of an accelerating component due to the electric field and a de-acceleration component which arises due to the collision of the carriers within the crystal. Therefore,

$$F = qE - m\frac{dv}{\tau_c} \tag{2.9}$$

Where τ_c is relaxation time which is the average time interval between two collision events. The charge carriers lose kinetic energy in each collision event and ultimately reach to thermal equilibrium with crystal lattice. In each collision of the charge carriers with the atoms, there is a transfer of kinetic energy so that the speed of carrier reduces. Due to these two components, the particles eventually reach to steady state motion where carriers move with the drift speed. The drift speed is proportional to the applied electric field. The mobility is defined as the gain in the speed by the charge carriers per unit electric field. Therefore, mobility is expressed as:

$$\mu = \frac{v_d}{E} = \frac{q\tau_c}{m} \qquad (2.10)$$

Diamond shows very high mobility of electrons and holes which are 4800 $cm^2\ V^{-1}\ s^{-1}$ and 3500 $cm^2\ V^{-1}\ s^{-1}$ respectively. Since the density of the phonons in the solid increases with the temperature, the scattering time reduces and hence the mobilities of electrons and holes decrease with the temperature. Near room temperature, the carrier mobility varies as $T^{-3/2}$, which indicates scattering by acoustic lattice vibration. At a higher temperature, the dependence is $T^{-2.8}$ due to interaction of the carriers with optical phonons.

2.5.4. Physical properties of diamond

Diamond is hardest known natural mineral found on the earth. It is approximately four times harder than the second hardest mineral which is Corundum. The density of diamond is 3.5 g/cm^3 but silicon has a density of only 2.3 g/cm^3. It has very high melting and boiling temperatures which are pressure dependent. Diamond looks to be very shiny due to its high refractive index (2.4) which is much higher than that of glass (1.5). Diamond has an atomic number of 6 due to pure carbon composition. Due to low atomic number, interaction cross-section of gamma rays in diamond is very less making it useful to monitor radiation in gamma background. The low atomic number of diamond also causes lower coulomb scattering of charged radiation which results in small angular spread of radiation.

2.5.5. Mechanical properties of diamond

Diamond shows excellent mechanical properties due to its extreme hardness. The strength of the material greatly varies with the area of the substrate and thickness. Sussman *et. al.* has reported that the strength of plate varies between 746 MPa for a 20 mm diameter x 296 µm thick plate to 1138 MPa for a 10 mm diameter x 187 µm thick plate [8]. As discussed in the section 2.1, the strength of material comes from strong covalent bonds between atoms and stable tetrahedral structure of the crystal. Approximately 50 eV energy is required to displace a carbon atom from the diamond lattice which is more than that required in silicon and germanium. Due to hardness of the material, diamond is quite favourable for making radiation hard detectors which can withstand high radiation field.

Diamond offers low coefficient of friction and high erosion resistance, therefore it is extensively used as an abrasive material for polishing, grinding, milling, etc. [9]. Some of the parameters of diamond calculated by Ruoff and Wangel [10] are tabulated in Table 2.2.

Table 2.2. Comparison of elastic constants of semiconductors.

Properties	**Diamond**	**Silicon**	**Germanium**
Young's Modulus (GPa)	1150	170	130
Bulk Modulus (GPa)	443	98	75
Shear Modulus (GPa)	550	70	54
Poisson ratio	0.07	0.25	0.21

2.5.6. Thermal properties of diamond

Diamond has excellent thermal conductivity despite of having very low electrical conductivity. There are two types of carriers who are responsible for thermal conduction in solids known as phonons and free electrons. Metals such as copper, silver, gold, etc., have high concentration of free electrons in the conduction band, therefore they easily conduct heat as well as electricity. On the other hand, diamond has very low concentration of free electrons and hence does not conduct electricity. However, due to phonons, it is a good thermal conductor. The phonons are quantized modes of vibration of crystal lattice. The vibrational energy is transferred from one part of the solid to the other part by phonons. Vibration in a crystal can be modelled as mass spring system as shown in Figure 2.7. The frequency of vibration is given by equation 2.11.

Fig. 2.7. Lattice vibration in solid modelled as spring mass system.

$$f_{vib} \propto \sqrt{\frac{k'}{m_{atom}}} \tag{2.11}$$

The frequency of vibrations is directly proportional to the effective spring constant (k') i. e. strength of C-C bond and inversely proportional to the mass.

Since C-C bond is very stiff in diamond and the mass of carbon atom is relatively small, the frequency of lattice vibration is very high in diamond lattice. Therefore, diamond is a very good thermal conductor. The thermal conductivity of diamond is generally > 1000 W m^{-1} K^{-1} and varies with the quality of diamond. The thermal conductivity of best quality of CVD diamond was reported to be as high as 2200 W m^{-1} K^{-1} [11] which is much higher than the thermal conductivity of copper and silver.

Diamond has a very high melting point and high heat capacity which makes it suitable for applications in electronics industry. The other thermal properties of diamond are listed in Table 2.3 [11].

Table 2.3. Thermal properties of diamond.

Properties	**Diamond**
Melting Point	4100 K
Debye temperature	2200 K
Heat Capacity	6.195 J/(mol.K)
Thermal expansion	0.8 X 10^{-6} /K

2.5.7. Optical properties of diamond

Due to high bandgap of diamond, it is transparent to photons having wavelength greater than 230 nm. Natural diamonds are found in colour mostly yellow and brown due to the presence of impurities. Nitrogen and boron are the major impurities found in diamond which cause absorption bands in the visible region of the spectrum. Sometimes, yellow colour is found in natural diamond which results due to the UV absorption because of nitrogen impurity. As the nitrogen content reaches 300-400 ppm, it shows green colour. On the other hand, metal impurities such as aluminium, iron, and magnesium cause brown coloration in diamond.

Diamond exhibits high refractive index with high dispersion in the visible range. The high refractive index of diamond is as a result of its high electrical polarizability. The refractive index of diamond is 2.4 at the wavelength of sodium D line. Diamond shows Raman active mode due to Rayleigh scattering of optical photons. A sharp peak at 1332 cm^{-1} occurs in the Raman spectrum which indicates sp^3 carbon atoms.

2.6. Growth of diamond substrate

Naturally occurring diamonds are formed over billions of years under intense pressure and heat. Diamond is believed to be crystallized in Kimberlite rocks which are formed deep inside magma. The rocks reach near the earth crust by an upward driven force exerted by excess CO_2 pressure. The natural diamond thus obtained is very costly limiting its widespread use in scientific research. The technology for synthetic diamonds was researched in the 1940's and the first synthetically created diamond was produced in the 1950's. There are two popular methods of the fabrication of diamond substrates; first is called high pressure and high temperature (HPHT) method which is older method and the other is called Chemical Vapor Deposition (CVD) method which is a more superior technique.

2.6.1. HPHT method to grow diamond

In this method, diamond is grown in the laboratory in the same way as natural diamond which is formed inside the earth surface. This method uses equipment, which creates pressure (using carbide anvil) and heat (using graphite heater), similar to that for natural diamonds which are found in the depth of the earth. The high temperature and pressure are very important factors required to crystallize diamond [12]. The HPHT method converts carbon to diamond at high temperatures and pressures using a molten metal catalyst in an environment where oxygen is not allowed. The HPHT diamond growth starts with a tiny diamond seed kept at the centre of a high pressure cell as shown in the Figure 2.8. Each seed is bathed in a solution of graphite and a metal based catalyst at very high temperatures and pressures in a diamond growth chamber. Under highly controlled conditions, the small diamond seed begins to grow molecule by molecule and then layer by layer which eventually leads to growth of diamond substrates.

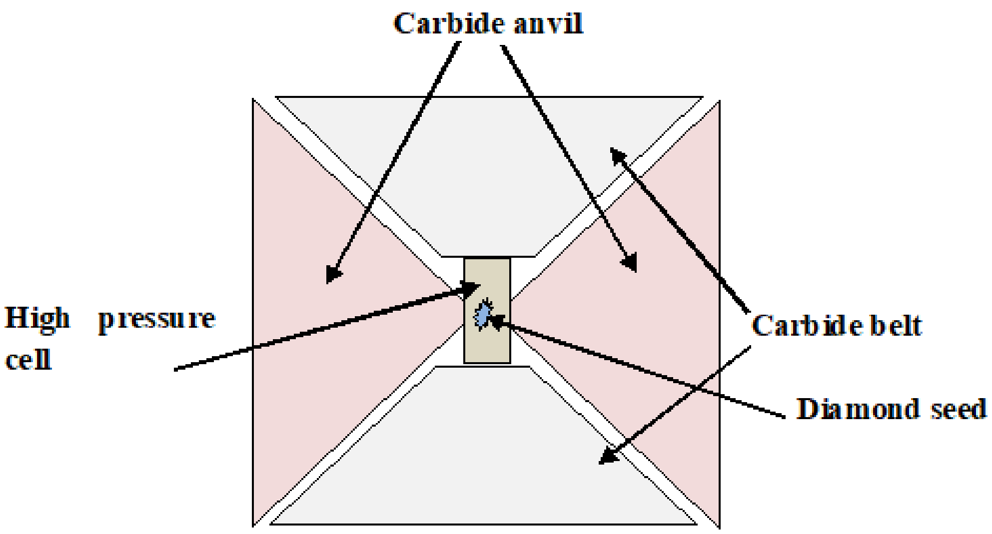

Fig. 2.8. Schematic showing HPHT method to grow diamond.

2.6.2. CVD method to grow diamond

Rather than trying to duplicate nature's method for creating diamond (as in the HPHT method), diamond could be produced if carbon atoms could be added one-at-a-time to an initial template, in such a way that carbon atoms are grouped in a tetrahedral network resulting in the growth of diamond substrate. CVD technique is conventional and the most widely used technique for the growth of diamond because this technique does not require the extensive apparatus to generate high pressure and high temperature. Therefore, CVD is also a more economical method for the production of diamond [13].

The general principle of CVD growth is to introduce a gas mixture containing carbon based radicals and hydrogen into a chamber at a high vacuum. The power is supplied to generate plasma that breaks down the gasses and deposits a crystalline carbon structure on a pre-existing substrate [14]. Therefore, the deposition of diamond film requires the activation of gas phase carbon containing precursors which can be achieved through the power supplied by micro waves, radio frequency, lasers, direct current, hot filament or chemical reactions [14, 15].The most commonly used means of activation are hot filament or plasma. In hot filament method, activation is done by the heating of a coiled filament maintained at a high temperature as shown in Figure 2.9 (a). In Plasma method, plasma is generated by either microwave or RF power. The principle of microwave plasma method is shown in Figure 2.9 (b) [16].

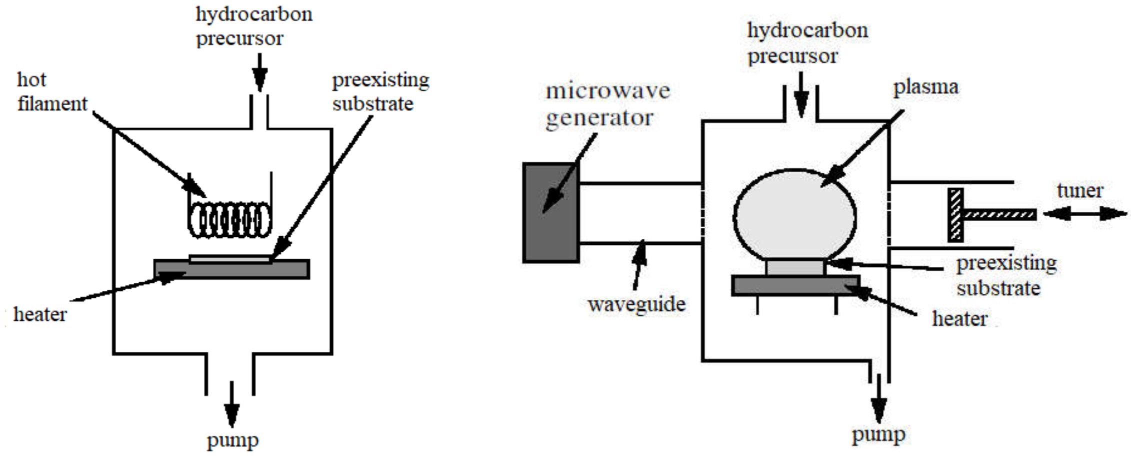

(a) (b)

Fig. 2.9. Schematic presentation ofCVD method to grow diamond substrates using (a) Hot filament method, and (b) Microwave plasma method [16].

The factors which determine type and quality of diamond substrates are following:

a. *Substrates*- Generally silicon or HPHT diamond are used as initial substrates for diamond deposition [14, 15]. These substrates are required to withstand a high temperature window of 1000-1400 ^{o}C for the growth of diamond. For getting free standing diamond, the initial substrates are chemically etched out. The nucleation and growth of a continuous diamond film requires a substrate with refractory characteristics and low thermal expansion coefficient.

b. *Gas mixture*- The gasses present during the deposition play a very prominent role in the quality of fabricated diamond substrates. In general, the gas mixture contains methane-hydrogen (~5% methane + 95% hydrogen). Methane supplies carbon atoms that crystallize on the substrate in tetrahedral form and hydrogen facilitates the plasma's presence. Sometimes dopants such as nitrogen and boron are added to the gas mixture to improve diamond growth but they have a negative effect on the electronic properties of the diamond film [14, 17]. The surface morphology of CVD grown diamond substrates is observed to be highly dependent on the C/H ratio in the gas mixture.

c. *Temperature and chamber pressure*- Pressure plays an important role in the stability of plasma during the growth of diamond [15]. Graphite is thermodynamically the more stable form of solid carbon at ambient temperature and pressure. Therefore, a suitable range of temperature and pressure is very important to get sp^3 bonded carbon for the growth of diamond. Temperature also plays important role in the surface morphology of diamond substrates. At low substrate temperatures, diamond substrates assume surface morphology having triangular [1 1 1] facets with twin grain boundaries.

The growth speed in CVD process is typically about 1 μm/h. After the growth process, the substrate is etched from the diamond, which is then cut and cleaned. Initially, there is a large number of small crystal seeds on the substrate, each oriented individually. As the deposition continues, the grains grow together, forming columnar single crystals with grain boundaries in between. On the substrate side, the lateral grain size is very small (in the order of micrometers), while the size continuously increases in the growth direction, reaching a diameter of the order of 100 μm with a diamond film thickness of 500 μm.

2.7. Types of diamond substrates

Depending upon the crystalline nature and occurrence of grains, diamond is classified into single crystal diamond (SCD) and polycrystalline diamond (pCVD).

Polycrystalline diamond is made of many differently orientated groups of atoms separated by grain boundaries. The size of individual grains increases from nucleation side to growth side and it can go up to ~10% of the film thickness. The grain boundaries contain impurities and affect the charge transport properties of the crystal [14, 17]. pCVD diamond substrates are generally fabricated on silicon substrates and defined by their numerous crystal orientation [18, 19].

In SCD, single orientation of atoms is present throughout the crystal lattice. SCD can be viewed as a single grain. Since SCDs have no grain boundaries, the charge trapping phenomena related to grain boundaries does not exist in the crystal. SCD is generally grown on high temperature high pressure (HPHT) substrate.

Depending upon impurity types, diamond is classified into Type I and Type II diamond. In the early 20th century, natural diamonds were divided into Type I, containing nitrogen impurities, and Type II, which were relatively free of nitrogen [20].

Those diamond substrates which contain nitrogen > 5ppm belong to this category. 98 % of the natural diamonds are of Type I where nitrogen content varies from 100-3000 ppm. They absorb UV and infrared light because of nitrogen impurities and have absorption edge of around 330 nm. Type I is further classified into two groups - Type Ia and Type Ib. Type Ia diamonds have nitrogen in aggregated from and Type Ib diamonds have single constitutional nitrogen which may be paramagnetic nitrogen atoms as part of the lattice. Most of the HPHT grown diamond falls in the category of Type 1b.

Those diamond substrates which have very low concentration of nitrogen (< 5 ppm) belong to the category of Type II. These diamonds usually transmit UV light due to very low content of nitrogen. Type II is further divided into two groups - Type IIa and Type IIb. Type II diamond has nitrogen as major impurity but they behave like intrinsic. Most of the CVD diamonds that are fabricated in laboratory are Type IIa. On the other hand, Type IIb diamond has boron as the major impurity and they behave like boron doped p-type semiconductor. Type IIa diamond is found very rare in the nature.

2.8. Advantages of diamond detectors over other semiconductor detectors

Conventional semiconductor detectors such as silicon and germanium have resistivity of the order of 10^{1}-$10^{5}\Omega$-m which results in a relatively high leakage current. The leakage currents and their fluctuations are an undesirable source of noise in radiation measurement applications which directly impacts the detector performance. These detectors employ p-n junction and are operated in the reverse bias mode to keep the leakage current low. Diamond has a very high resistivity of the order of 10^{11}-10^{18} Ω-m which results in a small leakage current [21]. Therefore, there is no need of junction to limit the leakage current which is required in silicon or germanium detectors.

Diamond has a very large bandgap which reduces thermal noise. In silicon and germanium, the bandgap is small, so concentration of the thermally generated charge carriers is high which results in relatively high electronic noise. These detectors especially germanium are needed to be cooled during the radiation measurement to reduce the thermally generated carriers. However, diamond can be easily operated at room temperature. The large band gap of diamond also reduces its sensitivity to visible photons and therefore the detector is not needed to be covered from visible light during the measurements. Diamond detector is called visible blind detector due to its insensitivity to visible light. A large bandgap of diamond results in a relatively smaller number of electron-hole pair generation [22]. The electrical signal obtained by the detector is comparatively low which results in low signal to noise ratio. Therefore, special type of backend electronics is required to improve the signal to noise ratio.

As discussed in previous chapter, the electron hole mobility in diamond is much higher than that in other semiconductor detectors. The high mobility of charge carriers opens the way to use detector in fast timing applications. The charge carriers in diamond have saturation drift velocity of the order of 10^5 $m.s^{-1}$, therefore they need only 1 ns (from equation 2.5) to cross a detector having thickness of 300 μm which results in signal pulse of nano second duration. Therefore, the detector has a potential to work for fast timing applications when integrated with high frequency electronics setup. Another interesting property of diamond is its atomic number (Z). Atomic number of diamond is close to the equivalent atomic number of tissues. Therefore, diamond detector can directly give the dose absorbed by the tissues without any specific calibration resulting in suitability for the use in personal dosimetry [23]. Another advantage of having its low atomic number is that it has very small interaction cross section with gamma rays. Therefore, the detector is able to measure radiations in high gamma background.

Diamond is a radiation hard detector which can be used in environment of high radiation flux. Generally, at the vertex position of several experiments such as CERN's LHC and ATLAS, radiation flux is extremely high which induces defects in the detector [24]. The concentration of these defects accumulates over a period of time and significantly affects the performance of detector. Therefore, detectors at these vertex locations are needed to be replaced frequently. Replacing the detectors at these locations is not a simple task as it is surrounded by very heavy trackers and electronic equipment. Diamond is expected to perform quite well due to its high radiation strength.

2.9. Fabrication methodology of diamond detector

Generally, diamond detectors are made in metal-insulator-metal (MIM) configuration where diamond as an insulator is sandwiched between two metal electrodes. The metal electrodes serve the purpose of applying electric field in diamond as well as to collect charge carriers. The performance of the detector is highly dependent on the metal-diamond interface. Therefore, the selection of contact metal is very important for diamond detector fabrication. The selection of a metal is done based on following considerations:

a. *Diamond-metal contact behavior* – The interface between diamond and metal directly influence the charge collection at metal electrode from diamond. For good charge collection, the diamond and metal interface is required to be ohmic. Therefore, metal should be carefully chosen to match the work function of diamond.
b. *Adhesion of metal to diamond surface* – Another important aspect of choosing the material for metallization is strong adhesion between metal and diamond. All carbon atoms in diamond are involved in covalent bonding with other carbon atoms and no vacant bonds are available to bond with foreign atoms as discussed in chapter 1. Therefore, diamond does not react with most of the metals. However, there are certain groups of metals which make carbide phase with diamond and result in strong diamond metal contact.
c. *Area of application* – Another important aspect to choose a metal is the field in which the detector is to be employed. For example, if detector is be used in high temperature field, the metal should withstand the required temperature.

2.10. Principle of radiation detection in diamond

The principle of diamond detector is based upon the generation and collection of electron hole pairs due to the interaction of radiation in diamond. There are various mechanisms (which will be discussed in Section 3.3) by which different types of radiations can interact with the diamond. Due to the interaction of incoming radiation with the detector, radiation particles lose their kinetic energy fully or partially.

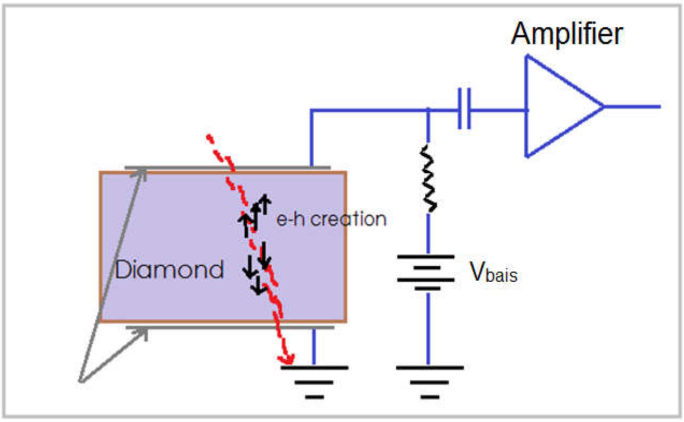

Fig. 2.10. Schematic showing principle of detection of radiation in diamond and signal processing.

If the energy is higher than the bandgap of diamond, it causes an electron to jump from conduction band to valence band and leaves a hole in the valence band. An average energy required to generate electron hole pairs is approximately three times of the bandgap of semiconductor. In diamond, 13.2 eV energy is required to generate one electron hole pair on an average. When the electric field is applied by means of biasing the detector, holes start migrating in the direction of electric field and electrons in the reverse direction. The motion of these electron hole pairs induces a current in the external electronic circuit which serves the purpose of generation of basic electrical signal. The induced current continues to flow unless the carriers are either trapped by any crystal defect or reach to the metal electrodes at the end of the detector volume.

Let us consider two electrodes separated by a distance of l and at a potential difference of V, so electric field between them is E=V/l. If charges +q and –q are generated and move apart a distance χ in this electric field E, then the work done by the power source maintaining the field is W = qχE = qχv/l. Because of this, a transient current is generated in the circuit and the time integral of this current gives the total charge Q which is given by:

$$\text{since } V = \frac{W}{Q} \tag{2.12}$$

$$\text{so,} \quad Q = \frac{W}{V} = \frac{q\chi}{l} \tag{2.13}$$

Q is the induced charge at the electrode due to one type of net charge q produced in diamond which traverses a distance of χ towards the electrode. So, if entire charge q reaches to the electrode i.e. χ =l, then the induced charge at the electrode would be equal to the total generated charge q. In practical cases, the entire charges generated do not reach to the boundary and some of them are usually trapped. In this case, induced charge at the metal electrode will be less than the charge generated. The induced charge Q can be obtained by integrating the current pulse that flows in the external circuit.

$$Q = \int_0^{t'} i(t)dt \tag{2.14}$$

Where, it is assumed that all charges are produced instantaneously at t = 0 and migration of charge carrier at t = t' either due to trapping or collection at electrode.

There are two modes of operations in which the detector can be operated depending upon the application.

a. *Pulse mode operation* - In pulse mode operation, detectors are operated to measure properties of individual quantum of radiation. In such measurement total charge produced in the detector is estimated which is directly related to the energy of individual quantum of radiation. The pulse mode operation of the detector is useful for energy spectroscopy and particle counting applications. This mode works well when the radiation rate is low.

b. *Current mode operation* - When radiation event rate is high, pulse mode operation become difficult because the individual pulses start overlapping with each other. Then, it becomes necessary to operate detectors to produce current proportional to the intensity of incident radiation. The detectors are operated in current mode for dosimetry applications, transient current response study, etc.

2.11. Diamond detector for measurement of various types of radiation

The principle of the detection of radiations is based on the interaction of radiations with the detector material. The mode of interactions greatly varies with the types of incident radiations.

2.11.1. Measurement of charged particles

Charged particles such as alpha, electrons, protons or heavy ions can directly ionize diamond through coulomb interaction. The detector medium acts as a cloud of electrons which gives rise to an electromagnetic field which exerts force on the incoming charged radiation. Ionization and excitation are the two major processes by which alpha particles, other charged particles or electrons lose energy in diamond. The alpha particles emitted from the radioactive sources such as Pu, Am, etc., have energy in the range of 5-5.5 MeV. The alpha particles from radioactive source lose almost its entire energy within a thickness of 16 µm in diamond [25].

Electrons also lose energy by the same process as alpha particles in diamond. However, as the mass of incoming electron is same as the mass of electrons inside the medium, a large portion of the energy will be transferred in each interaction compared to that of alpha.

2.11.2. Measurement of photons

Photons mainly undergo three types of interactions – photo electric effect, Compton scattering and pair production. These interactions lead to partial or complete transfer of photon energy to electrons in the detector medium. Therefore, photons either disappear or scatter through a significant angle. The cross-section of these interactions varies with photon energy and atomic number of the constituent atoms of detector medium as follows:

$$\sigma_{\mathrm{pe}} \propto \frac{\mathrm{Z}^{4-5}}{\mathrm{E}^{3.5}} \tag{2.15}$$

$$\sigma_{\mathrm{CS}} \propto \frac{\mathrm{Z}}{\mathrm{E}} \tag{2.16}$$

$$\sigma_{\mathrm{PP}} \propto \mathrm{Z}^{1-2} \tag{2.17}$$

Where σ_{pe}, σ_{cs} and σ_{pp} are cross-sections for photoelectric, Compton scattering and pair production respectively and Z is the atomic number of the detecting medium. As carbon has very low atomic number, the cross-section for these interactions is significant for low energy X-rays only and the sensitivity of diamond detector to gamma rays is very low. In fact, this is one of the advantages as the detector can be used to monitor several radiations in high gamma background.

2.11.3. Diamond for fast neutron measurement

Neutrons cannot directly ionize the diamond as they are neutral. Therefore, the detection of neutrons by diamond relies upon the following mechanisms:

a. *Elastic or inelastic scattering* – The scattering of the neutrons occur due to the collision with carbon nuclei in the diamond. In this scattering, a fraction of neutron kinetic energy is transferred to the carbon nucleus. In elastic scattering, energy lost by the neutron is entirely transferred as kinetic energy of nucleus but in inelastic scattering some part of the kinetic energy is lost in the excitation of nucleus. In both cases, the recoiled nucleus ionizes the material and gives signature of the energy of neutrons. The energy lost in scattering is a continuum ranging from 0 to a maximum value. Therefore, it is difficult to correctly deduce the neutron energy information and this requires a complicated mathematical modeling.

b. *Capture reaction* - The neutron may be captured by the nucleus which leaves nucleus in excited states. The nucleus then comes to the ground state by emitting one or more gamma rays. These gamma rays interact with diamond by one of the methods discussed in previous section.

c. *Nuclear reaction* - Another interesting mechanism by which neutrons can interact with the carbon is nuclear reaction where two or more charged particles can be produced. There are several possible ways by which nuclear reactions between neutron and carbon can take place as listed in Table 2.4 [26]. These reactions are $^{12}C(n, \gamma)^{13}C$, $^{12}C(n, n)^{12}C$, $^{12}C(n, \alpha)^{9}Be$, $^{12}C(n, n`)3^{4}He$, $^{12}C(n, n`, 2\alpha)$ ^{8}Be, etc. For 14.2 MeV fast neutrons, $^{12}C(n,\alpha)^{9}Be$ has maximum cross-section for which reaction Q-value is 5.7 MeV. So the remaining 8.5 MeV energy is distributed between ^{9}Be and alpha particles which is deposited in the detector.

Table 2.4. Possible channels of nuclear reactions between neutron and carbon with corresponding Q-values and threshold energies [26].

Reactions	Q-value (MeV)	Threshold Energy (MeV)
$^{12}C(n,\alpha)^{9}Be$	-5.701	6.180

$^{12}C(n,n'2\alpha)^4He$	-7.274	7.866
$^{12}C(n,n'\alpha)^8Be$	-7.366	7.985
$^{12}C(n,2\alpha)^5He$	-8.164	8.851
$^{12}C(n,p)^{12}B$	-12.586	13.644
$^{12}C(n,d)^{11}B$	-13.732	14.886
$^{12}C(n,2n)^{11}C$	-18.721	20.295
$^{12}C(n,T)^{10}B$	-18.929	20.520

2.11.4. Diamond detectors for slow and thermal neutron measurements

Neutrons with energy less than 1 eV are termed as slow neutrons and those slow neutrons which are in temperature equilibrium with its surrounding (energy ~ 0.025 eV) are called thermal neutron. Although, several possible nuclear reactions between neutron and carbon have been explained in the previous section, all these nuclear reaction have a certain threshold value. Slow and thermal neutrons do not have sufficient energy to induce such nuclear reactions. The measurement of slow and thermal neutrons relies on othertypes of nuclear reactions called exothermic reactions. For slow neutron detection, converting medium containing ^{10}B or ^{6}Li may be used which does not have threshold energy.

a. Based on ^{6}Li (n, α) reaction

   In this reaction, alpha particles and tritium are produced as products with reaction Q value of 4.87 MeV. These charged particles may then ionize diamond to produce electron hole pairs. The cross-section of this reaction is fairly high (940 b) for thermal neutrons and it drops to few hundred barns in slow neutron region.

$$ {}^{1}_{0}\mathrm{n} + {}^{6}_{3}\mathrm{Li} \rightarrow {}^{4}_{2}\mathrm{He} + {}^{3}_{1}\mathrm{H} \quad : \mathrm{Q} = +4.78\ \mathrm{MeV} \tag{2.18} $$

b. Based on ^{3}He(n, p) reaction

In this reaction, protons and tritium are produced with relatively very low Q value. However, the cross-section of the reaction is quite high (5330 b for thermal neutrons, and 500 b-1000 b for slow neutrons). Helium is generally incorporated in proportional gas counters which are not suitable for the integration with diamond.

$$ {}_{0}^{1}\mathrm{n} + {}_{3}^{6}\mathrm{He} \rightarrow {}_{1}^{1}\mathrm{p} + {}_{1}^{2}\mathrm{H} \quad : \mathrm{Q} = +0.764\ \mathrm{MeV} \tag{2.19} $$

c. Based on B (n, α) reaction

Boron is most commonly used material with diamond detector for the measurement of slow and thermal neutrons which is generally available as ^{10}B films. There are two channels of nuclear reaction between neutron and Boron as shown below. In both cases lithium and helium are produced but in one case lithium is in ground state and in the other case, it is in excited state. Most of the time lithium nuclei are left in the excited state.

$$ {}_{0}^{1}\mathrm{n} + {}_{5}^{10}\mathrm{B} \rightarrow {}_{3}^{7}\mathrm{Li} + {}_{2}^{4}\mathrm{He} \quad : \mathrm{Q} = +2.792\ \mathrm{MeV} \tag{2.20} $$

$$ {}_{0}^{1}\mathrm{n} + {}_{5}^{10}\mathrm{B} \rightarrow {}_{3}^{7}\mathrm{Li}^{*} + {}_{2}^{4}\mathrm{He} \quad : \mathrm{Q}\ + 2.310\ \mathrm{MeV} \tag{2.21} $$

2.12. Progress in the development of diamond detectors

The diamond detector was first time reported by B. Gudden *et al.* in 1923 as a photoconductor to study absorption characteristic of diamond [27]. These detectors were extensively used as photoconductive UV detectors. In 1934, existence of two types of diamond was found by Robertson [28] using photoconductivity analysis of diamond, and they are known as Type I which absorbs UV light because of Nitrogen impurity and Type II which is Nitrogen free and transmits UV light. Further work was done to observe charge carriers generated in diamond using electromagnetic radiation of short wavelength and its current mode operation in counting applications [29]. The response of diamond detectors to charged particles was observed by McKay and he showed that trapping of charge carriers in the crystal leads to space charge creation in active volume which leads to reduction in the current generated in the detector [30]. The thermal release of electrons and holes from the traps using electron bombardment technique was also observed in this work. In 1954, Benny and Champion studied the effect of radiation damage caused by neutron exposure and they postulated that some additional traps are produced because of irradiation which have a behaviour different from the internal traps [31]. Furthermore, the response of diamond detector as a counter of charged particles was examined and pulse height spectrum (PHS) was obtained for α and β particles [32]. The applications of diamond detector further progressed in to the field of X-ray dosimetry due to its low atomic number and this remains an active area of research since the last few decades of twentieth century [33].

Soon, many problems with diamond were realized like high cost, high impurity concentration, inadequacy of quality control of the sample and lack of reproducibility. However, diamond grown by CVD technique showed its potential to solve all these issues. In 1992, L. S. Pan reported his work on CVD diamond detector and he showed that the carrier drift length is limited by defects within the grains [34]. He obtained a PHS of diamond using alpha particles. A decrease in the charge collection efficiency was observed due to the bulk polarization in diamond and a polarization quenching by an 18 min continuous exposure of diamond with visible light was also observed [5, 35]. For the better performance of detector, it was necessary to address the issue of polarization in CVD diamond due to trapping. In 2002, C. Manfredotti *et al.* showed the priming effect due to pre-irradiation by two different radiations; X-rays and β-particles, and bleaching effect due to blue light [36]. It was also shown that priming has strong effect on holes while bleaching with light has a strong effect on electrons. In order to improve the charge collection distance, it was necessary to understand charge collection properties of diamond together with the distribution of traps. Bruzzi *et al.* experimentally estimated the concentration of traps in diamond along with their activation energies and capture cross-section by using photo induced current transient spectroscopy (PICTS) and thermally stimulated current (TSC) [37].

Diamond can also be used to monitor fast and thermal neutrons. Fast neutron can directly interact with the carbon and can be detected without any converter. M. Angelon *et al.* employed $^{12}C(n,\alpha)^{9}Be$ reaction [38] to monitor the fast neutrons. The thermal neutrons cannot be directly detected by diamond and a converter layer of lithium and ^{10}B is required with diamond substrate for their detection. In 2003, polycrystalline CVD diamond was successfully tested in Joint European Torous (JET) to monitor fast neutrons emitted from DT plasma [39]. This work was further extended for simultaneous detection of both fast and thermal neutrons by covering a SCD detector with ^{6}LiF film [40]. Further, a different method was proposed by C. Cazzaniga to simultaneously measure DD and DT fusion neutrons at JET by employing elastic scattering of carbon nuclei and $^{12}C(n, \alpha)^{9}Be$ reaction respectively [41]. M. Kim *et al.* studied the effect of oxygen plasma treatment on the shallow nitrogen vacancy centres. They found that short duration oxygen plasma treatment results in disappearance of nitrogen vacancy centres near the surface of diamond [42].

Several reports are available on transient current technique to estimate the charge carrier mobility and drift velocity in different materials. V. Eremin *et al.*, used this technique for the measurement of effective net concentration of ionized charges near p-n junction [43]. TCT measurement to study charge carrier properties in a SCD was reported by Pernegger *et al.*, where charge particles were introduced by α-particles [44]. On the other hand, some authors reported the introduction of charge carriers using laser source such as Nd-YAG [45].

2.13. pCVD based radiation detectors

One of the challenging issues with pCVD detectors is its low charge collection efficiency mainly because of short charge collection distance. pCVD substrates have a high concentration of defects which causes trapping and recombination of charge carriers and there is high probability of occurrence of such trapping and recombination sites at the grain boundaries. The trapping of charge carriers results in a space charge in diamond and causes bulk polarization in the material. The distribution of such space charge creates an internal field which causes distortion in the applied external field and this eventually degrades the charge collection efficiency [35, 46]. In order to improve the charge collection in diamond, either SCD should be used in which there are no grain boundaries which have most of the trapping sites, or existing traps should be filled. SCD exhibits almost 100% charge collection and can be used for the energy measurement of neutrons and charged particles with energy resolution of 0.4-1 % [47]. On the other hand, traps or recombination sites can be filled after irradiation of diamond called pumping or priming and the diamond film can be brought in fully pumped state for a total dose of about 2-3 krad [48]. The pumped state of the diamond is not stable and de-trapping may occur at relative high temperatures [49] and even with visible light illumination [50].

2.14. Application of diamond detectors

2.14.1. Beam conditioning and monitoring at LHC

Beam conditioning and loss monitoring in Large Hadron Collider (LHC) is very important to sustain several experiments at the site [51]. Neutron fluence or beam luminosity is generally very high at vertex locations which induce severe damages in the detectors. Due to the damage, the leakage current increases and the breakdown down voltage reduces. As diamond is a radiation hard detector, it can withstand high radiation environment and is considered to replace silicon detectors.

2.14.2. Fast neutron detectors for ITER experiment

ITER experiment aims to demonstrate power generation through fusion. Deuterium and tritium will be fused in test blanket module (TBM) at very high temperatures.

$$\mathrm{D} + \mathrm{T} \rightarrow \mathrm{n} + {}^{4}_{2}\mathrm{He} \tag{2.22}$$

The Q value of the reaction is 17.5 MeV which is distributed between alpha particles and neutrons. The neutrons and alpha have energies of 14.1 MeV of and 3.4 MeV respectively. Measurement of energy of these products would provide various useful information about plasma parameters. There is a requirement of detector which can monitor neutrons in and around test blanket module. The temperature in and around TBM is expected to vary from 300°C to 500°C. The flux of neutrons would be as high as 10^{10}-10^{13} $\mathrm{cm^{-2}.s^{-1}}$. The neutron flux and temperatures outside the TBM at various locations such as shield block, pipe forest, etc., are expected to be 10^{4}-10^{10} $\mathrm{cm^{-2}.s^{-1}}$ and ~50 °C–100 °C, respectively. Conventional neutron detectors cannot work at this temperature range and will be quickly degraded due to radiation damage in high radiation environment. Apart from these, space inside the TBM will be very limited and the detector response should be very fast. Considering all these requirements, diamond is considered to be most promising detector for fast neutron monitoring application in ITER experiment.

2.14.3. Diamond for medical dosimetry

Diamond is very attractive for dosimetry applications due to its near tissue equivalence i.e. atomic number of diamond ($Z = 6$) is very close to effective atomic number of human tissue ($Z_{eff} = 6$) [52-53]. This enables direct calculation of dose without a need of energy correction [54]. Another favourable advantage in diamond is its physical size. As diamond detector can be fabricated in small size with sizes of a few mm^3, it offers high spatial resolution. Silicon diodes have high spatial resolution comparable to diamond detectors but they offer non tissue equivalence ($Z_{Si} = 14$), requiring calibration for actual dose calculation.

2.15. Summary

Diamond is one of the allotropes of carbon where all atoms are arranged in a tetrahedral structure. The unit cell of diamond is known as diamond cubic crystal which is visualized as two interpenetrating FCC lattice. The calculations by Herman show that diamond is an indirect bandgap semiconductor with a bandgap of 5.45 eV. Diamond has outstanding electrical and semiconducting properties such as high bandgap (5.45 eV), high electron hole mobility (4800 and 3500 $cm^2V^{-1}s^{-1}$), high resistivity ($>10^{12}\Omega.m$), etc. Several other mechanical and thermal properties are also discussed in this chapter. There are two popular methods to grow diamond substrates named as HTHP method and CVD technique. HPHT is an old technique which utilizes high temperature and high pressure to replicate the actual conditions which are responsible for the formation of natural diamond. CVD technique is more elegant method to grow diamond using hydrocarbon precursors. The method is a highly controlled method for growing crystals with desirable size and thickness with very high grade purity. Diamond generally exists in two forms either single crystal having singer grain and polycrystalline having more than one grain. Diamond detectors have several advantages such as low leakage current which leads to low electronic noise in the detector, room temperature operation which removes the constraints to cool the detector at low temperatures, fast timing response, radiation hard, etc. Diamond detectors are generally fabricated in MIM configuration where diamond is sandwiched between two metal electrodes. The diamond metal contact has very high impact on the performance of the detector. Adhesion of the metal to diamond should be sufficient to withstand harsh conditions such as acid solutions, high temperature operation, etc., depending upon the applications.

The principle of diamond detector is based on interaction of radiation in diamond through several mechanisms which create electron hole pairs. The motion of these charge carriers under the influence of external electric field in the detector induces a signal pulse to the external circuit which contains many relevant information about the incident radiation. There are several mechanisms by which incident radiation may interact in diamond. There are several channel of nuclear reaction between fast neutrons and carbon such as $^{12}C(n, \gamma)^{13}C$, $^{12}C(n, n)^{12}C$, $^{12}C(n, \alpha)^{9}Be$, $^{12}C(n, n')3^{4}He$, $^{12}C(n, n'2\alpha)^{8}Be$. A minimum threshold energy required to occur the reaction is 6 MeV. Neutrons having energy less than 6 MeV cannot induce these nuclear reactions due to threshold energy of nuclear reactions greater than the energy of neutrons. Some types of convert layer are employed to convert neutron into charge particles which then enter into diamond and ionize the detector. Diamond based detectors have several applications involving high energy and nuclear physics experiments and dosimetry. In the present work, diamond based detectors were developed for charged particles and fast neutron measurements. The details of this work is presented in the next chapter.

CHAPTER 3: EXPERIMENTAL TECHNIQUES

Experimental setups play a prominent role in radiation measurement experiments using radiation detectors. The method of an experiment and strategy behind it greatly influence the results obtained in the experiment. In radiation measurement using diamond detectors, physical quantities to be measured are very small, e.g. leakage current are quite small and are in the range of pA-nA, detector signal is with charged particles is also very small. The detector and associated devices are very sensitive to noise pickup. Therefore, special precautions are required while experimenting with diamond detectors.

This chapter introduces experimental setup used to characterize the detector and to measure radiations during the doctoral work. The chapter is broadly divided into three sections to discuss about the; i) methods of fabrication of detectors, ii) principle and technique of characterization of diamond substrates as well as diamond detectors and iii) experimental methods to measure radiations using fabricated detector.

3.1. Fabrication of diamond detectors

The detectors were fabricated using commercially available single crystalline and pCVD substrates fabricated by CVD techniques. The substrates were of electronic grade with nitrogen content < 1 ppb. The both surfaces of diamond substrates were polished with surface roughness of less than 10 nm for Polycrystalline and less than 5 nm for SCD substrates. The diamond substrates of different area and thickness were used for the fabrication to study the sensitivity and charge trapping phenomena especially in pCVD. The following substrates were used for the fabrication of diamond detectors:

a. pCVD substrate of 100 mm^2 area and 100 μm thickness

b. pCVD substrate of 5 mm x 5 mm area and 300 µm thickness

c. SCD substrate of 5 mm x 5 mm area and 400 µm thickness

3.1.1. Cleaning of diamond substrate

The purity of the surface of diamond substrate is a very important factor because organic and inorganic impurities severely affect the detector performance. Diamond detectors have very low intrinsic leakage current but a small content of foreign atoms or molecules on the surface of diamond are known to cause surface leakage currents which may be several orders of magnitude more than the intrinsic leakage currents. Therefore, it is always advisable to properly clean diamond surface before detector fabrication as it dictates the device performance.

In the present work, a well established chemical method has been implemented to eliminate possible impurities on CVD grown diamond substrates [55, 56]. The method comprises of degreasing, piranha cleaning and acid treatment as discussed below.

Step 1: Degreasing - Degreasing of the diamond substrate was done to remove grease, lubricants, etc. on the surface. The diamond substrates were first cleaned in trichloroethylene (TCE) at 100^{o}C temperature and then dipped sequentially in acetone and methanol.

Step 2: Piranha cleaning - The organic solutions used in step 1 may leave traces of organic residues. Piranha cleaning was required to remove these organic residues on the substrates. The solution is prepared by adding hydrogen peroxide to sulphuric acid in 1:3. Piranha solution is highly exothermic and is known for attacking against the organic residues.

Step 3: Acid treatment - Acid treatment of the surface is done to remove any metal impurities on the surface. Acid cleaning also helps in reducing weakly bonded hydrogen from diamond surface. The diamond substrates were cleaned in chromic acid solution at 300°C for 30 minutes.

3.1.2. Pre-metallization annealing

Annealing of the substrate allows atoms to slowly diffuse throughout the crystal lattice. Atoms redistribute themselves to eradicate dislocations and defects and try to attain an equilibrium state. The undesired graphite layers are etched out by annealing in oxygen atmosphere where graphite burns and forms CO or CO_2 [57-58]. Annealing before metallization also softens the surface of diamond which allows metals to easily diffuse into surface during metallization.

Annealing of the substrates was done in a high temperature furnace in which desired temperature could be set. A proper care was taken to flow inert gasses such as nitrogen or argon during the annealing because a small content of oxygen in the furnace could lead to oxidation of the diamond surface at high temperatures. For annealing, the diamond substrates were placed in a quartz boat and loaded into the heating furnace as shown in Figure 3.1.

3.1.3. Oxygen plasma treatment of substrate

Generally, diamond substrates are fabricated using CVD technique where a high concentration of hydrocarbon precursor is used which leaves the surface hydrogen terminated. For hydrogen terminated surface, the vacuum level lies below the bottom of conduction band and it exhibits negative electron affinity. Therefore, the surface has tendency to donate electrons and it behaves like a quasi two dimensional hole surface which increases

Fig. 3.1. Heating furnace showing sample loading, sample is placed in quartz boat [59].

surface leakage currents. Oxygen plasma treatment was carried out in a radio frequency plasma etching system to reduce surface leakage. Oxygen plasma was maintained at a pressure of 25 mT by 25 SCCM flow rate of oxygen. The both sides of the diamond substrates were exposed to 50 W plasma for 15 minutes. The parameters used for oxygen plasma treatment are shown in Table 3.1.

Table 3.1. Parameters set for oxygen plasma treatment [59].

Parameter	**Value**
Flow rate	25 SCCM
Pressure	25 mT
RF Power	50 W
Time	15+15 min (Both surface)

3.1.4. Metallization on diamond substrate

The metallization on both the sides of diamond substrate was done for making electrical contacts. Electron beam physical vapour deposition technique was used for the metallization on diamond substrates at a vacuum of 10^{-6}-10^{-7} torr. During metallization, a set of metal masks was taken to avoid metallization at the edges of diamond substrate and to maintain a gap of 1 mm between edge and metallization. The substrates fitted in mask plates were mounted above the metal source as shown in Figure 3.2.

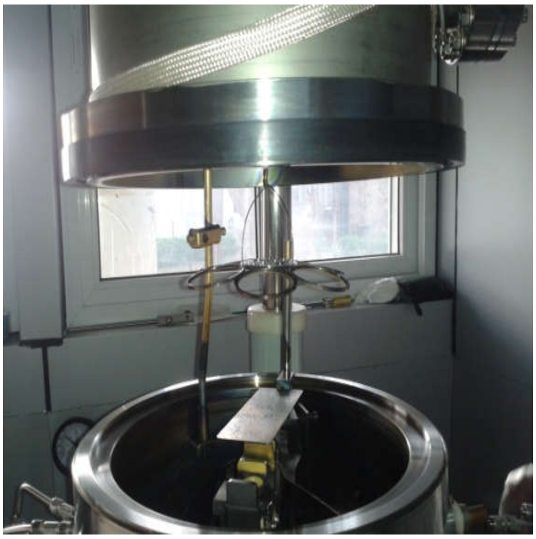

Fig. 3.2. e-beam evaporation chamber for the metallization on diamond substrates [59].

It has been discussed in previous chapter that metal should be properly chosen to obtain an ohmic contact and for strong adhesion. Aluminium is known to form low resistance and non-rectifying contact with semiconductors (especially in silicon devices). It makes good adhesion due to the physical bond with the surface. The disadvantage of Al is its low melting temperature (~ 650^{o}C) which limits its application at high temperatures. Another option for making ohmic contact is gold (Au) as its work function is close to diamond. Au was deposited on a few pCVD surfaces but adhesion of the Au with diamond was very poor. Au was observed to peel off even after touching the metal with a needle. For better adhesion of metal with diamond, it is important to choose metal which can make alloy at the interface. Ti and Cr are the metals which can form alloy at the interface and adhesion would be quite good. Hence, several batches of single and pCVD based detectors were fabricated with following combination of metals and the behaviour of detectors was studied.

a. Al

b. Ti/Au

c. Ti/Pt/Au

d. Cr/Au

Ti and Cr were deposited on diamond substrates which form carbide with diamond and then Au was deposited to prevent oxidation of the surface. The thickness of the metal on the substrate was controlled by time of exposure. The thickness of Ti, Pt and Cr was around 20 nm and gold was deposited up to a thickness of 200 nm.

3.1.5. Post metallization annealing

Thermal annealing of a few samples was done after metallization. The post metallization annealing was done from 200°C - 450°C in nitrogen environment. The annealing of the metalized substrates improves the carbide formation and also causes diffusion of metal into the diamond. Initially the changes in the metallization on the substrates at different annealing temperature were studied using a microscope for visual changes and the annealing temperature for different metal combinations was optimized.

3.1.6. Bonding and packaging

The metallized detector chip was mounted on a transistor outline (TO) header using a conducting epoxy and sintering was done at 150°C for 15 minutes. As the epoxy was conducting, the metal at the bottom side of the diamond chip was in electrical contact with the header. Therefore, the signal from the bottom could be directly taken from the grounded pin of the TO header. The contact from the top side was realized using gold wire bonding from the top metal to one of the three isolated header pin as shown in Figure 3.3.

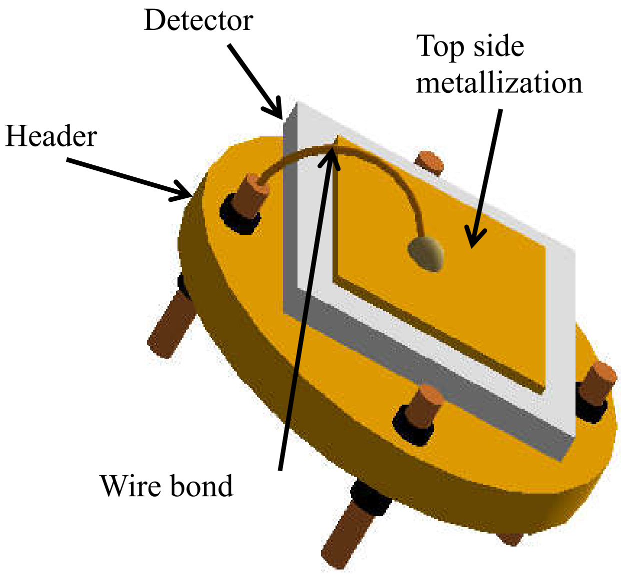

Fig. 3.3. Schematic of packaged diamond detector showing bonding from top metal to one of the header pin.

3.2. Characterization of detectors

The diamond substrates were characterized by Raman method, X-ray photoelectron spectroscopy (XPS) and Laue method before metallization. After metallization and packaging of detector, I-V characteristic and transient current spectroscopy were performed to evaluate the detector characteristics initially.

3.2.1. Raman Spectroscopy

Raman spectroscopy provides structural fingerprint and information about the phase of the material. Raman spectrum is obtained by exposing the sample with a monochromatic laser light and measuring the shift in its energy due to the interactions with the molecular vibrations or phonons. Raman spectroscopy can probe different forms of carbon i.e. sp^3, sp^2, etc. Carbon has sp^3 hybridization in the diamond structure which results in a peak in Raman spectrum at 1332 cm^{-1}.

The Raman spectra of the substrates were obtained prior to the detector fabrication. The Raman spectra were excited using a 532 nm laser focused to a spot size of 20 µm. The scattered light was analysed using an in house 0.9 m single monochromator, coupled with an edge filter and was detected by a cooled CCD (AndorTechnology) [60]. The entrance slit was kept at 50 µm, which gave a spectral band pass of 3.5 cm^{-1}.

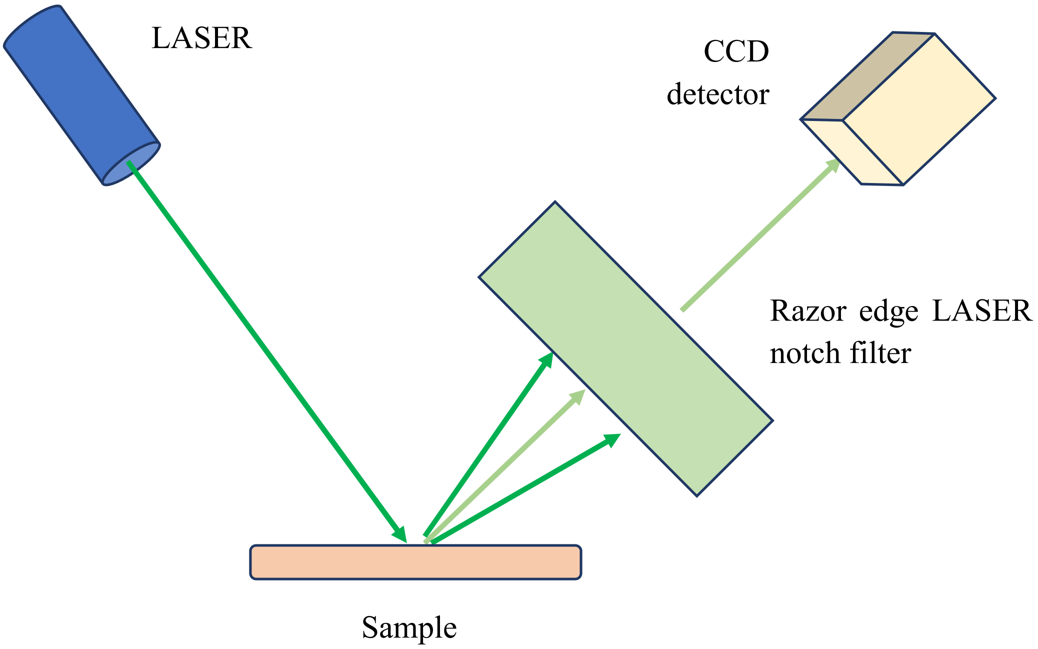

Fig. 3.4. Schematic showing operating principle of Raman spectroscopy.

3.2.2. X-ray photoelectron spectroscopy

X-ray photoelectron spectroscopy (XPS) is a surface sensitive technique to identify the composition and chemical states of the surface. XPS spectrum is obtained by exposing the sample surface with X-rays and measuring the kinetic energy and the number of electrons. The spectrum is basically a plot of number of photoelectrons at different binding energies which is a finger print of elements and their surrounding atoms. XPS analysis of the diamond surfaces just after oxygen plasma treatment was done using XPS spectrometer with an Al K_α

X-ray source. All binding energies were calculated based on the calibration by reference to the Au $4f_{7/2}$peak at 83.8 eV. The deconvolution of the C 1s and O 1s peaks was done using software inbuilt with the spectrometer. The composition of oxygen and carbon was obtained after normalizing the peak area by relative sensitivity factor using the following formula.

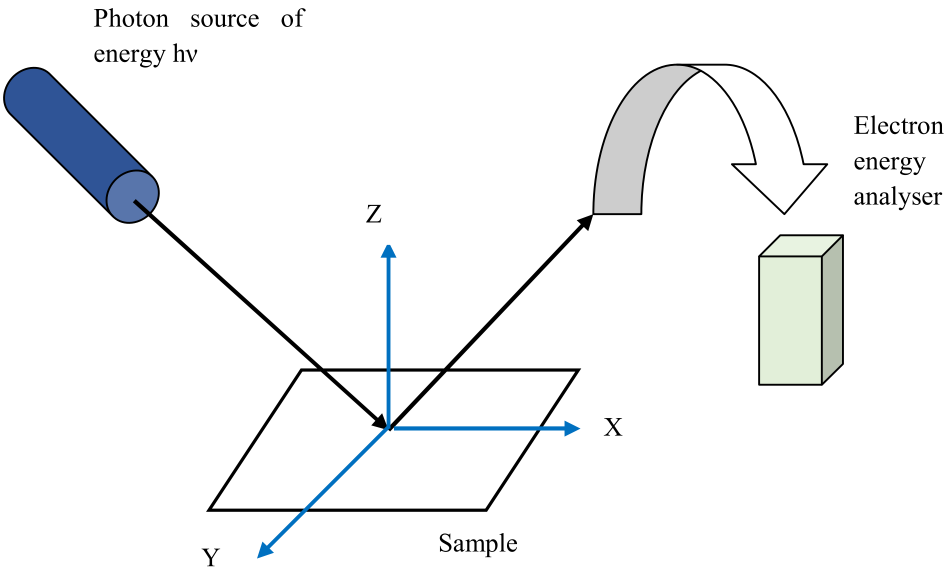

Fig. 3.5. Operating principle of XPS measurement.

$$\text{fraction of O on surface} = \frac{\frac{I_o}{S_o}}{\frac{I_o}{S_o} + \frac{I_C}{S_C}} \tag{3.1}$$

where I_o and I_C are intensity of O-peak and C-peak in the spectrum, S_o and S_c are sensitivity factors for O and C which were obtained from XPS-spectrometer database. Similarly, the fraction of C on the surface can be calculated.

3.2.3. Laue method of crystallography

Laue method is one of the diffraction technique used for qualitative analysis of crystal structure. The principle of the method is based on Bragg's law of diffraction where angle of incident X-ray beam with respect to crystal planes is fixed and the wavelength of photons varies. Laue reflection from a single crystal lies on the surface of a cone which intercepts the luminescent film (as shown in Figure 3.6.) and gives Bragg spots corresponding to the set of planes.

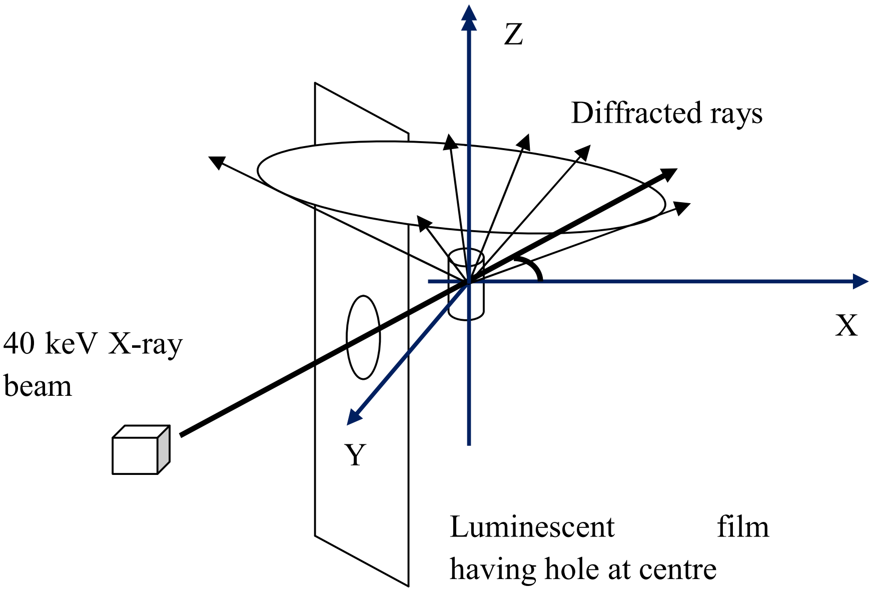

Fig. 3.6. Operating principle of Laue method in reflection mode.

Laue pattern of the diamond substrates were obtained for validation of single and polycrystalline nature of substrates. A 40 keV X-ray beam was used for the characterization and the beam current was set at 30 mA during the measurements. Laue pattern was obtained in back reflection mode where luminescent film was placed between incident beam and the diamond substrates so that back reflected rays were used to form the image. The luminescent film had a hole in centre to allow the incident X-ray beam to fall on the crystal. The reciprocal mapping of the crystal was done using inbuilt software after reading the luminescent film.

3.2.4. I-V characterization

First purpose of the current-voltage (I-V) characterization was to study the behaviour of metal-diamond interface i. e. whether it is behaving like schottky or ohmic. The I-V plot of an ohmic contact is linear and the order of current in the both positive and negative directions is similar. On the other hand Schottky contact does not exhibit linear I-V curve and the order of current magnitude is quite different for positive and negative biases. Apart from this, I-V characterization was done to measure the leakage currents at different bias voltages to determine a suitable voltage range for operating the detector during radiation measurement experiment. The schematic of the I-V measurement setup is shown in Figure 3.7.

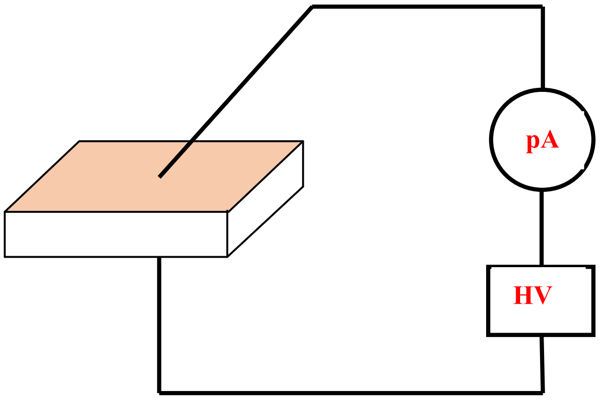

Fig. 3.7. Schematic of I-V measurement circuit consisting of a pico-ammeter, high voltage source and a detector.

I-V measurement was done using a programmable pico-ammeter which was controlled by software. The pico-ammeter had an inbuilt voltage source which was connected to the detector in series with the input of the pico-ammeter as shown in Figure 3.7. The voltage was varied in predefined steps through the software and the current was measured at each voltage step.

3.2.5. Transient response study of detector with alpha particles

Transient response study of the detectors is the study of current which flows with respect to time when the electrons-holes move after the interaction of radiation with the diamond. The transient current flows from the time the charged particles are generated by incoming quantum radiation and till the time they are trapped or reached to metal electrodes. The recorded current pulse with respect to time is very important to get information about the dynamics of charged particles (mobility, drift velocity, etc.) and material properties (trapping time, defects, etc.) [61]. The charge carriers may be generated either by a laser source or charged particles such as α-particles. The schematic of the setup used for this measurement is shown in Figure 3.8.

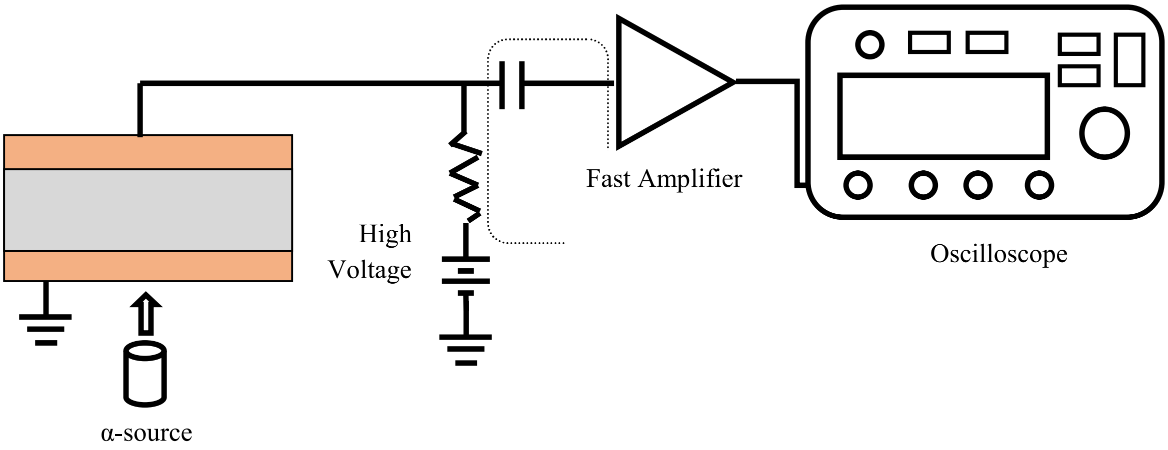

Fig. 3.8. Schematic of the setup for transient current study using alpha particles.

The transient current was measured using a fast broadband amplifier with a gain of 53 dB and bandwidth of 2 GHz. The charge carriers were introduced using 5.5 MeV α-particles generated from a ^{241}Am source. The range of 5.5 MeV alpha particles in diamond is 16 μm. Therefore, all electrons and hole will be generated within this length. These charge carriers are collected from the other end so that the charges drift through the bulk of diamond. The detector was biased at 250 V using a voltage source and the source was isolated from the input of wideband current amplifier using a Bias-T.

3.3. Study of the performance of detector to several types of radiation

After fabrication of the detectors, the response of detectors to charged particles and fast and slow neutrons was studied using methods and experimental setups discussed in the following subsections.

3.3.1. Alpha spectroscopy

Alpha spectroscopy of diamond substrate was done using a ^{238}Pu+^{239}Pu dual energy alpha source. ^{238}Pu emits alpha particles having energy 5.499 MeV and ^{239}Pu emits alpha of energy 5.156 MeV. The detector was placed in a vacuum chamber operated at a vacuum of 10^{-2} mbar. The alpha source was mounted at a distance of 5 cm above the detector. The detector was biased using a high voltage source. The signal from the detector was fed into a charge sensitive preamplifier and then signal was shaped using a shaping amplifier. Subsequently, the shaped signal was monitored on a cathode rays telescope (CRO) and was fed into an MCA to obtain the alpha spectrum. The PHS of alpha particles was recorded for a time of 15 minutes. The schematic of the alpha spectroscopy setup is shown in Figure 3.9 and the actual alpha setup used for the measurement is shown in Figure 3.10.

Dual alpha source:

^{239}Pu (5.156 MeV)

^{238}Pu (5.499 MeV)

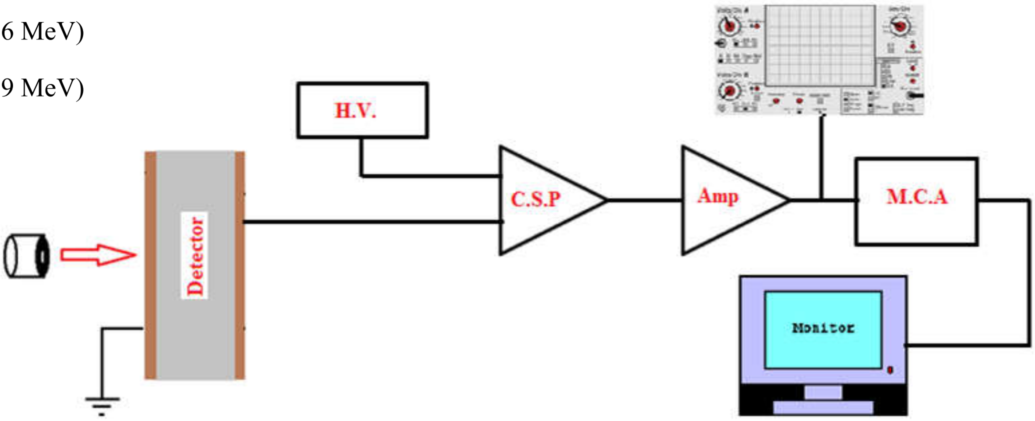

Fig. 3.9. Schematic of the setup used for alpha spectroscopy with diamond detector.

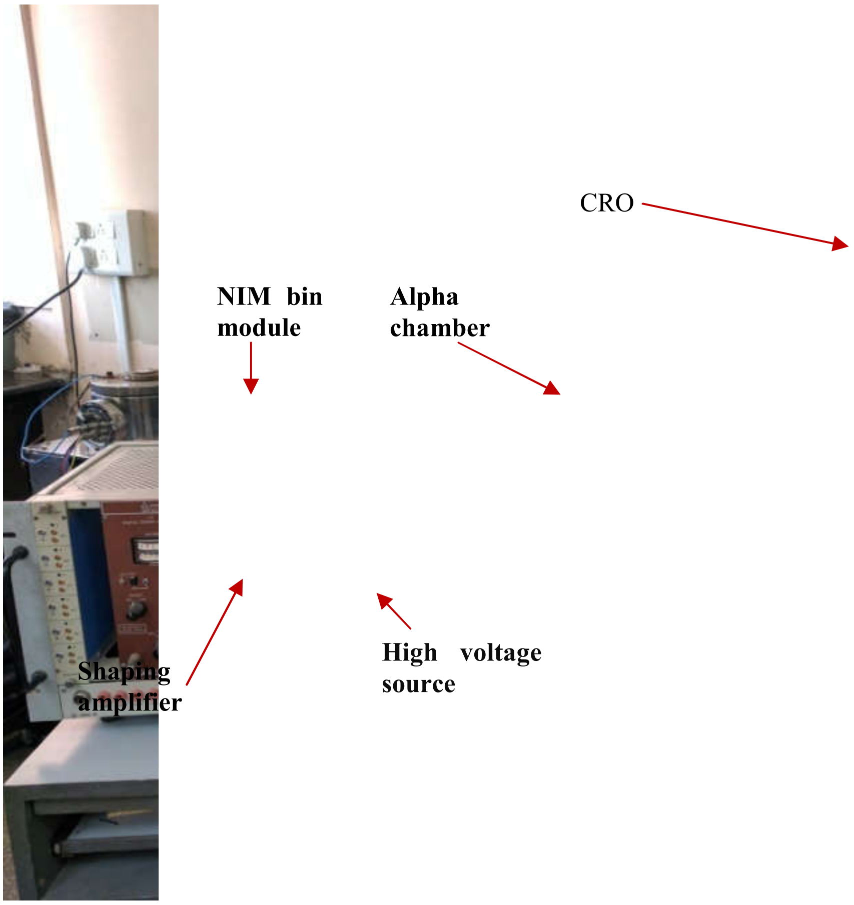

Fig. 3.10. Laboratory setup for the measurement of alpha radiation.

3.3.2. Fast neutron measurement

The performance of the detector to fast neutrons was studied at the fast neutron facility, TPD, BARC. The fast neutrons are produced in the fusion reaction of deuterium and tritium as below:

$$ {}_1^2D + {}_1^3T \rightarrow {}_2^4He + {}_0^1n \ + 17.6\ MeV \tag{3.2}$$

The deuterium ions are produced in RF ion source which are extracted through 1.5 mm canal using 6 kV DC and are then incident on the tritium target. The Q-value of the reaction is 17.6 MeV and the neutrons carry energy of 14.2 MeV.

For the measurement of fast neutrons, the detector was housed in an aluminium box for electromagnetic shielding and was placed in front of the D-T tube. Similar electronic setup as was used for alpha particle measurements was used for neutron measurements (Figure 3.9).The performance of the diamond detector to fast neutrons was further studied at different neutron fluxes. The neutron flux was varied by varying the distance between detector and D-T source.

3.3.3. Thermal neutron measurement

Thermal neutrons were measured using a Boron-10 film on the top surface of the detector. Boron film converts incoming slow neutrons into charged particles - Lithium and Helium with Q-value of 2.792 MeV and 2.310 MeV as shown by eq. (2.20) and eq. (2.21). Most of the time lithium nuclei are left in excited state then lithium and alpha particles carry energy of 0.84 MeV and 1.47 MeV respectively. In another case, lithium and alpha particles carry energy of 1.014 MeV and 1.77 MeV respectively.

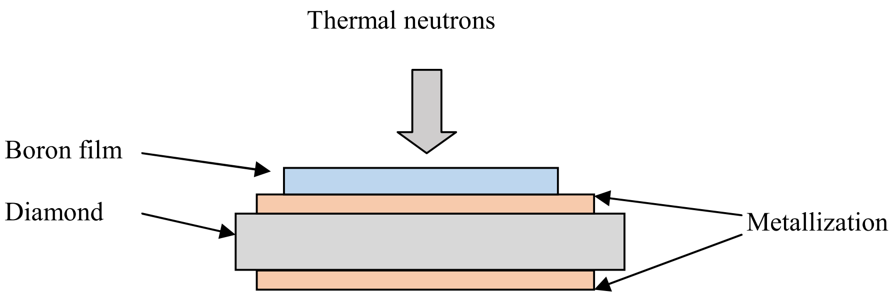

Fig. 3.11. Diamond detector integrated with Boron-10 film for the measurement of thermal neutrons.

Slow neutrons were obtained from the experimental nuclear reactor where neutrons were generated in the fission of ^{238}U. The generated neutrons were thermalized using a neutron moderator.

3.4. Summary

Several experimental setups were used to evaluate the quality of diamond substrates, fabrication detectors and for radiation measurement experiments which were discussed in this chapter. Diamond detectors were fabricated in several batches using commercially available SCD and pCVD substrates. The substrates were cleaned using well established chemistry techniques. The substrates were characterized by Raman spectroscopy and Laue crystallography. The detectors were annealed prior to metallization and subsequently oxygen plasma treatment of the substrates was done. XPS spectroscopy of the treated substrates was done to confirm presence of Oxygen termination. Different combinations of metallization were studied such as Ti/Au, Cr/Au Ti/Pt/Au and Al using e-beam thermal evaporation technique. The selection was the metal was based upon their work function matching so that contact would behave like ohmic. The sequence of the metallization was chosen as to get good adhesion between metal and diamond and capping of metal to avoid oxidation of the outer metal surface. The post metallization annealing of the detector was done in Nitrogen ambient. Further the metalized detectors were packaged on a TO header and bonded using Gold wire. The I-V characterization of the detector was done to study behaviour of metal diamond contact and study variation in the leakage current with bias voltage using a programmable Pico-ammeter. Subsequently transient current spectroscopy of the detector was done to study dynamics of charge carriers generated inside the diamond detector.

The fabricated detectors were subsequently used for the measurement of several types of radiations. The response of detectors to charge particles was evaluated using alpha particles from ^{238}Pu+^{239}Pu dual energy alpha source. The performance of detectors to fast neutrons was studied using 14.2 MeV neutrons from a D-T source. A proper packaging of the detector was developed for the experiments. The detector response to different neutron fluxes was obtained to check its linearity with the variation in flux. Further response of the detector to thermal neutrons was also evaluated using thermal neutron beam line coming from research reactor with a ^{10}B thin film as a converter. The details of fabrication and characterization of pCVD detectors and SCD detectors are described in chapter 4 and Chapter 5 respectively.

CHAPTER 4: FABRICATION AND CHARACTERIZATION OF PCVD BASED RADIATION DETECTORS

The doctoral work presented in this thesis was initiated with the study of pCVD based detectors. The pCVD substrates are easily available in the market with costs much lower than that of SCD substrates. The pCVD substrates contain several grains with size variations. pCVD substrates have higher density of defects which have a high probability of occurrence at the grain boundaries [35, 61]. These defects either act like charge trapping centres for electrons and holes where charge carriers are physically bonded to the defects or offer a favourable site for the recombination of electrons and holes. The trapping of charge carriers at the defect sites results in a space charge build up and induce polarization in the bulk of material. The bulk polarization sets up internal electric field which in turn distorts the externally applied electric field and affects the charge collection [46].

This chapter will begin with the results of characterization of pCVD substrates. In the subsequent sections, fabrication of pCVD detectors and their characterization will be discussed. At the end of the chapter, response of pCVD detectors to fast neutrons will be presented.

4.1. Raman spectroscopy of pCVD substrates

Raman spectroscopy of the diamond substrates was done to study the chemical structure of the diamond. The typical Raman spectrum of the diamond substrate obtained using 532 nm laser is shown in Figure 4.1. The spectrum shows a peak at 1332 cm^{-1} which is as expected due to sp^3 bonded carbon atoms and this confirms diamond structure. The spectrum does not contain any other peaks due to other forms of carbon which indicates high purity of the diamond substrate. The full width half maxima (FWHM) of the diamond peak was calculated to be 3.5 cm^{-1} by Gaussian fitting of the peak.

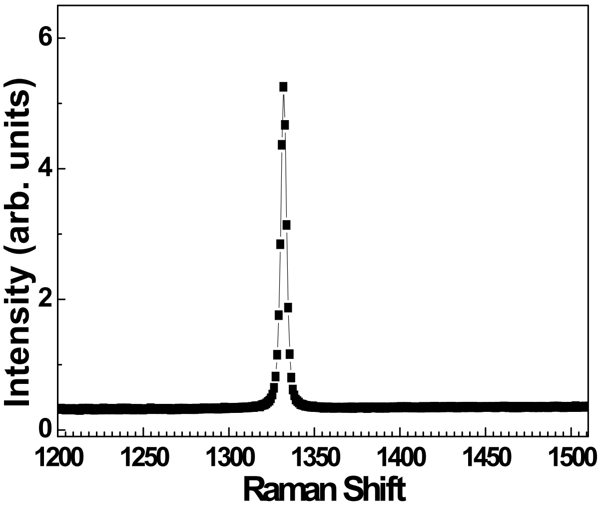

Fig. 4.1. Raman spectrum of diamond substrate showing a peak at1332 cm^{-1}.

4.2. Laue crystallography of pCVD substrate

The Laue pattern of 100 µm thick polycrystalline substrate was obtained to study the crystal structure. Prior to crystallography, the substrates were degreased and then cleaned in an acid solution as discussed in chapter 4. The Laue pattern obtained in reflection mode is shown in Figure 4.2. A circular pattern of the diffracted spots was seen in the spectrum which is indicating polycrystalline nature of substrate. As pCVD has a set of planes which satisfy Bragg condition for almost all incident X-rays falling at different angles, it results in a circular pattern of spots.

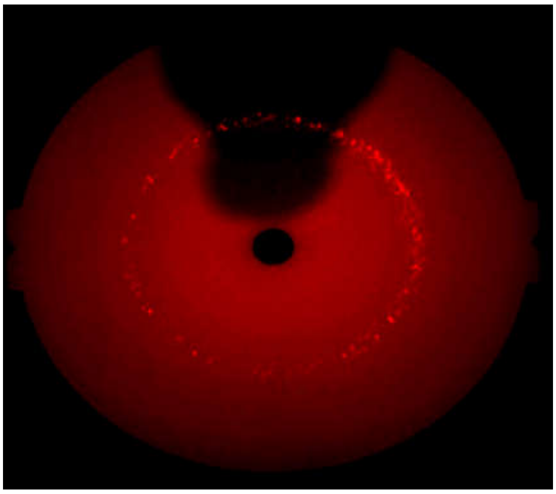

Fig. 4.2. Laue pattern of diamond showing Polycrystalline nature of substrate

4.3. Fabrication of pCVD detectors

pCVD based detectors were fabricated using two types of substrates having different size and thickness – square geometry of 5 mm x 5 mm x 300 μm and circular geometry of 100 mm^2 x 100 μm. As the aim of the detector development was the measurement of 14 MeV fast neutrons, the thickness of the detector was chosen accordingly. The range of 5.5 MeV alpha particles in diamond is around 16 μm and the range for 8.5 MeV alpha from $^{12}C(n, \alpha)^{9}Be$ reaction is around 40 μm. Therefore the thickness of diamond substrate of 100 μm was considered sufficient to obtain full energy deposition by the charged particles. Another important aspect of choosing lower thickness of the substrate was possibility of less trapping of charge carriers in pCVD substrates. The diamond substrates of 300 μm were chosen to study whether the neutron response is better in thicker detectors due to higher probability of nuclear interaction of neutrons with carbon. Prior to metallization, cleaning of the diamond substrates was done using the cleaning procedure discussed in chapter 4. A metal mask was used during the metallization to prevent the metal deposition along the edges. The size of the mask was carefully chosen to keep metallization edge at least 0.5 mm away from the substrate edges. Masks having circular pattern of 10.3 mm diameter and square pattern of 4 mm x 4 mm size were used during metallization on 100 mm^2 and 5 mm x 5 mm substrates respectively. The pCVD detectors were fabricated in three batches as per the following details:

Batch 1- Ti/Au metallization on each type of substrates i.e. 5 mm x 5 mm x 300 µm and 100 mm^2 x 100 µm was done by sequential deposition of Ti and Au on both sides of the substrates. Ti and Au were kept in two different boats and the e-beam was allowed to selectively incident on the boats one after the other to evaporate corresponding metal resulting in the deposition on the substrates. The time of evaporation was tuned to deposit metals for thickness of 20 nm of Ti and 200 nm of Au.

Batch II – Ti/Pt/Au metallization on substrates of each type as discussed above were done using e-beam thermal evaporation while placing Ti, Pt and Au in three separate boats. These metals were evaporated to deposit metals on both sides of diamond substrate for thickness of Ti (20 nm), Pt (20 nm) and Au (200 nm).

Batch III – Cr/Au metallization on substrates of each type were done by placing Cr and Au in two separate boats in e-beam chamber for sequential deposition of Cr (20 nm) and Au (200 nm).

Subsequent to the metallization, detectors were mounted on a TO package using a conducting epoxy as shown in Figure 4.3. A gold wire of 1 mil diameter was bonded from the top side of detector to one of the isolated pin on the header to make front side electrical contact and the back side contact was taken from the header itself (Figure 4.3(a) and (b)).

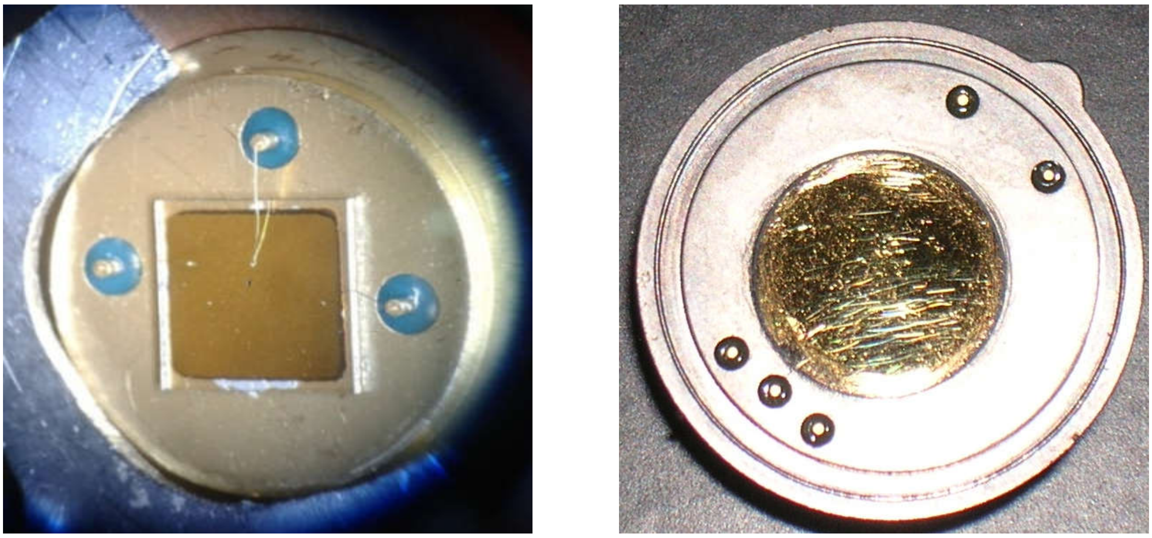

(a) (b)

Fig. 4.3. Packaged pCVD detector with wire bonding (a) 5 mm x 5 mm x 300 µm square size and (b) 100 mm^2 x 100 µm circular size.

4.4. I-V Characterization of the fabricated detectors

I-V characterization of the detectors was done to study the behaviour of metal diamond interface and leakage current variation with voltage. The leakage current in the detector was measured using a pico-ammeter with a programmable voltage source. The bias voltage was varied from 0 to a maximum voltage corresponding to 1 $V.\mu m^{-1}$.

4.4.1. I-V characteristic of the different metalized detectors

The I-V characteristics of three 100 mm^2 x 100 µm detectors fabricated in three different batches are compared in Figure 4.4. Leakage current of the chamber including cable without detector was measured and it was observed to be quite linear and symmetric in both positive and negative voltage range. The current was below pA for voltage ± 300 V. As shown in the Figure, the detectors with Ti/Au and Ti/Pt/Au did not show perfect ohmic contact behaviour, rather they are behaving like non ohmic. However Cr/Au metal contact on diamond shows behaviour very close to ohmic contact as the I-V curve appears to be symmetric in both directions with leakage current of 4.2 nA and 3.8 nA at -100 V and +100 V respectively (about 10 % variation). The Ti/Au contact on diamond appears to be more deviated from ohmic behaviour compared to that of Cr/Au as its I-V characteristic is more asymmetric. The leakage current in Ti/Au metalized detector was observed to be one third at + 100 V (2.6 nA) of the current at -100 V (7.9 nA). On the other hand the Ti/Pt/Au on diamond has shown highly asymmetric behaviour of I-V curve indicating a non ohmic type of contact. The leakage current in the detector was 11.9 nA and 2.3 nA at -100 V and + 100 V respectively.

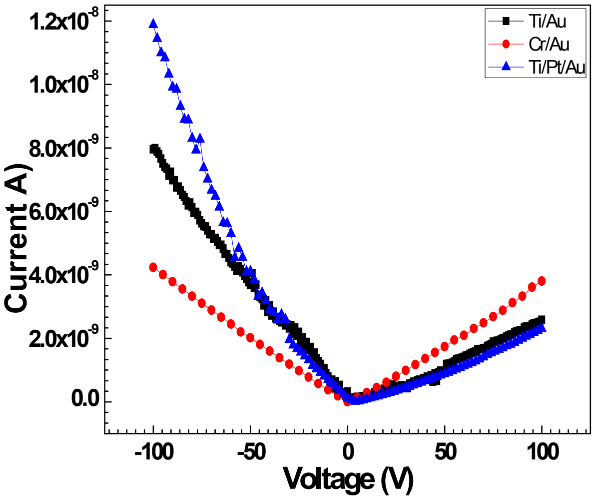

Fig. 4.4. IV characteristics of 100 mm^2 x 100 µm diamond detectors for three different types of metallization.

The behaviour of metal diamond contact may be ohmic or Schottky depending upon the metal used for contacts. The work function of the metal decides barrier height formed between metal and diamond. The work function of Ti (4.3 eV) and Cr (4.5 eV) is much closer to the work function of diamond. Therefore Ti and Cr are expected to give ohmic type of contact and therefore the I-V curves were observed to be close to ohmic behaviour. However, introduction of Pt (5.7 eV), which has work function slightly different from the work function of diamond, causes more deviation from ohmic character which reflects in the I-V curve. Out of the three detectors Cr/Au metalized detector has shown better ohmic response compared to other two detectors. The leakage current in positive bias region was observed to be similar for all three detectors but the difference was more in negative bias region.

4.4.2. IV characteristic of the pCVD detector having different thickness

The Cr/Au metalized detectors showed I-V response which was much closer to ohmic contact compared to other metallization. The I-V characteristic of two detectors fabricated in batch III with Cr/Au metallization on 5 mm x 5 mm x 300 μm and 100 mm^2 x 100 μm are compared in Figure 4.5. The leakage currents in the two detectors were observed to be very low and were about 4 nA at 100 V bias voltage for 100 μm thick detector and about 200 pA for 300 μm thick detector. The leakage current in 100 μm detector was expected to be larger than that in 300 μm due to larger area. Both detectors showed ohmic behaviour as the leakage current in both positive and negative direction is almost the same with linear relationship between current and bias voltage (current axis in Figure 4.5. is in logarithmic scale).

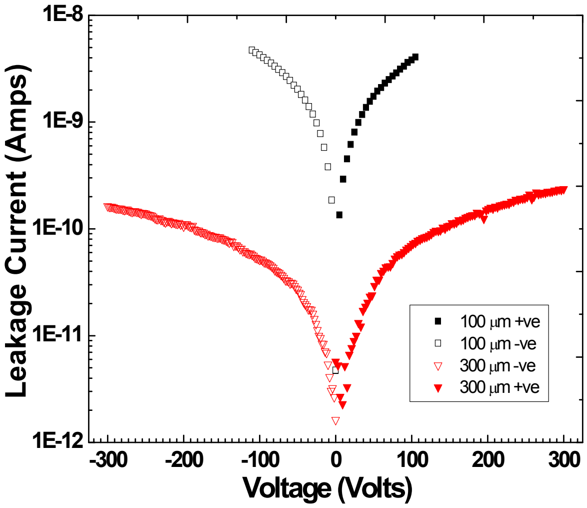

Fig. 4.5. I-V characteristic of the as fabricated diamond detectors with different geometries; i) 100 mm^2 x 100 μm and ii) 5 mm x 5 mm x 300 μm.

4.5. Alpha particle spectroscopy of the fabricated detectors

The performance of diamond detectors with charged particles was studied using ^{238}Pu+^{239}Pu dual alpha source which emits alpha particles of energies 5.1 MeV and 5.5 MeV. The charge generated in diamond by incident alphas was integrated by a charge sensitive pre-amplifier having a gain of 44 mV/MeV. The signal was further processed using a shaping amplifier having a gain of 50 and shaping time of 2 μs. The output of shaping amplifier was fed into a multi channel analyser (MCA) and an oscilloscope. During alpha particle response measurements, the detector and alpha source were mounted in a vacuum chamber at a pressure of 10^{-3} mbar. The diamond detectors were biased to obtain electric field of 1 V.μm^{-1}. The pulse height spectra obtained with the alpha source for the two types of fabricated detectors are shown in Figure 4.6. The low energy threshold for the MCA was set above the electronic noise level which was decided by taking the spectrum in the absence of alpha source. The PHS was observed to contain counts at all possible channels ranging from minimum set threshold to a maximum pulse height level without any specific peak. The absence of peak and continuous distribution in the spectrum indicate polycrystalline nature of the detector. The cut off of the spectrum towards higher channel number is observed to be about 200 channels for the 100 μm thick detector and 100 channels for the 300 μm thick detector.

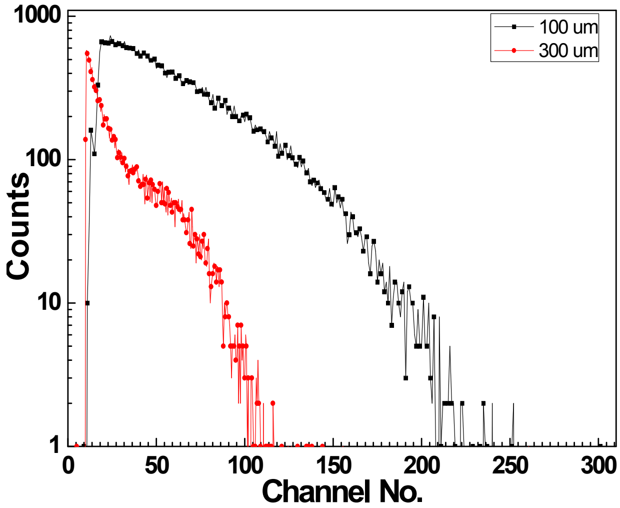

Fig. 4.6. Alpha spectra for diamond detectors with thickness of 100 mm^2 x 100 μm and 5 mm x 5 mm x 300 μm.

4.6. Stability test of the pCVD detectors

The stability of the detector response was studied by continuously operating the detector for a specific period and the pulse height spectra were recorded after every one hour. The response of 100 μm thick detector to alpha particles at different time intervals is shown in Fig 4.7 (a). The alpha response of the detector was not observed to be stable with time. The measurements carried out showed a significant shift in the spectrum to the lower energy side after first one hour and the counts at lower energies were observed to increase. Further shift of the spectrum after one hour up to six hours was observed to be quite less compared to that observed in the first one hour. The shift of the spectrum towards low energy channels reflects polycrystalline nature of diamond substrate, where there is trapping of charge carriers at the grain boundaries. The count rates were calculated by integrating the pulse height spectra to obtain the total counts and then dividing by the counting time (Figure 4.7 (b).

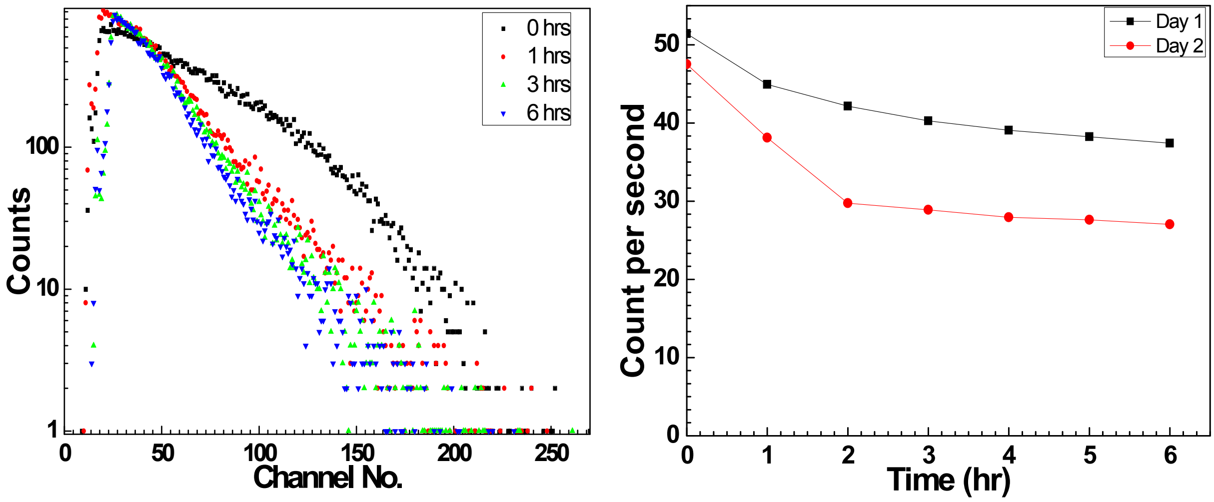

(a) (b)

Fig. 4.7. Stability tests for100 mm^2 x 100 μm pCVD detector showing (a) PHS at different time intervals, (b) variation in the count rate with time.

As shown in Figure 4.7 (b), the count rate was observed to decrease with time. The count rate measurement with time was repeated on the next day and similar trend was observed. The count rate was observed to decrease by 29% on the first day and about 42% on the second day. Another important observation in long term measurement was that count rate observed at the end of day one and count rate at the beginning of second day were not the same. During first day measurements, the count rate reduced from 52 CPS to 36 CPS but on the second day, the count rate started from 47 CPS and then decreased to 37 CPS. This behaviour indicates that some of charge carriers are loosely bound to the traps and they are released during the 18 hour of gap in these two measurements. The decrease in count rate was expected to be because of trapping of charge carriers at the defect sites. As trapping continues, the internal field developed due to polarization in the detector distorts the externally applied electric field. Therefore the charge collection reduces with time.

4.7. Priming of the pCVD detectors

As the detector performance was observed to degrade with time, it was required to passivate the charge trap centres. It is reported in the literature that these charge traps can be saturated by the technique of priming [62-64].

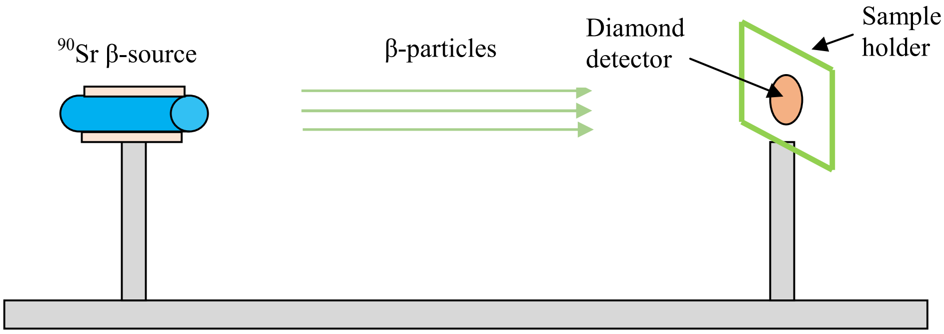

Fig. 4.8. Schematic of the setup used for the priming of diamond detectors using ^{90}Sr source.

For priming, the detectors were irradiated using β-particles emitting from a ^{90}Sr (energy 2.28 MeV, dose rate of 1.66 Gy h^{-1}) source for a total dose of 30 Gy. The source was a coin shaped electroplated source with a forward flux. During irradiation, the detectors were mounted with respect to the source so that complete active area was uniformly exposed. The β-irradiation was carried out at room temperature without application of a bias to the detector.

Subsequent to β-irradiation, stability test using the same method (as discussed in section 4.6) was again repeated for 6 hours on two consecutive days (day 1 and day 2). The PHS obtained with a 100 mm^2 x 100 µm pCVD detector after β irradiation is plotted in Figure 4.9 (a). The count rates observed with time are shown in Figure 4.9 (b). The PHS after β-irradiation shows a broad peak at channel number 158 instead of a continuum as was observed prior to priming. The maximum pulse height was also observed to shift from Channel number 100 to Channel number 250 indicating better charge collection. However, the PHS obtained with a 300 µm thick detector did not show such improvement.

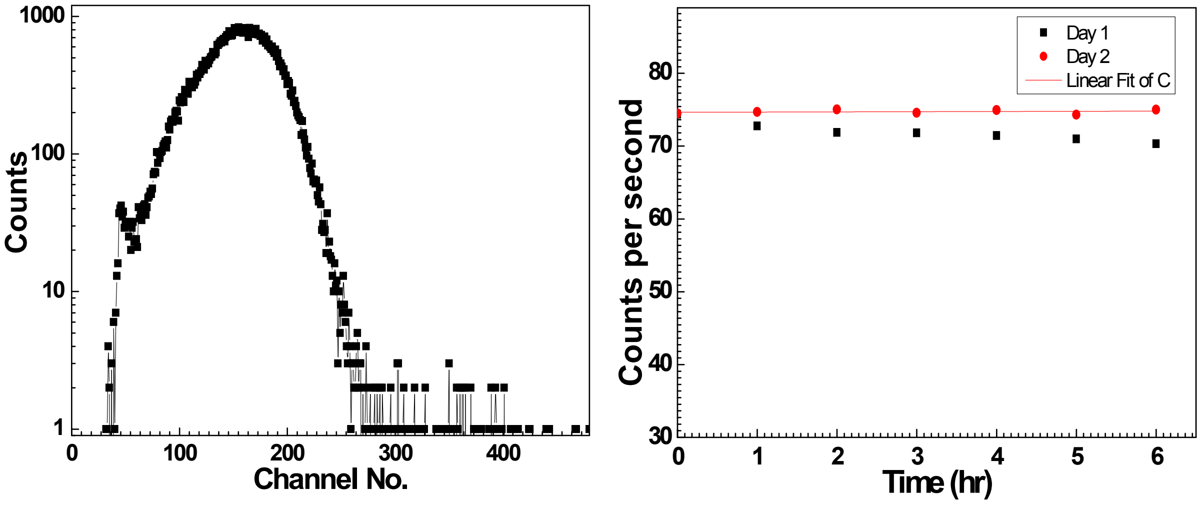

(a) (b)

Fig. 4.9. Results of the stability test of the detector after priming showing (a) improvement in the charge collection, and (b) stable count rate with respect to time.

The detectors show significant improvement in the count rate after β-irradiation. The count rate was observed to decrease by 5 % on the first day but on the second day, the response was observed to be stable with time with a count rate of 75 CPS. This improvement could be attributed to filling of traps due to β-irradiation resulting in negligible additional trapping of electrons and holes generated by the ionization with alpha particles.

4.8. Alpha response of the pCVD detectors with different metallization

To study the effect of different metal-diamond interface on charge collection, alpha response of pCVD detector with three different metallization was obtained. Three detectors of each type (i.e. 100 mm^2 x 100 μm and 5 mm x 5 mm x 300 μm which were fabricated in three batches) were evaluated to compare their alpha response. Priming of all these detectors using the method discussed in the previous section was done for a total dose of 30 Gy to stabilize the detector response. The responses of the detectors on the two types of substrates are compared one by one in the following sections.

4.8.1. Alpha response of the 100 mm^2 x 100 µm detectors with different metallization

The PHS obtained with three 100 mm^2 x 100 µm detectors with different types of metallization are shown in Figure 4.10. All three detectors have shown improvement in the alpha response after priming where the peaks in the spectra were observed to be within Channel No. 160 to 180. The maximum pulse heights obtained with the three detectors were almost similar, and were in the range of 230-250 indicating similar charge collection in the three detectors. Other details of the spectra are given in Table 4.1.

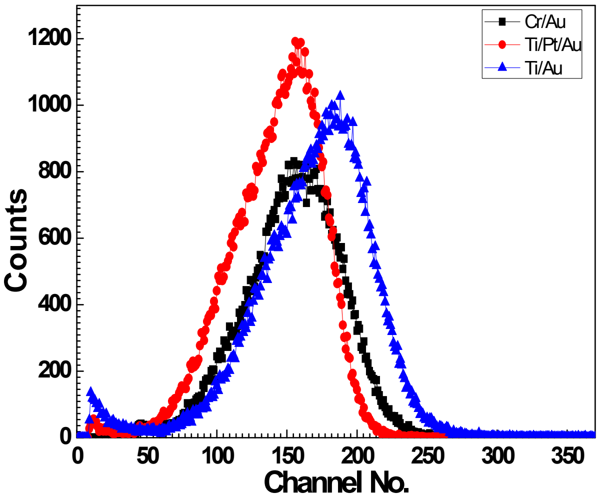

Fig. 4.10. Alpha histogram compared for three 100 mm^2 x 100 µm detectors metalized with Cr/Au, Ti/Pt/Au and Ti/Au.

Table 4.1. Details of alpha spectra obtained with 100mm2 x 100 µm detectors.

Detector Metallization	CPS	Peak Position	Peak Count	Cut Off
Cr/Au	74	163	805	240
Ti/Pt/Au	96	160	1177	230
Ti/Au	96	186	963	250

4.8.2. Alpha response of the 5 mm x 5 mm x 300 μm detectors with different metallization

The study of charge collection in 5 mm x 5 mm x 300 μm detectors was also done by obtaining the PHS with alpha particles (Figure 4.11). The improvement in the charge collection after priming was not observed to be as much for the 300 μm thick detectors as was observed in 100 μm thick detectors. However some improvement in the count rate was observed.

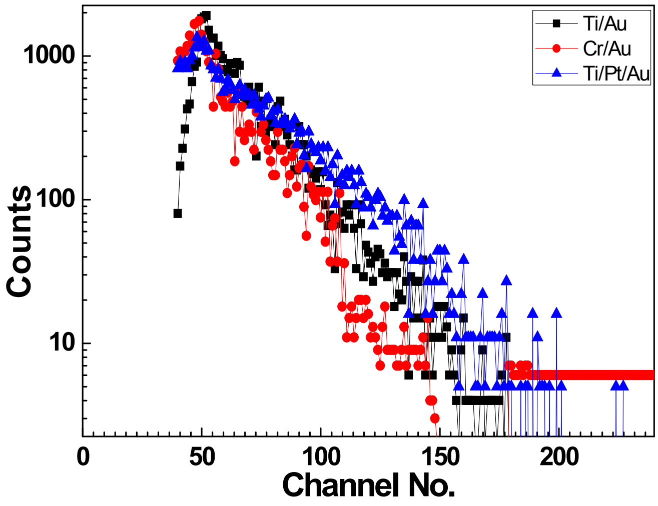

Fig. 4.11. Alpha histogram compared for three 5 mm x 5 mm x 300 μm detectors metalized with Cr/Au, Ti/Pt/Au and Ti/Au.

The maximum pulse heights obtained for three detectors were observed to be almost same and were in the range of 150-160. The analysis of the spectra obtained using the three types of detectors is listed in Table 4.2.

Table 4.2. Details of PHS obtained for three types of detectors.

Detector Metallization	CPS	Peak Position	Peak Count	Cut Off
Cr/Au	45	47	1700	150-160
Ti/Pt/Au	37	50	1261	150-160
Ti/Au	42	50	1915	150-160

4.9. Effect of heating on primed pCVD detector

The study of the effect of heating on the primed detector was done using a 100 mm^2 x 100 µm detector with Ti/Pt/Au metallization. The detector was heated up to 150^{o}C for a time of 15 minutes in steps of 50^{o}C. The alpha response of the pCVD detector was studied after each step. The PHS obtained after every heating steps are shown in the Figure 4.12 and compared to the responses of detector before heating and before priming.

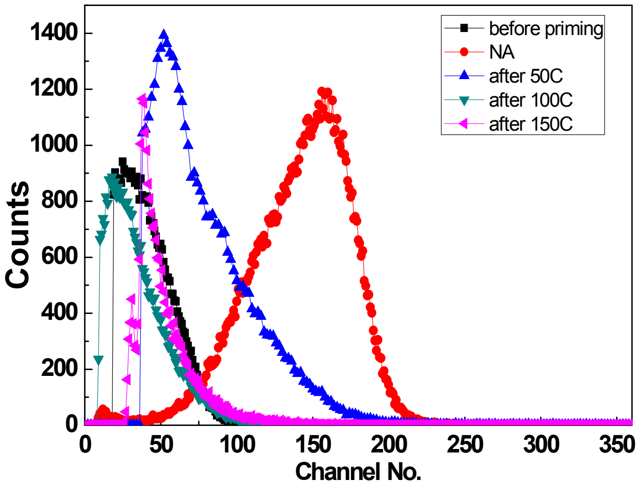

Fig. 4.12. PHS obtained for a 100 mm^{2}x 100 µm detector with Ti/Pt/Au metallization after heating at 50^{o}C, 100^{o}C and 150^{o}C. The results are compared to a non heated detector.

After heating at 50^{o}C, the count rate was observed to reduce from 96 CPS to 44 CPS and the peak position occurred at one third of the non heated detector. However, no significant reduction in the maximum pulse height was observed at high temperatures. However, as detector was heated to 100^{o}C the maximum pulse height was reduced by a significant amount. The Channel No. of maximum pulse height was very close to the Channel No cut off value observed before priming. The CPS and peak positions were observed to lie near 41 CPS and 27 CPS respectively.

After heating at still higher temperature (150°C), no significant degradation in the detector response was observed. The results show that the charge collection reduces after heating the detector. This indicates de-trapping of the saturated defect sites at high temperatures which was also reported in literature [65-66]. The analysis of the PHS obtained at different temperatures is presented in Table 4.3.

Table 4.3. Details of PHS obtained for three types of metallized detectors.

Temperature	**CPS**	**Peak Position**	**Peak Count**	**Cut Off**
Before Priming	27	39	1160	110
After priming and before Heating	96	160	1180	226
After heating at 50°C	44	52	1370	190
After heating at 100°C	41	27	925	95
After heating at 150°C	27	39	1160	110

4.10. Optimization of operating parameters for detector operation

The effect of different operating parameters such as bias voltage and shaping time on the performance of diamond detector was also studied. In order to study the effect of bias voltage, PHS with alpha particles was obtained at different bias voltages (Figure 4.13 (a)). As can be seen, the PHS at different bias voltage shows an increase in the pulse height with the increase in bias voltages. Since the increase in the bias voltage causes increase in the electric field, the charge collection improves. The count rates were calculated by integrating the PHS obtained at different bias voltages. The count rates were also observed to increase with the rise in the electric field as shown in Figure 4.13 (b).

During the measurements, a minimum threshold channel was set at channel No. 10 in the MCA which was decided by the noise level at the time of measurement. Hence, the events causing pulses with height less than the set threshold were not counted. When the electric filed applied to the detector increases, the pulse height increases due to better charge collection. Hence, those events which were earlier below the noise threshold are also counted, resulting in an increase in the count rate with the increase in electric field. The count rate was observed to increase by about 20 % due to the increase in bias from 50 V to 100 V.

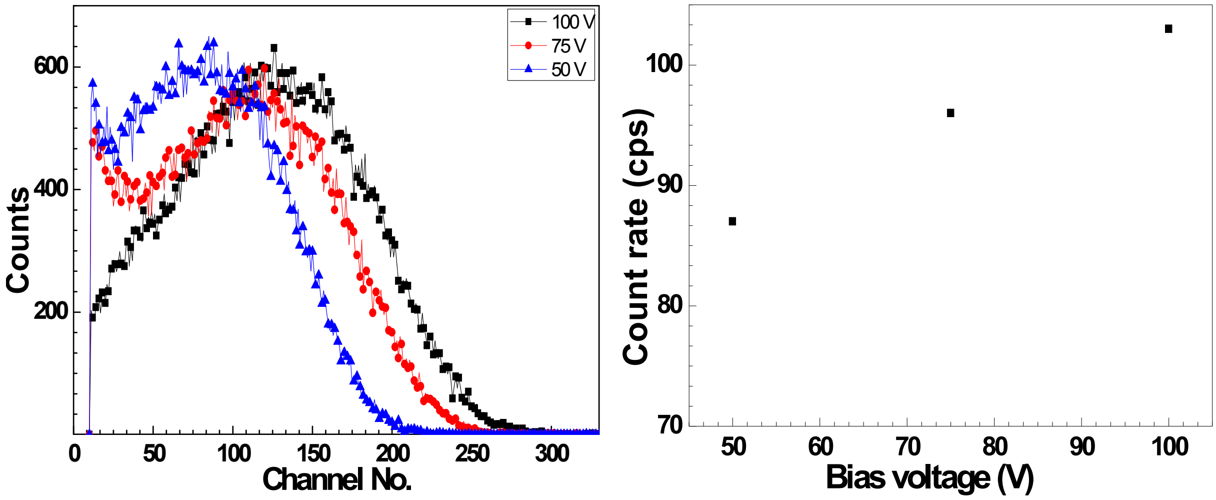

(a) (b)

Fig. 4.13. PHS obtained at different bias voltage shows (a) increase in pulse height and (b) increase in count rate.

Subsequently, the effect of shaping time on the charge collection was studied by varying the shaping time from 0.5 μs to 6 μs. The pulse height spectra obtained at different shaping times are shown in Figure 4.14 (a) which show increase in the pulse heights with the increase in the shaping time. The count rate was calculated for PHS obtained at different shaping times (Figure 4.14 (b)) which was observed to be almost constant at different shaping times.

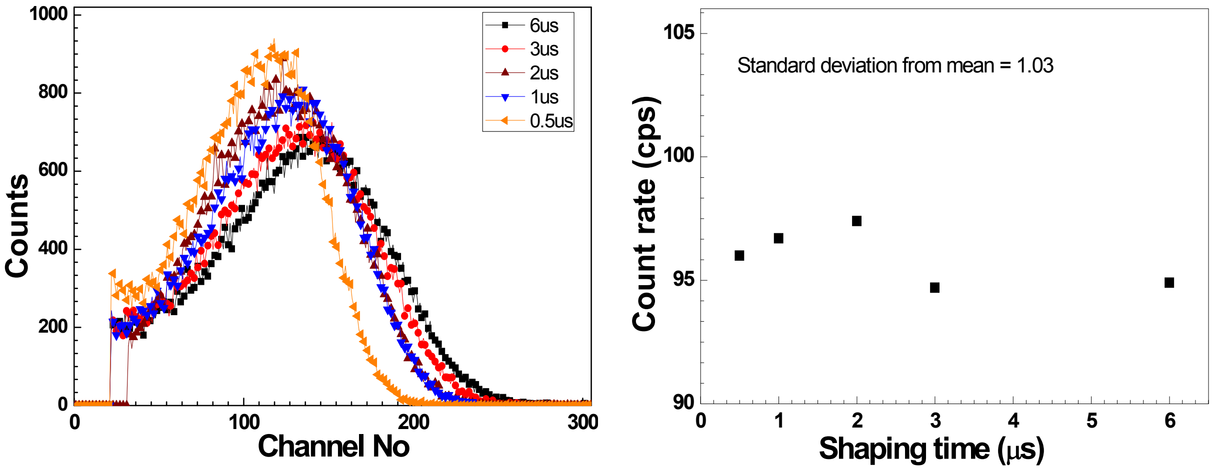

(a) (b)

Fig. 4.14. Effect of shaping time on (a) pulse height (b) Count rate.

4.11. Fast neutron measurements

The performance of the pCVD diamond detectors to fast neutrons was studied after achieving a stable response of the detectors to alpha particles. The fast neutron measurement of the detectors was done using a compact D–T neutron source. The D-T neutron source was a compact tube having isotropic emission of neutrons. The PHS obtained using the two detectors i.e. 100 mm^2 x 100 μm and 5 mm x 5 mm x 300 μm are shown in Figure 4.15. The actual neutron flux was calculated as 8.76 x 10^6 n cm^{-1}s^{-1} using activation foil measurements with 10% accuracy. The lower energy threshold for the MCA was set above the channel number corresponding to the electronic noise of the system in the absence of neutrons.

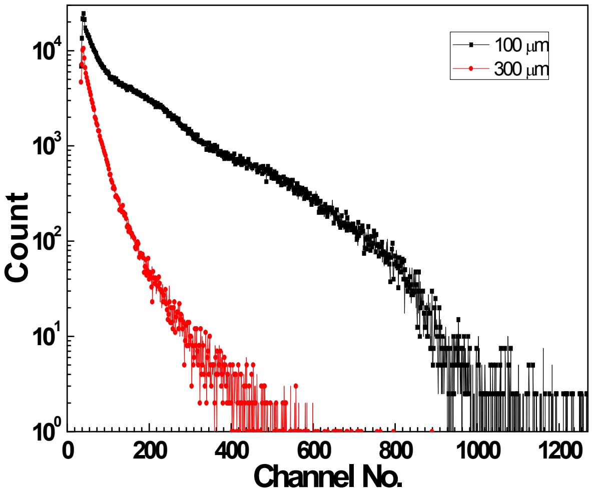

Fig. 4.15. Comparison of response of diamond detectors with thickness of 100 µm and 300 µm with fast neutrons.

The PHS with neutrons for the both detectors show a continuum without any peak. The detection of neutrons involves nuclear reaction between neutrons and carbon atoms. The location where interaction occurs along the path of beam is probabilistic. Therefore the amount of charge trapping in different interactions varies depending upon the exact location of the interaction. It was also observed that PHS with neutrons for 100 µm thick detector has counts on higher energy side compared to that observed for the 300 µm thick detector.

To see the response of the detectors for different neutron rates, the detector response was examined by varying the neutron flux at detector location from 2.86 x 10^5 n cm $^{-2}$ s^{-2} to 8.76 x 10^6 n cm^{-2} s^{-1}. The 100 µm thick detector was used for this study as it had better response compared to the 300 µm thick detector. The flux was varied by changing the distance of detector from the source. Figure 4.16 (a) shows the count rate observed for different neutron flux. The count rates were calculated by integrating the PHS with time and then dividing by the counting time. The count rate at different interval of times was recorded for the stability test of the detector to fast neutrons. The detector response was observed to be stable with time and count rate was constant at 4000 CPS as shown in Figure 4.16 (b).

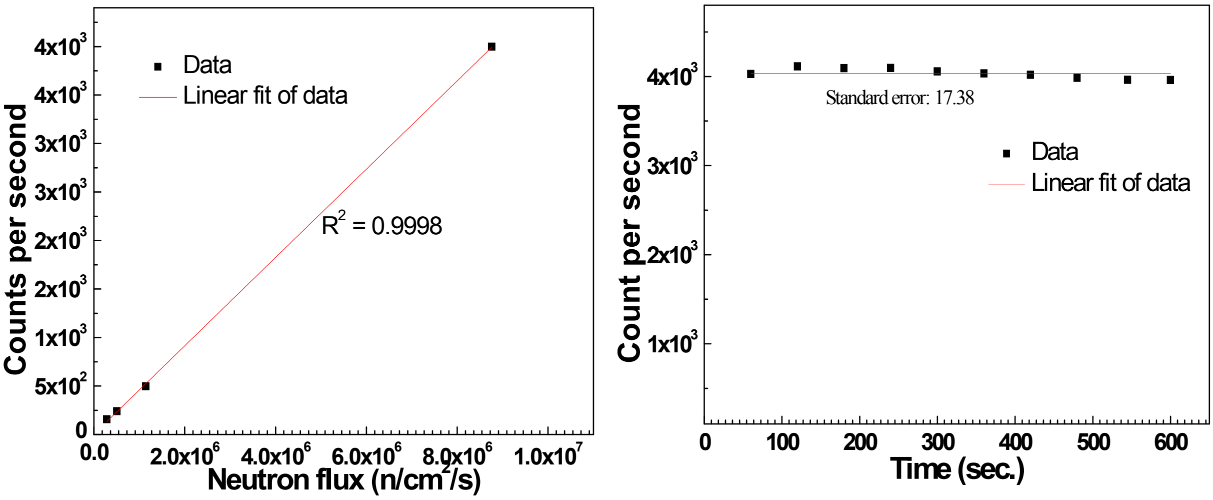

(a) (b)

Fig. 4.16. (a) Linear increase in count rate with neutron flux (b) Stable response of detector with time.

4.12. Summary

pCVD detectors were fabricated using commercially available substrates. Raman spectroscopy of the substrates has shown highly pure substrate without any trace of graphite or any other forms of carbon. Laue pattern of the substrate has shown Bragg spots in circular pattern indicating different set of planes oriented in different directions. The leakage current in 100 mm^2 x 100 µm detector was few nA on the other hand it was one order less in 5 mm x 5 mm x 300 µm detectors. The PHS with alpha particles obtained by the polycrystalline detectors was observed to be continuum without any peak. The maximum pulse height observed in the 100 µm thick detector was more than that observed in 300 µm detector which was indicating more trapping of charge carriers in thicker detector. The count rate shown by polycrystalline detectors was observed to decrease with time due to trapping of charge carriers. The priming of the pCVD detectors using β-particles has resulted in the stable response of the detector with improvement in the maximum pulse height seen in the PHS. Response of the pCVD detector to fast neutrons was studied using D-T neutrons. The detector has shown linear variation in count rate with the change in neutron flux indicating that pCVD detectors are suitable for fast neutrons counting application after proper priming of the detector.

CHAPTER 5: FABRICATION AND CHARACTERIZATION OF SCD BASED RADIATION DETECTORS

As discussed in the previous chapter, pCVD detectors can give a stable response to alpha particles and fast neutrons after suitable priming. These detectors can be used for counting applications where the number of incoming quanta of radiation is important. But even after the priming, detectors do not show adequate energy resolution for spectroscopy applications. Therefore, further work was done with single crystal diamond (SCD) substrates. As SCD has only one grain and there are no grain boundaries, the charge trapping is expected to be significantly reduced. SCD substrates fabricated with high purity method of CVD technique exhibit almost no trapping of charge carriers generated by incoming radiation. Therefore, SCD detectors have a great potential for spectroscopy applications.

In this chapter, fabrication of several batches of SCD detectors with different metallization and characterization is e discussed. Details of theoretical study of neutron Carbon interaction using Monte Carlo simulations are also presented.

5.1. Raman spectroscopy of SCD substrate

The Raman spectroscopy of SCD substrate was carried out in the similar manner as was done for polycrystalline substrates using 532 nm laser source. The typical Raman spectrum of the SCD detector is shown in Figure 5.1. The spectrum shows a peak at 1332 cm^{-1} indicating sp^3 bonded carbon in diamond structure.

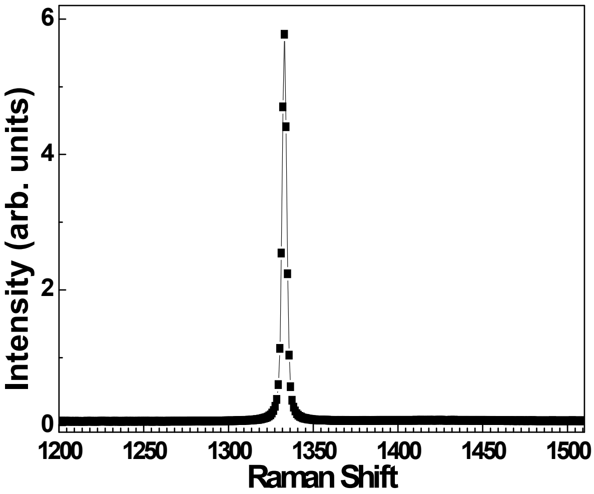

Fig. 5.1. Raman spectrum of a SCD substrate.

The FWHM of the Raman peak was calculated by fitting the peak using a Gaussian function. The FWHM was obtained to be 2.89 cm^{-1} which was comparatively lesser than the width obtained for a pCVD substrate. This was as expected as the SCD substrate has more ordered crystal structure than the polycrystalline substrate.

5.2. Laue pattern study of the SCD substrates

The Laue pattern of the SCD substrate was obtained using a 40 keV X-ray source. The pattern clearly shows Bragg spots where each spot corresponds to the different set of planes and exhibit single crystalline nature of the substrate as shown in Figure 5.2. The Laue pattern appears to have four fold symmetry which is a signature of lowest indexed set of planes i.e. [100], [010] or [001] at the surface of substrate.

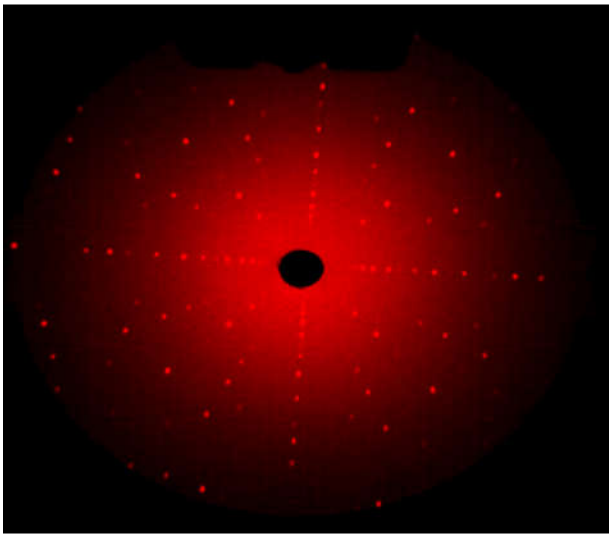

Fig. 5.2. Laue pattern of a SCD diamond substrate showing single crystalline nature of the substrate.

5.3. Fabrication of SCD detectors

The fabrication of SCD detectors was carried out using 5mm x 5mm x 400 µm SCD substrates. The substrates were cleaned in sulphochromic acid after degreasing and piranha cleaning as mentioned in chapter 4. Pre-metallization annealing of all the substrates was done at 400 °C in Nitrogen ambient for ½ hour. The SCD detectors were fabricated in three batches as described below:

Batch I – Both sides of SCD substrates were metalized by Al metal. Oxygen plasma treatment of the surface was done using the method discussed in chapter 4. The substrates were neither annealed before metallization nor after the Al metallization.

Batch II – The substrates were annealed at 400°C in nitrogen ambient for 30 minutes before metallization. The oxygen plasma treatment of some substrates was done after the annealing and some substrates were kept without this treatment. Subsequently, sequential deposition of Cr and Au was done using e-beam thermal evaporation on both sides of the substrates. The detectors were packaged without post metallization annealing.

Batch III – The detectors were fabricated in a similar way as discussed for Batch II with oxygen plasma treatment. However, the detectors were annealed at 300°C in nitrogen ambient for 30 minutes after metallization and then packaged on TO headers.

5.4. X-ray photoelectron spectroscopy

XPS spectroscopy of the samples was done using Al K_α X-ray source to identify the surface composition after oxygen plasma treatment. The XPS spectrum confirms the presence of oxygen on diamond surface as shown in Figure 5.3. The relative concentration of C and O is calculated to be 12.48 % and 87.52 % respectively. Other details about XPS spectrum are shown in Table 5.1.

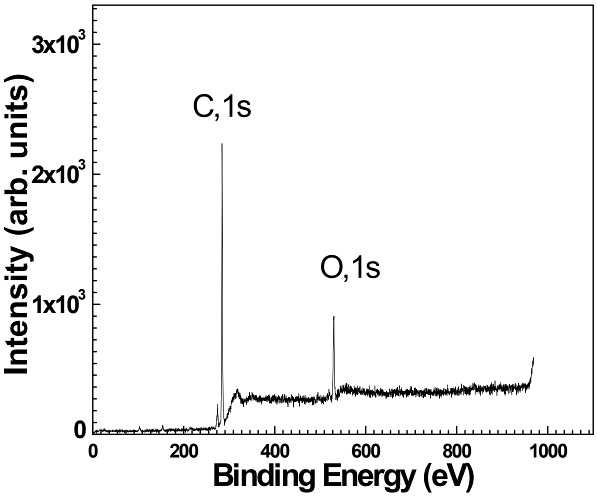

Fig. 5.3. XPS spectrum of diamond surface showing the presence of oxygen on the surface.

Table 5.1. Experimentally obtained data from the XPS spectrum.

Parameters	**Values**
C peak position	284.5
C peak area	39,495.4
FWHM of C peak	1.564
O peak position	529.8

O peak area	16,501.6
FWHM of O peak	2.225

5.5. I-V characterization

The leakage current variations in the detectors fabricated in different batches were studied by I-V measurements by varying the bias voltages. The SCD detectors with three different metallization were studied to investigate the contact behaviour and leakage currents.

5.5.1. I-V characterization of detector with different metallization

Det A - With Al metallization without post metallization annealing fabricated in Batch I.

Det B - With Cr/Au metallization without post metallization annealing fabricated in Batch II.

Det C - With Cr/Au metallization and with post metallization annealing fabricated in Batch III.

During the measurements, the bias voltage was varied from −400 V to +400 V and the leakage current was monitored. As shown in Figure 5.4. The leakage current was observed to be quite low for Det A, i.e. current of about 230 pA at +400 V. No breakdown was observed in positive bias region up to the measured voltage of 400 V which correspond to the electric field of 1 V/µm. For negative bias voltage, the current was of similar magnitude as was observed for positive bias voltages. However, the detector showed break down above -365 V. The leakage current observed in Det B was slightly more than that observed for Det A. The I-V curve of detectors Det A and Det B were symmetric in both positive and negative bias region which shows good ohmic behaviour. The I-V curve obtained for Det C shows a large variation in leakage current in positive and negative bias directions with the current in negative direction one order more than that in the positive direction before breakdown. The leakage current was observed to increase abruptly in the negative bias region after -175 V.

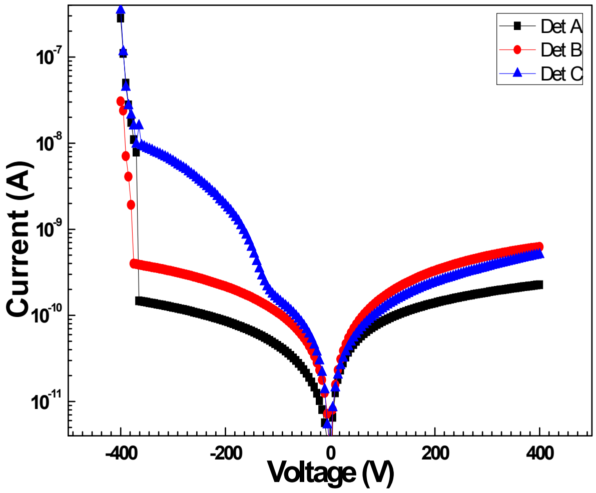

Fig. 5.4. Comparison of diamond-metal behaviour for three different types of detectors. Det A - Al metallization without annealing, Det B - Cr/Au metallization without post metallization annealing and Det C - Cr/Au metallization with post metallization annealing.

All the three detectors showed breakdown in the negative bias region at applied voltages between −370 V to −380 V. The detectors did not show any breakdown in the positive bias region when bias voltage was raised up to 400 V.

5.5.2. Study of effect of oxygen plasma treatment on leakage current

To study the effect of oxygen plasma treatment on the leakage current, I-V characteristic of two detectors, one with oxygen plasma treatment (fabricated in Batch II) and the other without oxygen plasma treatment (both were fabricated in Batch II) are compared in Figure 5.5. The leakage current was observed to reduce from 10 nA to below nA after oxygen plasma treatment. The higher current was expected due to the contribution of surface leakage current to the bulk leakage current. Oxygen plasma treatment was observed to reduce leakage current of all samples by approximately one order. The reduction in leakage current is attributed to removal loosely bound H atoms and oxygen termination of the surface. Oxygen plasma treatment also removes organic residues which may terminate stray leakage path over the surface.

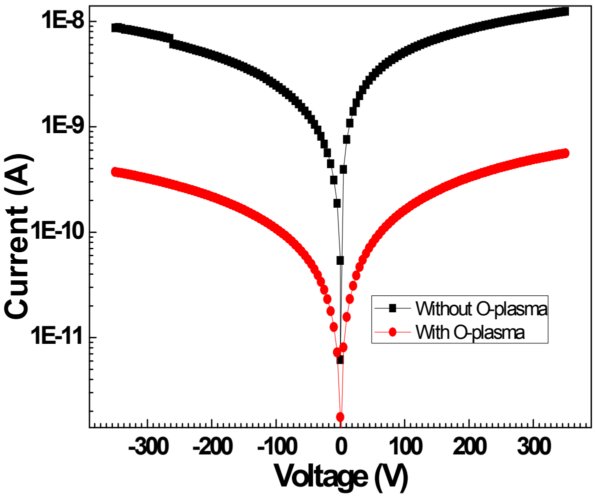

Fig. 5.5. Leakage current variation with bias voltage for Det B detectors with and without oxygen plasma treatment.

5.6. Study of charge collection properties

The charge collection property of a detector greatly varies with the applied bias voltage and it plays a very prominent role in spectroscopy applications. As charge carriers are generated in the detector due to the interaction of incident radiation, they immediately tend to recombine or get trapped at the crystal defect sites. When electric field is applied to the crystal, these charge carriers are separated and the recombination rate reduces with the increase in the field. The charge collection in a detector can be best estimated from the quantity known as 'charge collection distance (CCD)'. The charge collection distance is average distance travelled by charge carriers inside the detector crystal before recombining or getting trapped [61]. The charge generated in the detector and collected at the electrodes can be related to the charge collection distance using equation 2.13 as follows [67]:

$$Q_C = \frac{Q_g x_{ccd}}{l} \tag{5.1}$$

where

Q_g - total charge generated in the detector due to the interaction of radiation

Q_c - amount of charge collected at the electrodes

l - thickness of the detector

x_{ccd} - charge collection distance.

The CCD can be estimated if the absolute values of measured detector signal (Q_c) and the total generated charge (Q_g) are known. The charge collected at the electrodes (Q_c) is converted to a voltage signal pulse having amplitude 'v′ which is proportional to the collected charge itself. An increase in the electric field improves the amount of the charge collected at the electrodes. Therefore, the pulse amplitude (v) rises with increase in detector bias voltage and reaches to a maximum value (v_{max}) corresponding to the full charge (Q_g) collection. Therefore

$$v = kQ_c \tag{5.2}$$

and

$$v_{max} = kQ_g \tag{5.3}$$

Where k is a constant of proportionality which depends upon the parameters of the electronics and under normal working conditions can be considered as a constant. Therefore from equations (5.1), (5.2) and (5.3) we can write

$$x_{ccd} = \frac{v}{v_{max}}.l \tag{5.4}$$

Once the maximum pulse amplitude (v_{max}) is measured, CCD (x_{ccd}) can be calculated for each measured signal (v) at a particular applied electric field. CCD measurements were carried out in the positive bias region as the detector showed lower leakage current in this region.

In order to calculate CCD, the detector bias was varied using a high voltage source and the output of the detector was fed into the input of an in house charge sensitive pre-amplifier (gain - 44 mV/MeV). The output of the amplifier was monitored on a CRO to record the signal amplitude. The detector bias voltage was varied from zero to a maximum voltage equivalent to 1 V. µm^{-1} and the signal output of the preamplifier was noted. The variation in the signal amplitude with applied electric field is shown in Figure 5.6 (a) which shows that the pulse amplitude initially increases and then saturates for electric fields > 0.13 V/µm. If we consider that the maximum pulse amplitude (v_{max}) is reflecting the full charge collection (Q_g), then CCD as a function of applied field can be calculated according to Equ. (6.4). The variation of CCD at different electric fields is shown in Figure 5.6 (b). The charge collection distance was observed to saturate as the electric field crosses 0.13 V/µm and it becomes equal to the thickness of diamond substrate. Similar increase in CCD with the applied field was observed when applied bias voltage was reversed. Therefore, the detector bias voltage of 100 V (corresponding to 0.13 V/µm) was considered as a suitable voltage for the operation of the detector.

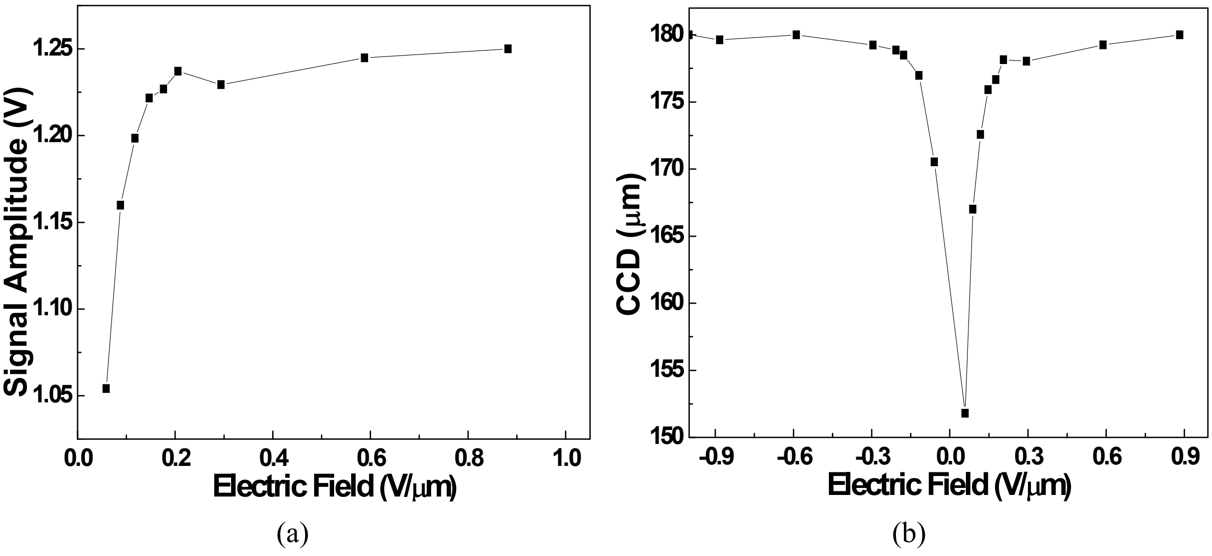

(a) (b)

Fig. 5.6. (a) Signal amplitude increases with electric field and saturate at 0.13 V/µm, (b) CCD variation with electric field calculated from the saturated value of signal amplitude.

5.7. Alpha response study of SCD detector

The performance of fabricated detectors to charged particles was studied using $^{238+239}$Pu dual energy alpha source. For alpha particle measurement, detector was placed in a vacuum chamber and the alpha source was mounted at a distance of about 5 cm above the detector. The detector signal pulse was measured using the electronics discussed in chapter 4. Since it was observed that the full charge collection occurs at 100 V, the pulse height measurements with alpha particles were carried out at a bias voltage of 100 V. The detector was kept at a vacuum of 10^{-2} mbar using the setup discussed in chapter 4. The channel number to energy calibration was performed using the two known alpha energy peaks corresponding to 5.156 MeV (^{238}Pu) and 5.499 MeV (^{238}Pu). The PHS obtained with the detector shows that the two peaks corresponding to the two energies of alpha particles i.e. 5.499 MeV and 5.156MeV are well resolved (Figure 5.7). From the alpha peak at 5.499 MeV, it is estimated that the detector has an energy resolution of 1.9 %. The detectors with an Al metallization and with a non-annealed Cr/Au metallization showed similar alpha spectra.

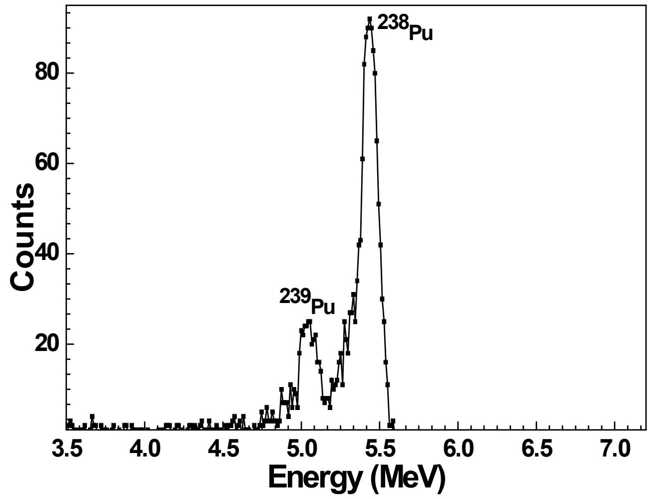

Fig. 5.7. Alpha spectrum of a SCD detector obtained using dual alpha source of ^{238}Pu (5.156 MeV) and ^{239}Pu (5.499 MeV).

5.8. Study of dynamics of charge carriers

Further transient current measurement of the detector was carried out with alpha particles to study the charge transport in the bulk of diamond. The details of experimental setup for the measurement of transient response of detector were discussed in chapter 4. The current pulse was observed for both types of charge carriers using a 2 GHz CRO. The current pulses due to charge generation in the detector with ^{241}Am alpha particles are shown in Figure 5.8.

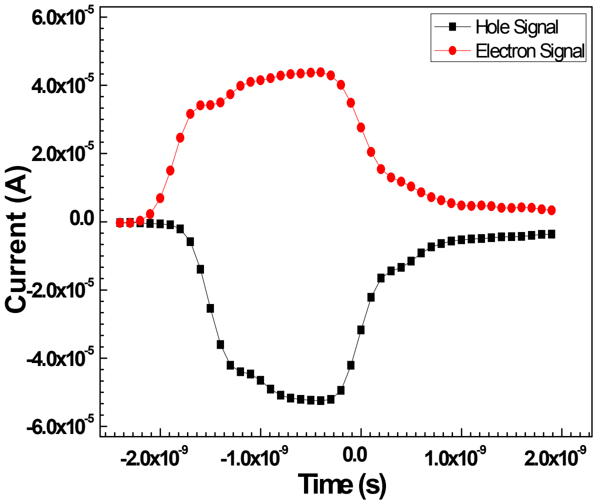

Fig. 5.8. Transient response of diamond detector for electrons and holes.

The pulses due to electrons and holes were recorded by applying a voltage of ±250 V to the detector. The signal current amplitude due to holes was around 50 nA which was 10 % more than that observed for the electrons (45 nA). The FWHM of hole signal (1.6 ns) was less than that of electrons (1.9 ns) which reflects the drift time of each type of carriers inside the detector. The electron and hole mobilities were calculated from the drift time of each types of carrier using Drude model.

From eq. 2.10 (chapter 2)

$$\mathrm{v_d} = \frac{\mu}{\mathrm{E}} = \frac{\mu}{\mathrm{V/d}} \tag{5.5}$$

if d is thickness of detector and t_d drift time then

$$v_d = \frac{d}{t} \tag{5.6}$$

From eq. (5.5) and (5.6)

$$\mu = \frac{d^2}{V.t} \tag{5.7}$$

From the equation (5.7), mobilities of about 4000 $cm^2V^{-1}sec^{-1}$ and 3368 $cm^2V^{-1}sec^{-1}$were calculated for electrons and holes respectively. Similar mobilites were estimated Jan Isberg et al. which were 4500 $cm^2V^{-1}sec^{-1}$ and 3800 $cm^2V^{-1}sec^{-1}$ for electrons and holes respectively [68].

5.9. Theoretical study of diamond detector response to fast neutrons

GEANT4 based Monte Carlo simulation study was done to study the nuclear interaction between fast neutrons and carbon. The four mandatory classes of the GEANT4 are primary generator action, detector construction, physics list and action initialization. Primary generator action class has information about the primary fast neutrons having energy of 14.2 MeV which were considered as a pencil beam of 1 mm diameter. The detector construction class incorporated the detector as diamond with density of carbon atoms of 3.5 g/cm^3. The physics list incorporated "QGSP_BERT_HP" physics model to study the nuclear reaction between carbon atom and neutrons which is a high-precision model suitable for medium neutron energy <20 MeV. The simulation was done for 10^7 primary neutrons. A theoretical PHS was obtained using these simulations based upon the energy deposited by neutrons in the individual event interactions with carbon in the diamond. The theoretical PHS is presented in Figure 5.9. Neutron cannot ionize diamond directly but it can undergo several possible channels of nuclear reaction between carbon and neutron such as $^{12}C(n, \alpha)^9Be$, $^{12}C(n, p)^{12}B$, $^{12}C(n, d)^{11}B$ and $^{12}C(n, n)^3He$ [62]. These interactions have different reaction cross sections which vary with the energy of neutrons. The cross sections for some of these reactions have been experimentally measured as $^{12}C(n, \alpha)^{9}Be$ (~0.065 barns), $^{12}C(n, p)^{12}B$ (~0.01 barns), $^{12}C(n, d)^{11}B$ (~0.04 barns) and $^{12}C(n, n)^{3}He$ (~0.25 barns) [63].

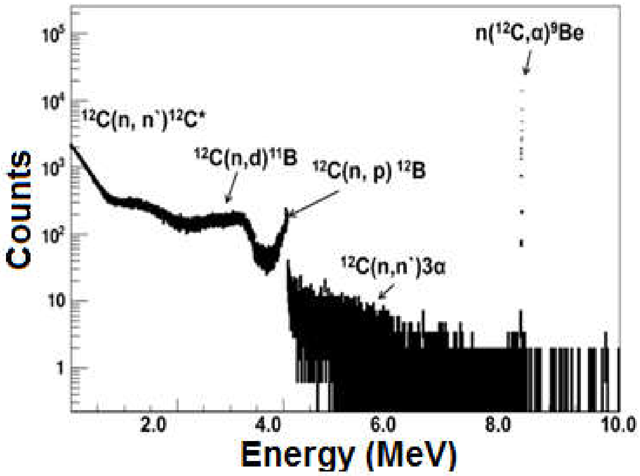

Fig. 5.9. Simulated PHS for neutron–carbon interactions showing various peaks corresponding to different channels of n-C reactions.

All these neutron events are characterized by unique Q-values of the corresponding reactions as listed in Table 3.1 (chapter 3). The energy of the products in these events is the difference of the energy of the incoming fast neutron and Q value of the reaction. Therefore, each of these events appears at different energy channels in the PHS. As can be seen from the simulated spectrum, the $^{12}C(n, \alpha)^{9}Be$ interaction peak appearing at 8.5 MeV is well isolated from the other peaks. Therefore, this reaction is most important for the spectroscopy of the fast neutrons.

5.10. Fast neutron measurements

The fast neutron response of the detector was also investigated experimentally using 14 MeV neutrons from deuterium- tritium (D-T) source. During the experiment, the detector was mounted in an aluminium enclosure. The detector was placed at a distance of 10 cm from the

D-T source. The neutron yield rate at the source was 2.5 x 10^9 n/s. Considering the isotropic emission of neutrons from the D-T source, neutron flux at the detector position which was at a distance of 10 cm from the source was 2 x 10^6 n/cm^2/sec. The PHS obtained with 14 MeV fast neutrons shows several peaks corresponding to the various possible nuclear reaction between carbon and neutrons i.e. $^{12}C(n, \gamma)^{13}C$, $^{12}C(n, \alpha)^9Be$, $^{12}C(n, p)^{12}B$, $^{12}C(n, d)^{11}B$. The experimentally observed PHS is in well agreement with that obtained by Monte Carlo simulation. Using the alpha spectra obtained with a dual energy source as shown in Figure 5.7, the channel numbers were calibrated to energy. The peak of $^{12}C(n, \alpha)^9Be$ reaction appear at 8.5 MeV which was observed to be sharp and well separated from other peaks. The SCD detector shows an energy resolution is 4 % for the 8.5 MeV energy peak. The sensitivity of the detector was calculated to be around 4.8 x 10^{-2} counts per neutron.

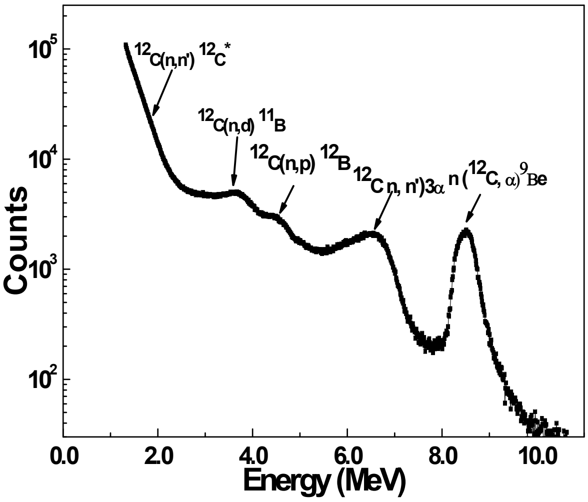

Fig. 5.10. Experimentally obtained PHS with a SCD diamond detector for fast neutrons showing various peaks.

The experiments were further conducted to see the linearity of the detector response with change in the neutron flux. The neutron flux was varied from 3.2×10^5 n/(cm^2 s) to 2.0×10^6 n/(cm^2 s) by increasing the distance of the detector from the neutron source. The spectra obtained at different neutron fluxes are compared Figure 5.11 (a). The position of peaks corresponding to different nuclear reaction was observed to appear at the same energy channel in all the spectra obtained at different neutron flux. As expected, the height of the spectra was observed to increase with increasing the neutron flux indicating increase in count rate. The count rates were calculated by integrating the spectra per unit time duration of measurement and are plotted in Figure 6.11 (b) as a function of neutron flux. The detector shows a very good linear response to the variation in neutron flux.

The neutron spectra obtained for the detectors with Al metallization and with a non annealed Cr/Au metallization were similar. The energy resolution (FWHM) for each detector was obtained by fitting the 8.5 MeV peak in the spectrum. The energy resolution was observed to be about 3.5% for all the three types of detectors. The sensitivities for detectors were calculated using the count rate shown by the detectors and the actual flux of neutrons falling on the active area of detector. The Det A, Det B and Det C show sensitivity of 3.4×10^{-2} count/n, 4.8×10^{-2} count/n and 4.5×10^{-2} count/n respectively.

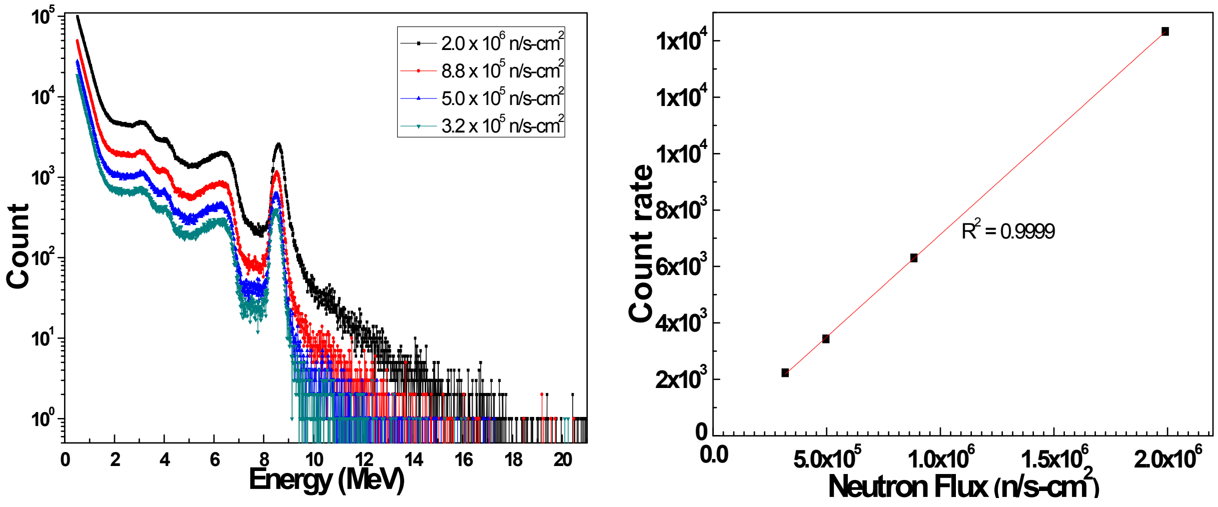

(a) (b)

Fig. 5.11. (a) Experimentally obtained PHS of fast neutrons at different neutron fluxes, (b) Linear variation (with $R^2 = 0.9999$) in count rate with respect to change in neutron flux.

5.11. Thermal neutron measurements

Diamond detectors cannot measure thermal neutrons directly using the principle discussed above as the minimum threshold energy required for the nuclear reactions is 6 MeV. As discussed in Section 3.4.4 (chapter 3), for thermal neutron detection, a suitable converter material is required to convert the neutrons into charged particles. For slow neutron measurement, ^{10}B film are usually used which converts neutron into alpha and ^{7}Li particles.

$$ {}_{0}^{1}\mathrm{n} + {}_{5}^{10}\mathrm{B} \rightarrow {}_{3}^{7}\mathrm{Li} + {}_{2}^{4}\mathrm{He} \quad : \mathrm{Q} = +2.792\ \mathrm{MeV} \ \ (6\%) \tag{5.8} $$

$$ {}_{0}^{1}\mathrm{n} + {}_{5}^{10}\mathrm{B} \rightarrow {}_{3}^{7}\mathrm{Li}^{*} + {}_{2}^{4}\mathrm{He} \quad : \mathrm{Q} = +2.310\ \mathrm{MeV} \ \ (94\%) \tag{5.9} $$

Most of the times, ^{7}Li remains in the excited state in the reaction which has Q-value 2.310 MeV. Then the charged particles i.e. ^{7}Li and α ionize the diamond and creates electron hole pairs. For studying the thermal neutron response of SCD detector, thermal neutron beams provided from a research reactor at BARC was used. The thermal neutrons are produced by the fission of natural Uranium.. The experiment to measure thermal neutrons was conducted at a beam line outside the reactor. The detector was mounted in front of the beam line. Similar set of electronics setup which was used for alpha and fast neutron measurements was used for this experiment. The PHS with thermal neutrons was acquired by ^{10}B integrated SCD detector. For reference, thermal neutron spectrum was also obtained using a 10 mm x 10 mm silicon detector integrated with similar ^{10}B thin film. The silicon detector was reverse biased at 40 V and the detector signal was fed into a preamplifier and shaping amplifier. Thermal neutron spectra obtained by SCD and silicon detectors are shown in Figure 5.12. As shown in the Figure, the maximum pulse height for a SCD detector was within the Channel No. 100-200. On the other hand it was within Channel No. 700-800 for silicon detector. The pulse height obtained in the spectrum was approximately five times more than that seen in the spectrum of SCD detector. However, the ratio was expected to be around four times as the energy required to create the electron hole pairs in diamond (13.2 eV) is about 3.7 times more than that of silicon (3.6). Further study of the change in the response of the detector to different neutron fluxes was done to check its linearity. The neutron flux was reduced by placing a number of 5mm SS plates. The SS plates were marked as number 1, 2, 3, 4 and 5. The PHS obtained for different neutron fluxes are compared in Figure 5.13 (a). The count rate from each spectrum was calculated from the experimental data and is plotted as a function neutron flux in Figure 5.13 (b). The variation in count rate with thermal neutron flux was not as linear as seen in case of fast neutrons. This may be due to presence of ^{10}B film which may itself attenuate energy of the charged products of the reaction. The maximum pulse height observed to be the same after placing SS plates of different thickness. As the SS plates reduce neutron flux and not energy, the change in the pulse height was not expected.

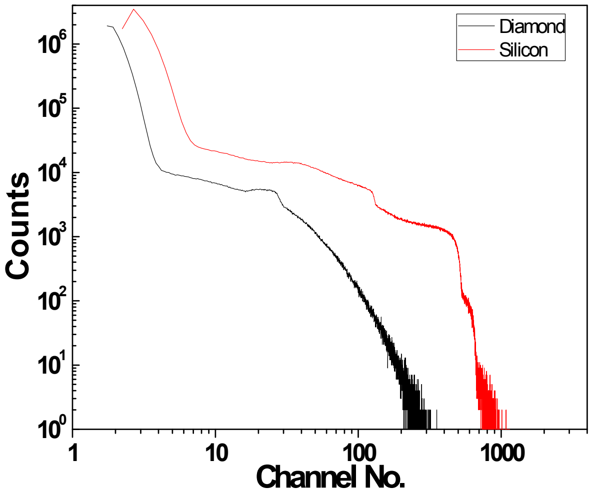

Fig. 5.12. Thermal neutron spectra obtained by a SCD detector and a silicon detector. Both detectors were integrated with 10B films.

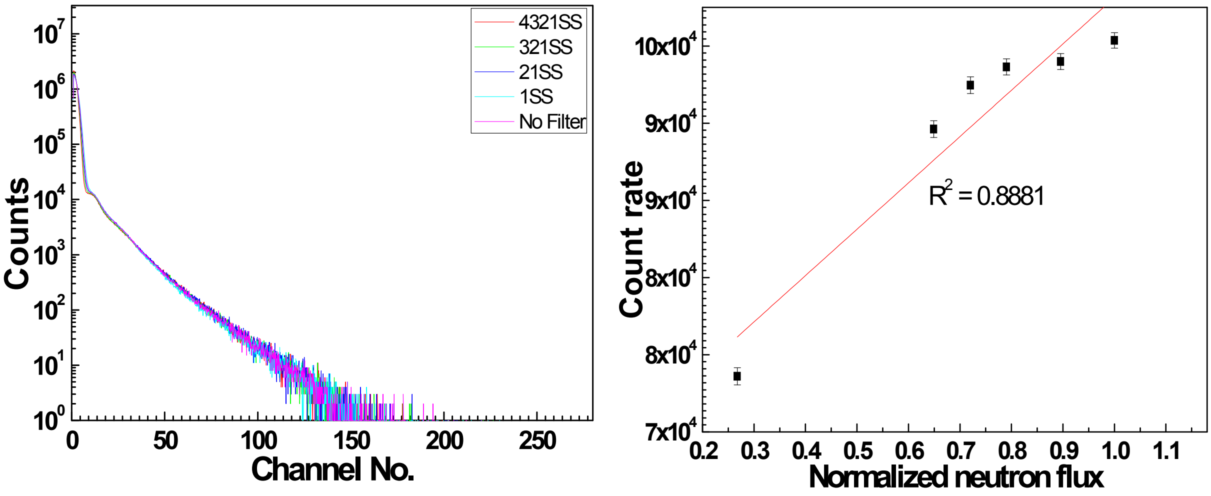

(a) (b)

Fig. 5.13. (a) PHS of thermal neutrons obtained at different neutron fluxes, (b) The variation in detector count rate as a function of change in neutron flux.

5.12. Summary

SCD substrates were commercially procured for the fabrication of detectors. The substrates showed very high purity as revealed by Raman spectroscopy and good crystallinity as observed by Laue crystallography. Oxygen plasma treatment of the substrates was done to get oxygen terminated diamond surface. XPS spectrum of the SCD substrates showed the presence of oxygen atoms on the diamond surface. The SCD detectors were fabricated using different types of metallization and it was observed that Cr/Au metallized detector show good ohmic contact. The Leakage current in the SCD detector was observed to be quite less and was of the order of few hundred pA in Cr/Au metallized detectors. The SCD detectors showed very good response to alpha particles with energy resolution of around 2 % at 5.5 MeV energy. Subsequently response of SCD detector to 14.2 MeV neutrons was studied by acquiring PHS. The experimentally obtained PHS with fast neutrons was observed to be in good agreement with the theoretical result obtained by Monte Carlo simulation. The PHS showed several peaks corresponding to different channels of nuclear reactions between carbon and neutrons. The SCD detectors showed energy resolution of about 4 %

corresponding to the peak at 8.5 MeV. The detectors demonstrated liner variation in count rate with the neutron flux. Initial studies of the performance of SCD detector integrated with ^{10}B film carried out to monitor thermal neutrons from experimental nuclear reactor showed the potential of SCD detector to monitor thermal neutrons also. In the next chapter, the performance studies of SCD detectors at high temperatures are presented.

CHAPTER 6: STUDY OF SCD DETECTORS FOR HIGH TEMPERATURE APPLICATIONS

Considering the potential of the SCD detectors for operation in ITER Experiment in a high temperature environment, the fabrication aspects and performance of the detectors at high temperatures were studied. In this chapter, the details of the fabrication of three batches of detectors and their performance study at high temperatures are presented.

Diamond detectors were fabricated to evaluate their performance at high temperatures. The detectors were fabricated in two batches using both pCVD and SCD substrates. The substrates were again processed in acids and other chemicals as discussed in chapter 4. Subsequently all substrates were annealed at 400^{o}C in nitrogen ambient prior to metallization. The fabrication of the detectors was done in two batches as per details given below:

Batch I – The detector were fabricated using pCVD substrates of 5 mm x 5 mm x 300 μm. The pCVD detectors were fabricated to evaluate the quality of different metallizations on diamond at high temperatures. As SCD substrates were costlier and limited in number, pCVD substrates were used for this study. Ti/Au, Cr/Au and Ti/Pt/Au were metalized using the same procedures discussed earlier. After metallization, annealing of the substrates was done at high temperatures up to 400^{o}C-500^{o}C.

Batch II – The SCD detectors were fabricated with Cr/Au metallization just after annealing. The post metallization annealing of detectors was done at 300^{o}C in nitrogen ambient.

6.1. Study of the of metal surface on diamond at high temperatures

The effect of temperature on metal diamond interface was examined to check whether the metallization would be suitable for high temperature applications. pCVD detectors with the three types metallization – Ti/Au, Cr/Au and Ti/Pt/Au were annealed at high temperatures up to 400°C-500°C in steps of 50°C in nitrogen ambient for 15 minutes. The condition of metal surface was visually monitored by seeing the surface through an optical microscope after annealing at every step. The metallized diamond-surface was observed to be normal without any changes up to 250 °C for all three types of metallzations. However, as the annealing temperature was raised to 300 °C, Ti/Au metallization showed changes in the colour. Spots were clearly observed on the metalized surface of Ti/Au from 350°C which could be due to the diffusion of Ti. The image of Ti/Au metal surface after 400 °C annealing is shown in Figure 6.1 (a). At some spots, change in the colour was observed probably due to inter-diffusion between Ti and Au. The Cr/Au metallization was observed to remain as it is up to 400 °C except that the surface became little dark. As the temperature was raised to 500°C, a few black spots were observed on the surface. A picture of Cr/Au metal on diamond after annealing at 500 °C is shown in Figure 6.1 (b). The Ti/Pt/Au metallization on diamond was observed to be intact up to 500°C as shown in Figure 6.1 (c) except that the surface became dark.

The I-V characteristics of the detectors with three types of metallization was obtained (shown in Figure 6.2) after different annealing temperatures to study the changes in the contact properties. The Ti/Au metalized detector showed leakage current of 0.8 nA at -200 V before annealing and the current at +200 V was one order more. After annealing the detector at 300°C, the leakage current was observed to increase in both directions.

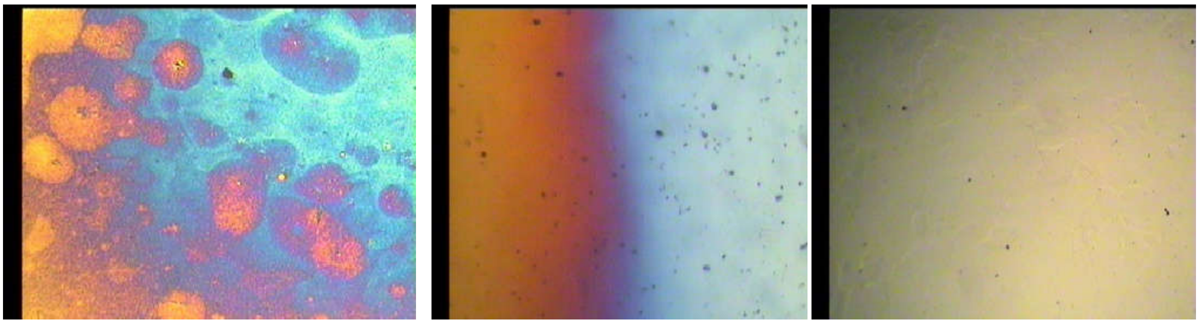

(a) (b) (c)

Fig. 6.1. Microscopic image of metal surface over diamond after different annealing temperatures; (a) Ti/Au after annealing at 400 ^{o}C, (b) Cr/Au after annealing at 500 ^{o}C, (c) Ti/Pt/Au after annealing at 500^{o}C.

The I-V plots obtained at 300 ^{o}C was observed to be relatively more symmetric in both directions showing improvement in the ohmic character after annealing. After annealing at 400 ^{o}C, the leakage current was observed to fall suddenly with very small increase in the leakage current with increase in the voltage. The results of I-V measurement after annealing at 400 ^{o}C show that the contact has probably gone bad due to burning of metal from the surface as shown in Figure 6.1 (a). The leakage current in Cr/Au detector was around 1 nA with ohmic behaviour prior to annealing. The leakage current behaviour was observed to shift on higher current (tens of nA) side while maintaining the ohmic behaviour. After annealing the detector at 500 ^{o}C, the leakage current was observed to decrease at 1 nA level. The I-V characteristic was still observed to be ohmic except in the positive bias region between 150 V-200 V as shown in Figure 6.2 (b).

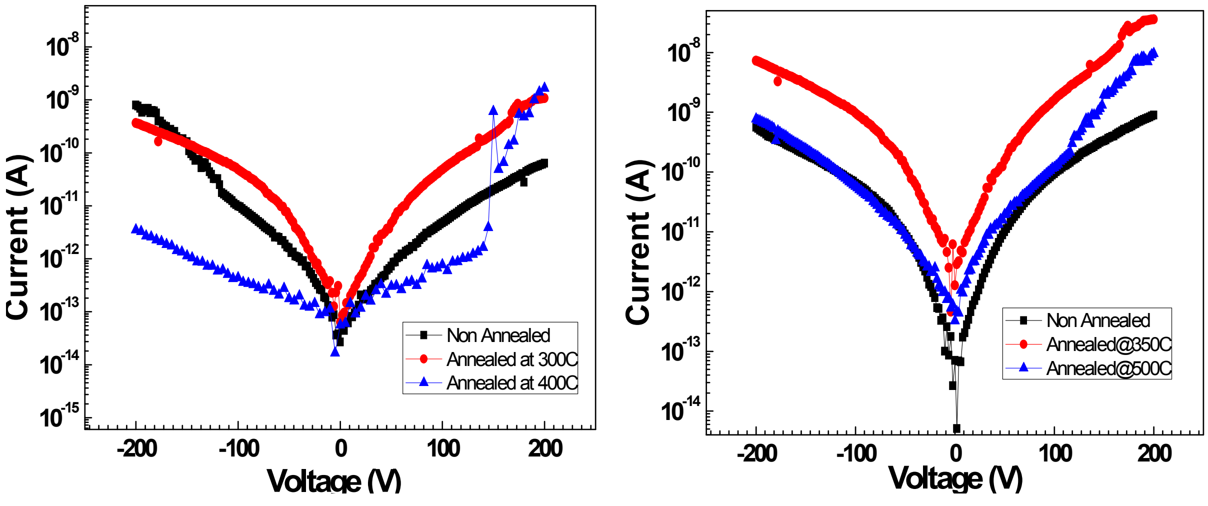

(a) (b)

Fig. 6.2. IV characteristic of pCVD detectors after different annealing temperatures for (a) Ti/Au metallized detector after annealing at 300 °C and 400 °C and (b) Cr/Au metallized detector after annealing at 350 °C and 450 °C.

The leakage current in Ti/Pt/Au metalized detector was around 1 nA at +200 V and one order less at -200 V. After annealing at 350 °C, the leakage current in the negative bias direction increased slightly but with large increase of current in the positive bias direction. The I-V characteristics became symmetric indicating improvement in the ohmic nature of the contacts. After annealing at 500°C temperature, the current in the both directions increased and became of the order of tens of nA (Figure 6.2 (c)).

From the comparison as discussed above, Cr/Au and Ti/Pt/Au metalized detectors showed their stability and were observed to maintain the I-V behaviour after heating up to 500°C. Therefore these contacts show potential to work in high temperature measurements. The Ti/Au contact did not show the stability after heating at 400°C.

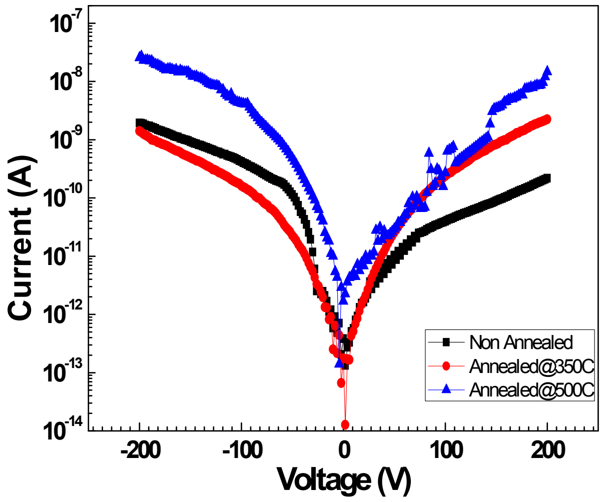

Fig. 6.3. IV characteristic of pCVD detectors with Ti/Pt/Au metallization after annealing at 350 °C and 500 °C.

6.2. Development of high temperature measurement setup

In this work, a complete setup to characterize the detectors at high temperatures was designed and fabricated. The setup consists of a heating chuck, contact probes, a temperature controller and a temperature sensor and provision to mount an alpha source above the detector. A flange with BNC connectors was provided for the external connections to the equipment. The chamber was connected to a vacuum pump for maintaining vacuum of about 10^{-2} torr-10^{-3} torr (Figure 6.4 (a) and (b)). The heating chuck incorporated a nichrome heater for increasing the chuck temperature. The chuck was designed to hold flat detector samples up to the diameter of 15-20 mm. The top of the heating chuck was covered by a thin sheet of mica to electrically isolate detector samples from the heater which prevented electrical noise coupling during the measurements. Total six contact probes were provided for making electrical contacts with the detector. Out of these, two were grounded and four were completely isolated from the heating chamber. These contact probes were connected to BNC connectors fixed at the bottom flange where heat radiated from the chuck is minimum resulting minimum heating of BNC connectors. A holder to mount a one inch disk shaped alpha source was designed to hold the source as available in the laboratory. The distance of the source from the detector was adjustable from 0.5 cm to 5 cm above the detector. Valves were provided to the chamber to connect to a vacuum pump. A pressure gauge was also connected to monitor the vacuum.

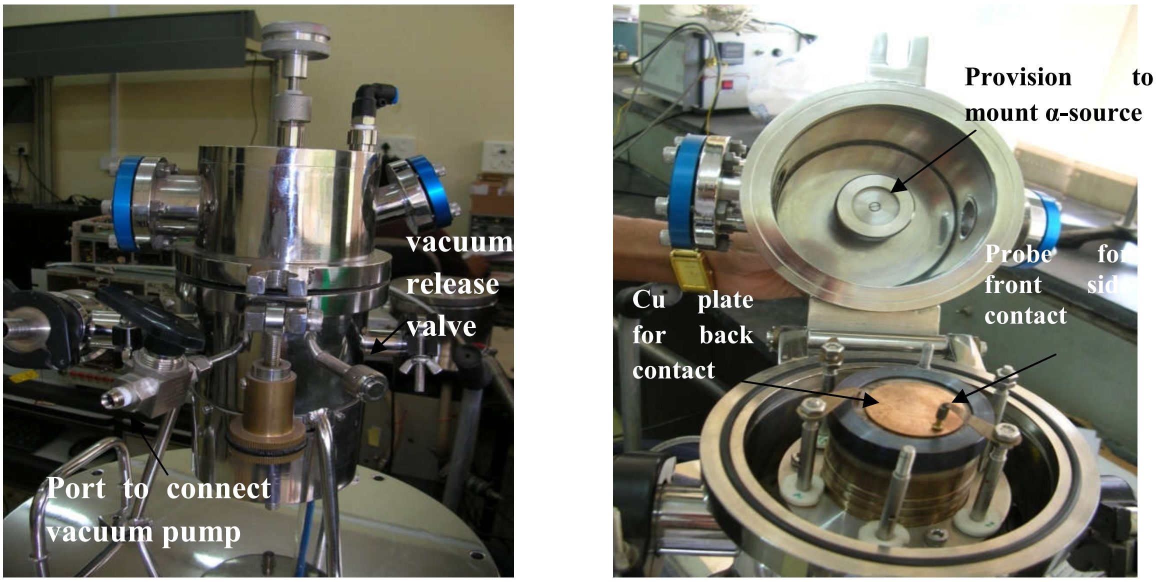

(a) (b)

Fig. 6.4. The fabricated high temperature setup for alpha and I-V measurements; (a) outer view, (b) inner view.

6.3. Study of I-V characteristics at high temperatures

The leakage current variation with the bias voltage was studied at high temperatures for the detectors fabricated in batch II. The detectors were mounted on the chuck and the contacts from top and bottom sides were taken using contact probes shown in Figure 6.4 (b). A Picoammeter and inbuilt voltage source were connected to the BNC connectors fitted at the bottom flange of the chamber. The bias voltage was varied from -400 V to +400 V and the leakage current was measured using an automated setup. The temperature was varied from room temperature up to 300 °C in steps of 100 °C. The temperature of the chuck as measured by a K-type thermocouple was also displayed by the temperature controller. The thermocouple was located inside the chuck and not at the surface where the detector was placed. The temperature attained at the top of the chuck (on which the detector was placed during measurements) was lower by a few degrees than the temperature shown by the temperature controller. The temperature at the top of the chuck was calibrated with the set temperature of controller so as to obtain desired temperature at the top of the heating chuck.

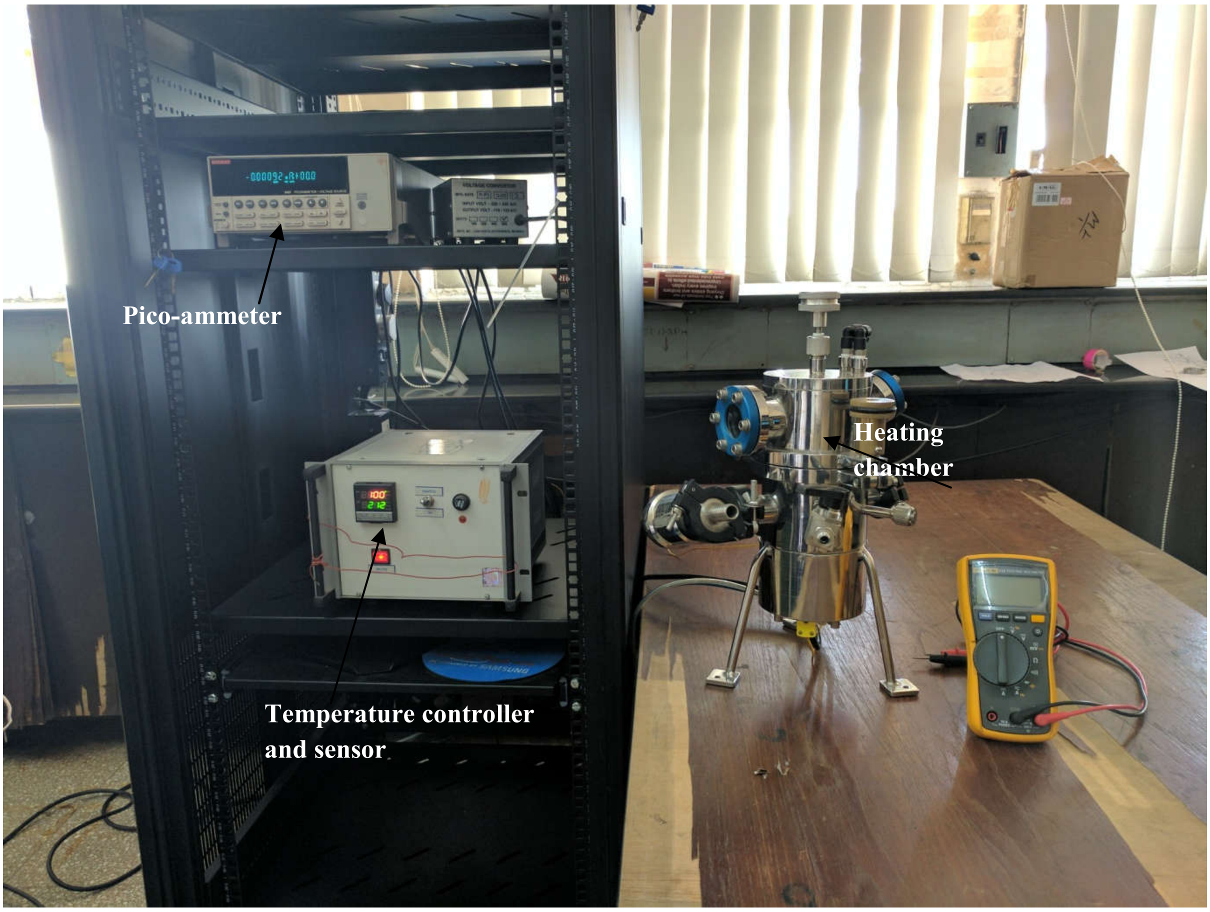

Fig. 6.5. The setup used for I-V measurements of detectors at high temperatures.

The I-V characteristics of the detectors fabricated in batch II at high temperatures are compared in Figure 6.6 (a). The detector shows leakage currents of few hundred pA at +300 V and the current was one order more at -300 V. As the temperature increases, a small change in the leakage current is observed up to 200 ^{o}C. When temperature increased from 100^{o}C to 200^{o}C, the leakage current is observed to increase by an order of magnitude. From

200°C to 300°C, a sharp increase in current was noticed in the positive bias region and the leakage current increases up to 24 nA as shown in Figure 6.6 (b).

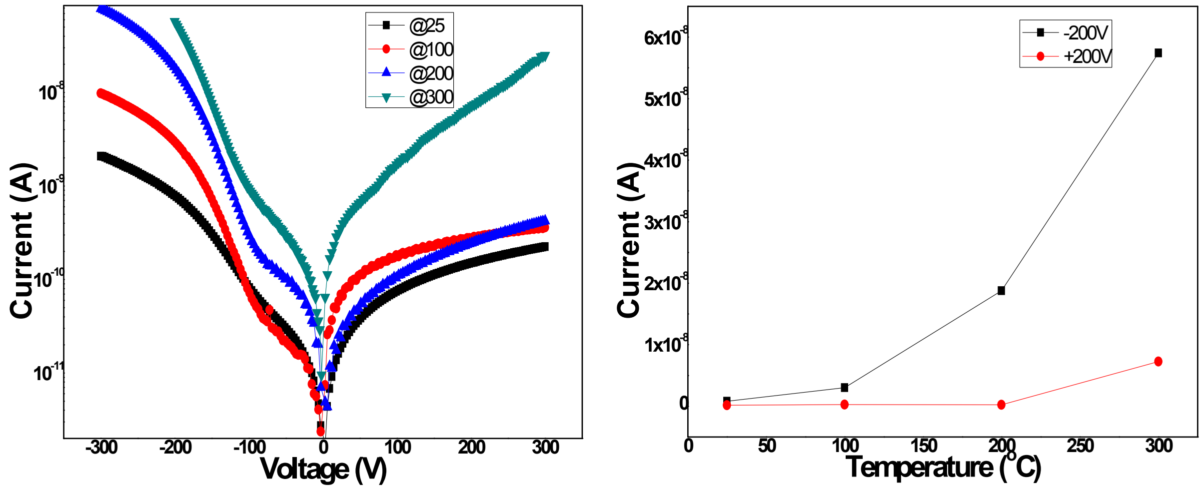

(a) (b)

Fig. 6.6. (a) I-V characteristics of 5 mm x 5 mm x 400 µm detector obtained at different temperatures, (b) Leakage current at ± 200 V vs temperature plot.

6.4. Alpha response study at high temperatures

The alpha response of the fabricated 5 mm x 5 mm x 400 µm SCD detector to charged particles was studied at high temperatures. For these measurements, the detector was placed on the chuck of the heater and a dual energy alpha source $^{238+239}$Pu was mounted in the source holder above the detector. As alpha source had a very thin coating of Pu on a disk, it could have degraded due to heating. Therefore, the alpha source was mounted at a distance of about 5 cm from the detector so that temperature at the source location would be always less than 50°C. The entire heating system was kept inside an SS chamber which was maintained at a vacuum of 10^{-2} mbar using a rotary pump. The back end electronics was connected to the heating chamber (as shown in Figure 6.7 (a)) to process the signal received from the detector.

As discussed in chapter 6, the detector bias voltage for the measurements with alpha particles was optimized based on the voltage required for full charge collection. The leakage current was observed to be reasonably low at 100 V bias @ 300 °C in Det C, therefore this detector was used to obtain the alpha spectrum at 300 °C. The PHS with alpha particles at RT and 300°C is compared in Figure 6.7 (b). It can be seen from the figure that there is an improvement in the charge collection causing the shift in the alpha spectrum to the high energy side at 300 °C. No significant change in energy resolution of the detector was observed between from RT and 300°C.

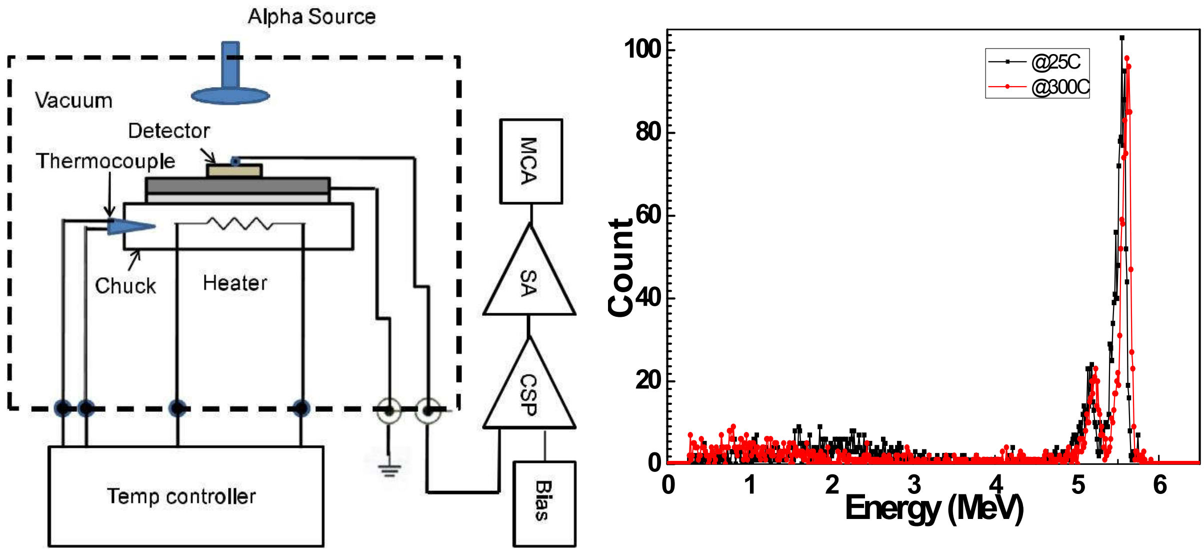

(a) (b)

Fig. 6.7. (a) Schematic diagram of the high temperature setup for alpha response measurements, (b) PHS obtained with Cr/Au metalized detector (fabricated in Batch II) at RT and 300°C.

6.5. Fast neutron measurement at high temperature

Considering the application of the detectors for neutron diagnostics in ITER Experiment, the performance of the detectors with fast neutrons was studied at high temperatures. A detector enclosure was fabricated and the measurement setup was prepared for the measurements up to 300°C.

The detector enclosure was fabricated as a 30 cm long aluminium tube. One end of the tube was fixed with a BNC connector and the detector was mounted at the other end of the enclosure as shown in Figure 6.8 (b). The length of the tube was kept long enough to reduce the temperature at the BNC end of the enclosure below 250 °C. This limitation of the temperature was set due to the maximum operating temperature of the coaxial cable polyether ether ketone (PEEK) used during the measurements. The electrical contact to the top side of detector was provided by a long stainless steel wire of diameter of 1 mm which was mechanically crimped over the contact pin of the TO header. The pin was connected to the top side metallization by gold wire bond as shown in Figure 6.8 (a).

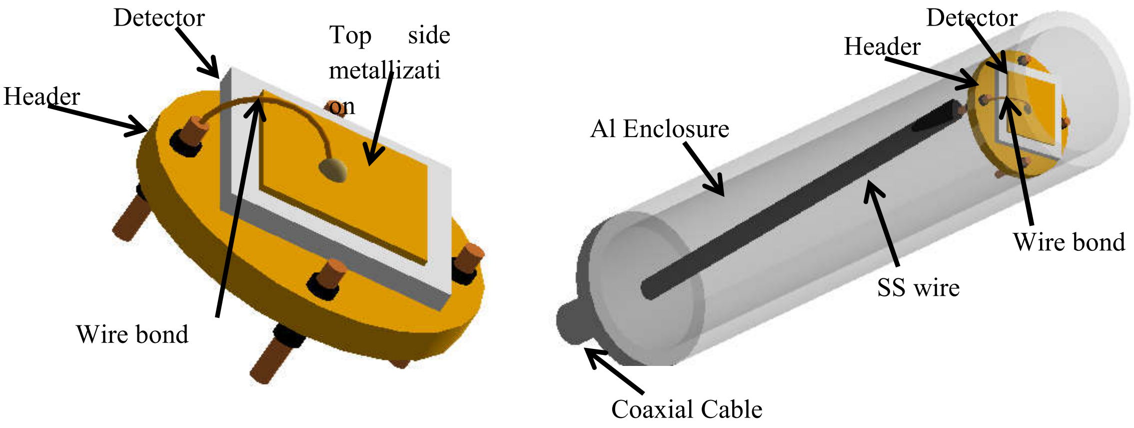

(a) (b)

Fig. 6.8. Schematic showing (a) gold wire contact between top metal of detector to one of the pin of TO header, (b) 30 cm long aluminium tube holding detector at one end with SS wire connecting the header pin to BNC connector.

The contact to the back side of the detector was provided by the body of aluminium enclosure itself which was in contact with the body of the detector TO header. The detector end of the cylindrical enclosure was inserted in a solid copper block so that the detector is placed in the middle of the block. The copper block was placed over the chuck of the heating chamber using a heat sink paste. The temperature was set by a digital PID programmable temperature controller and a K-type thermocouple was used to monitor the temperature. The thermocouple was kept in contact with the heating chuck. The copper block was directly placed upon the heating chuck using a heat sink paste. Therefore, some drop in the temperature was observed between the thermocouple location and detector location. A temperature calibration was done using a PT100 temperature sensor. During measurements, the temperature was set in the PID controller so that the temperature at the detector location was at the desired temperature.

The fast neutron measurements at high temperatures were done using the same set of electronics that was used during the alpha spectroscopy. A schematic of the measurement setup and associated electronics is shown in Figure 6.9. The detector was kept at a distance of 12 cm from the D–T neutron source. The flux calculated at the detector location was about 6.37×10^5 n/cm^{2}s. The detector was biased at 100 V during the measurement. The detector was allowed to stabilize for 10 minutes before taking the neutron spectra.

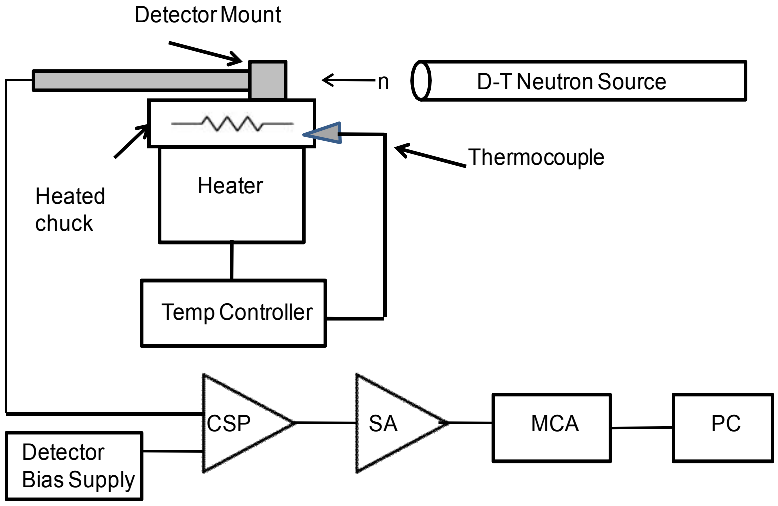

Fig. 6.9. Schematic of the experimental arrangement used during fast neutron measurement. The detector enclosure inside a copper block is placed over the heating chuck and the back end electronics is connected to the BNC connector carrying the detector signal.

The output of the shaping amplifier was fed into a MCA as well as a CRO to see the signal pulses. The signal output of the shaping amplifier at room temperature is shown in Figure 6.10 (a) which shows pulses of varying height from 500 mV to 2 V. The pulses of different heights arise due to different channels of nuclear reactions having different threshold energies. Due to the difference in threshold energies, the products of nuclear reactions carry different amount of energy which leads to the signal with different amplitudes.

The PHS of fast neutrons obtained at different temperatures varying from RT to 300°C are shown in Figure 6.10 (b). The spectra contain all peaks as theoretically expected from Monte Carlo simulations. Compared to the theoretical spectrum, the peaks are broadened due to the electronic noise of the detector and electronics. The pulse height spectra from RT to 300°C are observed to be identical with maintaining the shape of each peak. No degradation of the spectroscopic performance up to the maximum studied temperature of 300°C was observed. The $^{12}C(n, \alpha)^9Be$ peak at 8.5 MeV which contains most relevant information about the incident fast neutrons is observed to be well separated even at 300°C.

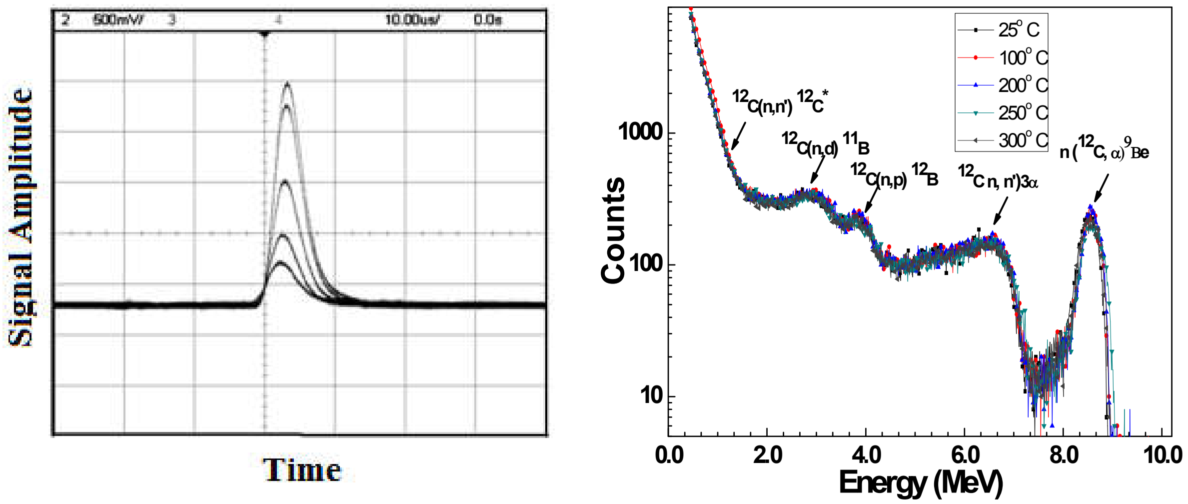

(a) (b)

Fig. 6.10. (a) Signal output of shaping amplifier for fast neutrons at RT, (b) PHS of fast neutrons from RT to 300°C.

Further analysis of the obtained PHS at different temperatures was done by studying the change in the count rate with temperatures. The count rate corresponding to (n, α) reaction was calculated by integrating the counts under (n, α) peak.

The total integrated counts from the spectra obtained at each temperature were about 3×10^5 for the counting time of 5 minutes. The variation in the count rates at different temperatures is shown in Figure 6.11 (a) where total count rate and count rate for counts related to (n, α) reactions are shown separately. The change in the count rates observed at different temperature is not significant. The SCD detector shows average total count rate of 1040 CPS with statistical variation of 30. The count rate under the (n, α) peak is around 32 CPS. Considering the detector area of 16 mm^2, count rate of 1058 CPS, and the neutron flux of 6.37×10^5 $n/cm^2 \cdot s$, the detector sensitivity was observed to be 10^{-2} count per neutron for the total integrated counts.

The effect of temperature on the energy resolution of the detector was studied from the obtained PHS. The energy resolution of the detector was obtained by Gaussian fitting of the peak at 8.5 MeV and FWHM was calculated. The energy resolution corresponding to the 8.5 MeV peak of the neutron spectra at different temperatures is shown in Figure 6.11 (b). The energy resolution was observed to vary within 3.3-3.8 % with a standard deviation of ±0.2% at different temperatures. The detector does not show any significant degradation in the energy resolution with the increase in the temperature of the detector. Therefore, the results indicate that the SCD detector could be used for the measurement of fast neutrons up to the studied temperature of 300C.

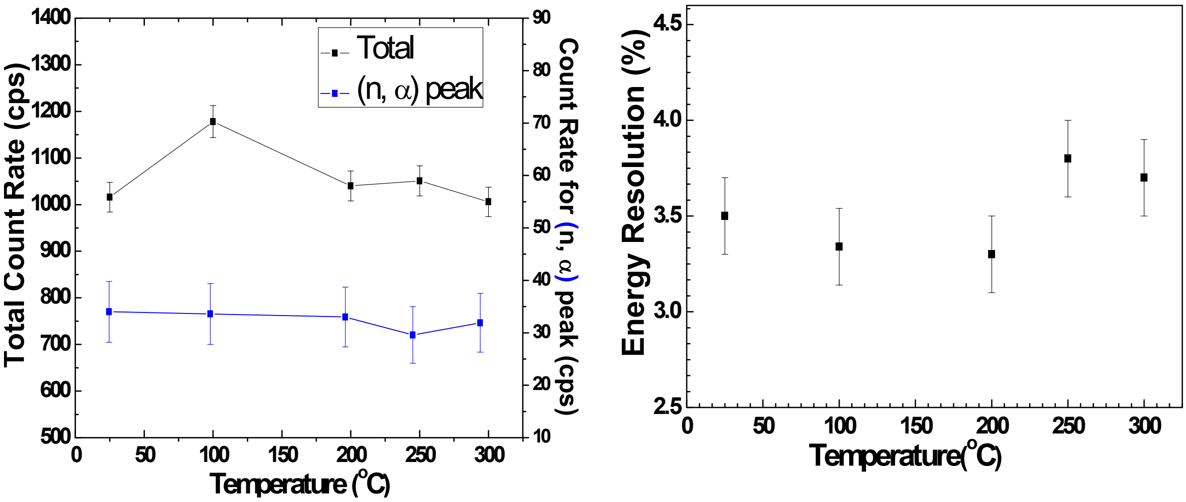

(a) (b)

Fig. 6.11. (a)Variation in count rates with temperature considering total counts and counts under (n, α) peak, (b) Energy resolution variation of the detector with temperature calculated at the (n, α) peak.

6.6. Summary

The study of diamond detectors for alpha and fast neutron measurements up to 300°C was carried out. The Cr/Au and Ti/Pt/Au metallized detectors showed comparatively better metal adhesion up to 500°C compared to Ti/Au metallized detector. A high temperature setup comprising a heating chuck, temperature controller and sensor, provision to mount alpha source, contact probes etc. was developed to test the performance of the detectors at high temperatures. The leakage current measurements in SCD detectors were performed at high temperatures up to 300°C. The leakage currents were observed to increase from few hundred pA to few hundred nA. Subsequently, the response of detectors to alpha particles was investigated at high temperatures. It was observed that PHS of alpha particles remains as it is up to 300°C along with maintaining its energy resolution of 2 % for 5.5 MeV alpha particles. A suitable package was developed to mount detector for fast neutron measurements at high temperatures. Subsequently experiments were conducted to monitor fast neutrons at high temperatures. The PHS with fast neutrons was acquired at high temperature up to 300°C at a step of 50°C and it was observed that there is no significant change with temperatures. All the peaks corresponding to different channels of nuclear reaction between carbon and neutron remain intact up to 300°C and there is no degradation of the energy resolution of 4 % up to the studied temperature of 300°C.

CHAPTER 7: CONCLUSIONS AND FUTURE SCOPE

Unique properties of diamond mainly electrical, mechanical and thermal properties open up wide area of applications for diamond such as heat sink in electronics chips, abrasive, jewellery etc. Radiation detection is one of the most eminent applications of diamond which has been of prime interest for many research groups over the world. Diamond has outstanding electrical and semiconducting properties such as high bandgap (5.45 eV), high electron hole mobility (4800 and 3500 $cm^2V^{-1}s^{-1}$), high resistivity ($>10^{12}\Omega$.m), etc. Diamond detector has several advantage over other semiconductor detectors such as low leakage current, fast response, very high radiation hardness etc. Diamond based detector falls under the category of semiconductor detectors such as silicon and germanium. Diamond offers many advantages over these detectors which allow the detector to work in certain applications where other semiconductor detectors do not work. The inherent potential of the material and promising advantages of the detector was the motivation to carry out this research work based involving study of SCD and pCVD detectors. The doctoral work was focussed on the development of detector fabrication technology and to investigate the performance of SCD and pCVD based radiation detectors with radiations such as alpha particles and fast neutrons. Another objective was to explore the potential of detector for applications involving high temperature environment such as ITER. The mains results and findings of the doctoral work on pCVD detector are as follows:

- A study of pCVD detectors with different types of metallizations has been carried out. Detectors with low leakage currents of about nAs have been realized by optimizing the fabrication process. Cr/Au metallized detectors show I-V characteristic much closer to ohmic behavior compared to Ti/Pt/Au andTi/Au metalized detectors..

- The fabricated pCVD detectors show a good response to alpha particles with a continuum in the alpha spectrum without any peak due to charge trapping effects.
- The thinner detectors with 100 μm thickness show better performance compared to 300 μm thick detectors due to reduced due to reduced trapping of charge carriers in the substrate.
- The as fabricated pCVD detectors show unstable response with the decrease in count rate with time. The Priming of the pCVD detectors for a total dose of 30 Gy using β-particles results in the stability of detector response as count rate was observed to be stable with time after priming. The priming also resulted in improvement in the charge collection.
- Although pCVD detectors do not give energy information of fast neutrons, they are suitable for measurement of flux of neutrons as count rate of the detector was observed to vary linearly with neutron flux.

Main results and findings of the doctoral work on SCD detector are as follows:-

- Oxygen plasma treatment of the diamond substrates results in the oxygen termination of the diamond substrates as revealed by the XPS results.
- The I-V characteristics of Al and Cr/Au metallized detectors show ohmic type behavior.
- SCD detectors exhibit leakage currents of a few hundred pico-amperes for Cr/Au and Al metalized detectors.
- Oxygen plasma treatment of the substrates reduces leakage current by at least one order of magnitude by reducing the surface leakage current.
- Charge collection study of the detector in terms of CCD shows full charge collection at an applied bias voltage corresponding to an electric field of 0.13 V/μm.

- SCD detectors demonstrate alpha response suitable for spectroscopy of alpha particles. The energy resolution shown by the fabricated detectors is about 2 % for 5.5 MeV alphas.
- Transient current study of SCD detector reveals very high electron and hole mobilities (4000 cm^2/V-sec and 3368cm^2/V-sec). The results are in agreement with the results reported in the literature.
- Monte Carlo simulation results demonstrate that the SCD detectors can give peaks in neutron pulse height spectrum corresponding to different channels of nuclear reaction between 14 MeV fast neutrons and carbon.
- The experimentally observed response of SCD detectors to 14 MeV fast neutrons is in agreement with the theoretically predicted reposne from Monte Carlo siumation studies.
- SCD detectors exhibit very linear response with respect to variation in the neutron flux.
- ^{10}B film integrated with SCD detector can be used for the measurement of thermal neutrons.

Main findings of the study of diamond detector at high temperatures of 300^{o}C are as follows:-

- Ti/Au metallization as contact material cannot sustain temperature above 300^{o}C
- Cr/Au and Ti/Pt/Au metallized detectors sustain annealing temperatures of 500^{o}C. The detector leakage current increases significantly from a few hundred pA to few tens of nA at 300^{o}C.
- No significant degradation in the alpha response of the detectors is observed up to 300^{o}C. The detector energy resolution at 300oC remains the same (2 %) as observed at room temperatures.

- SCD detector response to neutrons at high temperature has sown that all peaks in the neutron PHS remain unchanged up to 300^{o}C.
- The energy resolution was observed to vary from 3.3 % to 3.8 % for the high temperature operation from RT to 300^{o}C.

Future Scope

In this work, performance of the detector to alpha particles and fast neutrons was tested up to 300^{o}C. Due to limitation of PEEK cable and BNC connector, experiments could not be carried beyond 300^{o}C. However, performance of the detector up to 400^o C can be evaluated using ceramic based BNC connector and MI cables.

Diamond is also suitable for dossimetry applications due to its tissue equivalent atomic number. Further experiments may be conducted to evaluate dossimetric response of the detector.

REFERENCES

1. R. Saito, Physical properties of carbon nanotubes, Imperial college press, (1998).
2. D. J. Chadi and Marvin L. Cohen, Phys. Rev. B 8, 5747-5753 (1973)
3. F. Herman, et al., J. Phys. Soc. Jpn. 21, Suppl., 7 -11 (1966)
4. F. Borchelt et al., Nucl. Inst. and Meas. A 318-327 (1995)
5. D.R. Kania, L.S. Pan, P. Bell et al., J. Appl. Phys. 68, 124-130 (1990)
6. R. Vaitkus, T. Inushima, S. Yamazaki, Appl. Phys. Letters, 62, 2384-2386 (1993)
7. C. Canali et al., Nucl. Instr. And Meth. 160, 73-77, (1979).
8. J. E. Field, Rep. on Prog. in Phys. 75, 126505 (2012).
9. Tabor D and Field J E, The Properties of Natural and Synthetic Diamond, 547–71(1992)
10. Ruoff A, High-Pressure Science and Technology, 525–48(New York: Plenum, 1979).
11. D.J. Twitchen et al., Diam. and Rel. Mat. 10, 731-735 (2001)
12. Harris J W and Gurney, The Prop. of Diam., 555–91(1979)
13. A.J. Kordyasz, et al., Nucl. Instr. and Meth. A 530 87-91, 530 (2004)
14. Isberg et al., Science *297*, 1670-1672 (2002).
15. J J, Gracio et al., Jour. of Phys.: D Appl. Phys. 43, 374017 (2010).
16. W. Paul, Phil. Trans. R. Soc. Lond. A 358, 473-495 (2000).
17. A. V. Krasilnikov et al., Nucl. Fus., 45, 1503–1509 (2005).
18. F. Huegging, et al., Nucl. Instr. and Meth. A 565, 278-283 (2006).
19. Borchi, Emilio et al., Phys. Rev. B 71 104103-1-04103-8 (2005).
20. R. Robertson et al., Philos. Trans. R. Soc. Lond. A, 232, 463-535 (1934).
21. B. V. Spitsyn et al., J. of Crys. Grow. 52, 219-226 (1981).
22. E. Pace et al., Diam. and Rel. Mat. 9, 987-993 (2000).
23. F. Schirru et al., J. Phys. D: Appl. Phys. 43, 265101-265105 (2010)
24. Moritz et al, Nucl. Instr. and Meth. A 730, 168-173 (2013).
25. E. K. Souw and R. J. Meilunas, Nucl. Instr. and Meth. A, 400, 69-86 (1997).
26. M. Pillon et al., Nucl. Instr. and Meth. Phys. Res. A 640, 185-191 (2011).
27. B. Gudden and R. Pohl, Z. A Hadr. &Nucl. , 17 331-346 (1923).
28. R. Robertsonet al., Philos. Trans. of the R. Soc. of Lond. A, 232, 463-535(1934).
29. H. Friedman, L.S. Birks and H.P. Ganvin, Phys. Rev. 73, 186 (1948).

30. K. G. McKay, Phys. Rev. 77,816 (1950).
31. A. H. B. Benny and F. C. Champion, Nature 173, 1087 (1954).
32. P. J. Dean and J. C. Male, J. Phys., Chem. Solids 25, 311 (1964).
33. R. J. Keddy and T. L. Nam, Radiat. Phys. Chem. 41 767-73 (1993).
34. L.S. Panet al., Science 255,830-833 (1992).
35. M. Pomorski et al.,Phys. Stat. Sol. 202, 2199-2205(2005).
36. C. Manfredotti et al., Dia. and Rel. Mat. 11,446-450 (2002).
37. Mara Bruzziet al., J. of Appl. Phys. 91,5765-5774 (2002).
38. M. Pillon et al.,Nucl. Instr. and Meth. Phys. Res. B 101,473-483 (1995).
39. M. Angelone et al., Rev. Sci. Instr. 76, 013506 (2005)
40. M. Angelone et al., Nucl. Instr. and Meth. in Phys. Res. A 595 616-622(2008).
41. C. Cazzaniga et al., Measurement of DD and DT fusion neutrons using single crystal diamond detector at JET (EFDA-JET, 2012).
42. M. Kim et al., Appl. Phys. Lett. 105, 042406 (2014)
43. V. Eremin et al., Nucl. Instr. and Meth. in Phys. Res. A 372, 388-398 (1996)
44. H. Pernegger et al., J. of Appl. Phys. 97, 073704 (2005).
45. J. Isberg et al., Phys.Stat.Sol. 202, 2194-2198 (11) (2005).
46. U. Wolfram, Phys. In Med. & Bio. 44, 2183 (1999).
47. J.H. Kaneko et al., Nucl. Instr. and Meth. in Phys. Res. A 505 187-190 (2003)
48. M. Marinelli et al., Nucl. Instr. and Meth. A 476 (2002) 701-705.
49. M. Marinelli et al., Appl. Phys. Lett. 83, 3707-3709 (2003).
50. C. Manfredotti, E. Vittone, F. Fizzotti, A. Lo Giudice, C. Paolini, Dia. and Rel.Mat. 11, 446-450 (2002).
51. S. Muller, Ph.D. Thesis, CERN-THESIS (2011).
52. N. Ade et al.,Radiat. Phys. Chem. 81, 232-239 (2012).
53. P.W. Hoban et al., Phys. Med. Biol. 39, 1219 (1994).
54. M.G. Guerrero et al., Diamond and Rel. Mater 13, 2046-2051 (2004).
55. O. M. Suprun, J. of Superhard Mater. 37, 211-214 (2015)
56. Handbook of semiconductor wafer cleaning technology, W. Kern New Jersey (1993).
57. M. C. Granger et al., Analy. Chim. Acta, 397, 145-161 (1999).
58. N. R. Parikh, Appli. Phys. Lett. 61, 3124-3126 (1992).
59. Internal report
60. A. P. Roy et al., Indian J. of Pure & Appl. Phys. 30, 724-728 (1992).
61. H. Pernegger et al., J. of Appl. Phys. 97, 073704 (2005).

62. M. Marinelli et al., Phys. Review. B 195205-1-8 (2001).
63. M. Pillon et al., AIP Conf. Proc. 1412, 121-128 (2011).
64. M. Bruzzi et al., J. Appl. Phys.. 91, 5765-5774 (2002).
65. S. Wang et al., Appl. Phys. Lett. 88, 023501-1-3 (2006).
66. A. Lohstro et al., J. of Appl. Phys. 101, 063711-1-7 (2007).
67. R. J. Taper, Rep. Prog. Phys. 63, 1273-1316 (2000).
68. Jan Isberg et al., Science, 297, 1670-1672 (2002).